Dynamic Development of Hydrofractures

Dissertation zur Erlangung des Grades
„Doktor der Naturwissenschaften“ im Promotionsfach Geologie

am Fachbereich Chemie, Pharmazie und Geowissenschaften
der Johannes Gutenberg-Universität Mainz

Irfan Ghani
geb. in Lahore / Pakistan

Mainz, July 2013

Erklärung

Hiermit versichere ich, die vorgelegte Arbeit selbständig und unter Verwendung der angegebenen Quellen und Hilfsmittel zu haben.

Mainz, July 2013

Dekan:

Table of Contents

Table of Contents I
Abstract V
Zusammenfassung VII
Nomenclature IX

1. Introduction 1

1.1 General introduction: 1
1.2 Motivations and objectives: 3
1.3 Existing literature 5
1.3.1 Analogue models 5
1.3.2 Engineered hydraulic fractures 6
1.3.3 Natural hydrofractures 6
1.4 This work 8
1.5 Organization of the thesis 10
1.6 References 11

2. Mechanics of rock fracture 15

2.1 Rock failure modes 15
2.2 Hydrofracture 16
2.2.1 Stress Intensity Factor and Subcritical Crack Growth 16
2.2.2 Pore pressure conditions for vertical hydrofracturing in a poroelastic medium 18
2.3 References 20

3. Theory and Model Workflow 21

3.1 Hydrodynamics – mass conservation and darcy flow 22
3.2 Particle Dynamics – Newton's second law 23
3.3 Implementation – Fluid-Solid Interaction 24

3.4 Brittle Deformation and Physical Features of the Coupled Model 25
3.5 References 26

4. Dynamic Development of Hydrofracture 27

4.1 Introduction: 27
4.2 Formulation 29
4.2.1 Methodology 30
4.2.2 Discrete elastic model 31
4.2.3 2D Pressure diffusion field 32
4.2.4 Two way solid-continuum interaction 34
4.2.5 Deformation mechanics 35
4.2.6 Assumptions 38
4.3 Model verification 39
4.4 Model implementation 41
4.4.1 Point source in a homogeneous porous medium 42
4.4.2 Hydrofracturing in a homogeneous medium under gravity loading 44
4.5 Discussion and conclusion 46
4.6 Appendices 48
4.6.1 Appendix-A: ADI – 2D Pressure Diffusion 48
4.6.2 Appendix-B: Hydrofracture patterns as function of the ratio of external stresses 50
4.6.3 Appendix-B: Hydrofracturing in pure shear stress field 51
4.7 References 51

5. Dynamics of hydrofracturing and permeability evolution in layered reservoirs 55

5.1 Introduction 55
5.2 Fluid association in subsurface rock deformation 58
5.3 Field observation 60
5.4 Numerical model 64
5.4.1 Governing equation of fluid diffusion 64
5.4.2 Discrete model of elastic solid 65
5.4.3 Force pertaining to elasticity 66

5.4.4 Fluid seepage force 66
5.4.5 Gravity loading 67
5.4.6 Implementation 67
5.5 Results 70
5.5.1 Fracturing in single layer confined reservoirs 71
5.5.2 Transition from fracturing to faulting in multilayer systems 76
5.6 Discussion 78
5.7 Conclusion 80
5.8 References 81

6. Summary and concluding remarks 85

6.1 General conclusion 85
6.1.1 Efficiency of the numerical model 85
6.1.2 Interplay between seepage forces and fracture propagation 86
6.1.3 Control of physical properties and stress permutation 87
6.2 Suggestion for further improvements 88
Acknowledgements 89

Abstract

Fluid driven natural hydrofracturing is a prevalent and significant deformation process occurring at all depths of the Earth's crust. It imparts strong bearing on the evolution of effective permeability and fluid transport at a wide range of scales by developing hydraulic connectivity. The process is dynamic and complex, it is dynamic as it involves strong coalescence of brittle deformation and hydraulic evolution with respect to the active hydraulic and tectonic loadings, and the complexity arises from the potential poroelastic response to the pressure field and fracture growth upon volume change. The formation of a hydrofracture is composed of three stages: 1) initiation and nucleation, 2) time dependent quasi-static growth as long as fluid pressure heads the rock's tensile strength, 3) and during propagation its containment or reorientation at layers contacts with contrasting mechanical and sedimentary properties in heterogeneous rocks. In addition, the course of fracture growth is also strongly affected by the background anisotropy i.e., pre-existing micro cracks in natural rocks. Fracture propagation pathways can either be formed by gradually linking up low strength discontinuities ahead of the fracture tip or they can be terminate or abut when the fracture encounters discontinuities of high strength. Such interaction results in fracture networks of complicate geometries, reflecting complex local deformation histories and the dynamics of the driving physical mechanisms.

Natural hydrofracturing has important implications for research and private sectors in various fields of Geoscience. Since the mid twentieth century controlled hydraulic fracturing has been implemented intensively for the permeability stimulation in oil and gas reservoirs. Field observations, isotopic studies, laboratory experiments and numerical analysis reveal the critical role of pore fluid pressure gradients in conjunction with the poroelastic effects as main driving forces to manipulate the local state of stress and the conditions of hydrofracture formation and propagation. Most of the presented numerical hydro-mechanical models account coupling between fracturing fluid and growing fractures by presuming predefined fracture geometry with constant fluid pressure in a homogeneous and isotropic elastic medium for the sake of keeping the problem computationally tractable. However, natural rocks are seldom that simple, hence these models are generally not efficient to analyze this complex process and neglect the real aspect of poroelastic effects and its influence on intimate fluid-solid coupling i.e., pore pressure evolution and failure behavior or vice versa.

In this work, a two-dimensional coupled poro-elasto-plastic model is presented for the qualitative and to some extent quantitative analysis of the role of localized or homogenously developed seepage forces on the dynamic propagation of hydrofractures and the concurrent evolution of effective permeability. The numerical program is computationally efficient and

takes its robustness from the use of a simple Darcy based pressure diffusion equation sans redundant components in the description of the fluid dynamics. This also exhibits Biot's compressibility in the porous rocks and is implemented to address the controlling conditions for the mechanics of hydrofracturing corresponding to pore fluid pressure gradients in specified geological scenarios i.e., mechanically and hydraulically homogeneous and heterogeneous sedimentary sequences. Results reveal that fluid pressure gradients in confined sediments introduce local perturbation in the background stress field. Depending on the boundary conditions it may also promote permutation of principal stress tensors to eventually provoke reorientation of propagating hydrofractures. With effects on the local stress state high pressure gradients may also cause bedding parallel fracturing or slippage in undrain heterogeneous media. An example of particular interest is accretionary wedging, where the highly dynamic nature of tectonic activity together with extreme pore pressure causes intensive local perturbation in stress fields which subsequently result in complex structural evolution including vertical and horizontal hydrofracture networks. Likewise, transport properties of rocks are strongly influenced by the dynamics in the evolution of local permeability by dilation fractures and faulting. It is shown that there may possibly be a strong correlation between the formation of normal faulting and large scale fluid migration.

The consistency between the simulated results with previous experimental and numerical results suggests that the described numerical procedure is worthy of simulating qualitative dynamic aspects of hydrofractures. However, there are some drawbacks in the scheme when attempting to analysis the fluid flow or drainage through the induced fracture planes quantitatively in deformed rocks. In addition, the coupling with thermo-chemical evolution is recommended to extend the presented scheme further in order to study vein growth problems in dynamically developed hydrofractures.

Zusammenfassung

Natürliche hydraulische Bruchbildung ist in allen Bereichen der Erdkruste ein wichtiger und stark verbreiteter Prozess. Sie beeinflusst die effektive Permeabilität und Fluidtransport auf mehreren Größenordnungen, indem sie hydraulische Konnektivität bewirkt. Der Prozess der Bruchbildung ist sowohl sehr dynamisch als auch hoch komplex. Die Dynamik stammt von der starken Wechselwirkung tektonischer und hydraulischer Prozesse, während sich die Komplexität aus der potentiellen Abhängigkeit der poroelastischen Eigenschaften von Fluiddruck und Bruchbildung ergibt. Die Bildung hydraulischer Brüche besteht aus drei Phasen: 1) Nukleation, 2) zeitabhängiges quasi-statisches Wachstum so lange der Fluiddruck die Zugfestigkeit des Gesteins übersteigt, und 3) in heterogenen Gesteinen der Einfluss von Lagen unterschiedlicher mechanischer oder sedimentärer Eigenschaften auf die Bruchausbreitung. Auch die mechanische Heterogenität, die durch präexistierende Brüche und Gesteinsdeformation erzeugt wird, hat großen Einfluß auf den Wachstumsverlauf. Die Richtung der Bruchausbreitung wird entweder durch die Verbindung von Diskontinuitäten mit geringer Zugfestigkeit im Bereich vor der Bruchfront bestimmt, oder die Bruchausbreitung kann enden, wenn der Bruch auf Diskontinuitäten mit hoher Festigkeit trifft. Durch diese Wechselwirkungen entsteht ein Kluftnetzwerk mit komplexer Geometrie, das die lokale Deformationsgeschichte und die Dynamik der unterliegenden physikalischen Prozesse reflektiert.

Natürliche hydraulische Bruchbildung hat wesentliche Implikationen für akademische und kommerzielle Fragestellungen in verschiedenen Feldern der Geowissenschaften. Seit den 50er Jahren wird hydraulisches Fracturing eingesetzt, um die Permeabilität von Gas und Öllagerstätten zu erhöhen. Geländebeobachtungen, Isotopenstudien, Laborexperimente und numerische Analysen bestätigen die entscheidende Rolle des Fluiddruckgefälles in Verbindung mit poroelastischen Effekten für den lokalen Spannungszustand und für die Bedingungen, unter denen sich hydraulische Brüche bilden und ausbreiten. Die meisten numerischen hydromechanischen Modelle nehmen für die Kopplung zwischen Fluid und propagierenden Brüchen vordefinierte Bruchgeometrien mit konstantem Fluiddruck an, um das Problem rechnerisch eingrenzen zu können. Da natürliche Gesteine kaum so einfach strukturiert sind, sind diese Modelle generell nicht sonderlich effektiv in der Analyse dieses komplexen Prozesses. Insbesondere unterschätzen sie die Rückkopplung von poroelastischen Effekten und gekoppelte Fluid-Festgestein Prozesse, d.h. die Entwicklung des Porendrucks in Abhängigkeit vom Gesteinsversagen und umgekehrt.

In dieser Arbeit wird ein zweidimensionales gekoppeltes poro-elasto-plastisches Computer-Model für die qualitative und zum Teil auch quantitativ Analyse der Rolle

lokalisierter oder homogen verteilter Fluiddrücke auf die dynamische Ausbreitung von hydraulischen Brüchen und die zeitgleiche Evolution der effektiven Permeabilität entwickelt. Das Programm ist rechnerisch effizient, indem es die Fluiddynamik mittels einer Druckdiffusions-Gleichung nach Darcy ohne redundante Komponenten beschreibt. Es berücksichtigt auch die Biot-Kompressibilität poröser Gesteine, die implementiert wurde um die Kontrollparameter in der Mechanik hydraulischer Bruchbildung in verschiedenen geologischen Szenarien mit homogenen und heterogenen Sedimentären Abfolgen zu bestimmen. Als Resultat ergibt sich, dass der Fluiddruck-Gradient in geschlossenen Systemen lokal zu Störungen des homogenen Spannungsfeldes führen. Abhängig von den Randbedingungen können sich diese Störungen eine Neuausrichtung der Bruchausbreitung zur Folge haben kann. Durch den Effekt auf den lokalen Spannungszustand können hohe Druckgradienten auch schichtparallele Bruchbildung oder Schlupf in nicht-entwässerten heterogenen Medien erzeugen. Ein Beispiel von besonderer Bedeutung ist die Evolution von Akkretionskeilen, wo die große Dynamik der tektonischen Aktivität zusammen mit extremen Porendrücken lokal starke Störungen des Spannungsfeldes erzeugt, die eine hoch-komplexe strukturelle Entwicklung inklusive vertikaler und horizontaler hydraulischer Bruch-Netzwerke bewirkt. Die Transport-Eigenschaften der Gesteine werden stark durch die Dynamik in der Entwicklung lokaler Permeabilitäten durch Dehnungsbrüche und Störungen bestimmt. Möglicherweise besteht ein enger Zusammenhang zwischen der Bildung von Grabenstrukturen und großmaßstäblicher Fluid-Migration.

Die Konsistenz zwischen den Resultaten der Simulationen und vorhergehender experimenteller Untersuchungen deutet darauf hin, dass das beschriebene numerische Verfahren zur qualitativen Analyse hydraulischer Brüche gut geeignet ist. Das Schema hat auch Nachteile wenn es um die quantitative Analyse des Fluidflusses durch induzierte Bruchflächen in deformierten Gesteinen geht. Es empfiehlt sich zudem, das vorgestellte numerische Schema um die Kopplung mit thermo-chemischen Prozessen zu erweitern, um dynamische Probleme im Zusammenhang mit dem Wachstum von Kluftfüllungen in hydraulischen Brüchen zu untersuchen.

Nomenclature

Intrinsic elastic constant	k_{ij}
Kronecker delta	δ_{ij}
Mode-I Stress intensity factor	K_I
Mode-I driving stress	σ_I
Normal stress	σ_n
Maximum principal compressive stress	σ_1
Minimum principal compressive stress	σ_3
Real scale (dimension)	S
Real scale constant	$s = \frac{2}{3}\frac{E_m}{E_R}\frac{A_m}{A_R}$
Vertical stress (gravity)	σ_v
Horizontal strain	ε_h
Vertical strain	ε_v
Young Modulus	E
Poisson Ratio	υ
Solid mass density	ρ_s
Fluid mass density	ρ_f
Effective stress	$\rho_{eff} = (\rho_s - \rho_f)gz$
Mass of solid particle	m_s
Solid volume fraction	ρ
Particle number density	ρ_n
Porosity	ϕ
Permeability	K
Solid particle velocity	u_s

Fluid velocity	u_{f}
Fluid viscosity	μ
Adiabatic compressibility	β
Ambient fluid Pressure	$P = P_{\circ} + \rho_{\mathrm{f}} gz$
Fluid overpressure/hydraulic head	$P_{\circ}$
Pore pressure	P_p
Fracture filled fluid pressure	P_{f}
Hydrostatic pressure	$\rho_{\mathrm{f}} gz$
Reynold's number	Re
Area weight smoothing function	$s(r - r_{\circ})$
Fluid drag force	f_{p}
Inter-particle contract force	f_{e}
Force of gravity	f_{g}

1. Introduction

This thesis focuses on the dynamic growth of fluid-driven natural fractures, a prevalent and significant process occurring at almost all depths of the Earth's crust. First, a relatively detailed introduction into the process of hydrofracturing in relation to pore fluid overpressure is given in the following section. The main focus of the introduction is to explain mechanisms involving the production of high pore fluid overpressure and their implication on the large-scale physical (micro-macro scale fracturing) and hydraulic properties (permeability evolution) of the Earth's crust. Second, the chapter provides the basic motivations of the work lifted from the applied fields of hydrofractures and the corresponding objectives of the thesis. Onwards, a comparative note on previous studies and research developments is presented. The next section emphasizes the key features of the developed numerical model and its advantage over previous numerical tools. Finally, the last section outlines the structure of this thesis.

1.1 General introduction:

The interaction between crustal fluids and porous rocks provides dynamic mechanisms which alter the fundamental material properties (geophysical, geochemical and hydrologically) of the Earth's crust in geological time frames. The mechanical consequences of fluid-solid interaction correspond to the mechanics of brittle deformation (fracturing and faulting), which has a strong bearing on the effective permeability and fluid transport on a wide range of scales under panoptic conditions of pressure and temperature. Changes in porosity and effective fluid pressure lead to corresponding variations in the physical properties of the rock mass e.g., fracture strength relative to the stress intensity factor, which in turn follows initiation of discrete fractures or quasi-static sub-critical growth of existing cracks. Hydrofracturing thus contributes significantly to the anastomosing development of fracture networks, which is case sensitive to the transient evolution of the overall permeability and in turn influences fluid transport in the crust substantially.

A natural elevation of crustal fluid pressure can be classified into two modes, either localized elevation of pressure or a large-scale elevation. Injection of external fluids e.g., emplacement of piercement structures such as magmatic dykes and sills, mud volcanoes, hydrothermal vent complexes, and veining following a metamorphic devolatilization process reflect a local and abrupt increase in pressure [1]. Local induction of stress and thermal anomalies in sedimentary basins by ascending dykes result in conversion of formation pore water to steam which then acts as a driving fluid in the process zone of the propagating

fracture. Several time dependent geological phenomena result in a homogeneous increase in pore pressure and the subsequent expulsion of interstitial fluids in sedimentary sequences [2] and include: (1) reduction of porosity due to increase of compressive stress during burial, (2) pore fluid expansion mechanisms (clay-mineral diagenesis, kerogen decomposition, aquathermal expansion etc.), and (3) internal fluid production (dehydration of sediments in subduction zones, hydrocarbon generation, production of methane in organic-rich shales etc.).

The build up of fluid pressure gradients due to a spacial variation in pore pressure is one of the main driving forces that manipulate the conditions of hydrofracture formation and propagation in geo-pressured sedimentary rocks [3], where the mechanical failure yields pore pressure diffusion and thus temporal relaxation in the system. A continuous increase in pore pressure in a confined rock volume produces a steep gradient across impermeable barriers which ultimately provokes hydrofracturing and seal failure, where the generated seepage forces couple the pore pressure diffusion with rock deformation. These directional forces introduce perturbation in the local stress field and depending on the boundary tectonic and hydraulic conditions may also promote permutation of principal stress tensors and show strong bearing on the overall failure patterns e.g., transition from vertical to near horizontal fracturing. With effects on local stress state high pressure gradients may also cause bedding parallel fracturing or slippage in an undrain heterogeneous medium, an example of particular interest is accretionary wedging [4] where the highly dynamic nature of tectonic activity together with extreme pore pressure causes intensive local perturbations in stress fields which subsequently result in complex structural evolution including vertical and horizontal hydrofracture networks.

In a more general model, hydrofracturing involves the coupling of at least two sub-processes: 1) the evolution of pore fluid pressure, and 2) the deformation of the host rock as a result of fluid flow within induced fractures. The process is dynamic and complex; it is dynamic as it involves strong coalescence of brittle deformation and hydraulic evolution with respect to the active fluid and tectonic loadings, whereas complexity arises from the potential poroelastic response upon volume change. The poroelastic parameter α through the Poisson ratio υ plays a major role in the evolution of the local stress field by an increase in pore pressure P_{p} [5]. The fluid induces local stress anomalies in the system as an attempt to balance its internal pressure distribution immediately after a deformation event. On other hand, the formation of hydrofractures is composed of three stages: 1) initiation and nucleation, 2) quasi-static growth as long as fluid pressure heads the rock's tensile strength, 3) and during propagation its containment or reorientation at layers contacts with contrasting mechanical and sedimentary properties in heterogeneous rocks. In addition, hydrofracture propagation is also strongly affected by the background discontinuities in natural rocks. Fracture propagation pathways can either be formed by gradually linking up low strength discontinuities ahead of the fracture tips or terminate or abut when met with discontinuities of high strength [6]. This results in fracture networks of complicated geometries, which reflects a complex deformation history and the physical driving-mechanisms.

Transport properties of rocks are strongly influenced by the formation of dilation fractures and faulting since these may have a highly dynamic permeability. Field studies and numerical results show that there may be a strong correlation between tectonically oriented layer perpendicular fracturing and fracturing due to significant fluid pressure gradients across layered anisotropies. Numerical studies show that layered systems that are under lateral extensional stresses experience a transition from layer failure to large scale dilation faulting through the interconnection of isolated tectonic fractures in the competent layers [7], when subject to seepage forces generated by the prevailing fluid pressure gradient [8, 9]. Fracturing in the system seems to take place on the local scale, whereas faulting contributes significantly to system drainage through the formation of large-scale connectivity [10, 11]. Faults in sedimentary basins can be fluid pathways or permeability barriers to fluid flow properties [12, 13]. The enhanced permeability characteristics of fault zones is significantly controlled by changes in the local stress field as a function of fluid overpressure, which directs fault initiation, reactivation or expansion of the fault core and subsequently enhance the permeability of the faulted zone. On the contrary, expansion of fault void space results in a fluid pressure drop and leads to the process of healing and sealing by the mineralization of the fracturing fluid [14-16] and hence limiting the fluid transport.

In this thesis, the development and propagation pathways of hydrofractures that develop due to high pore-fluid pressure gradients and the respective poroelastic effects under different tectonic and sedimentary conditions are investigated in homogeneous (chapter 4) and heterogeneous (chapter 5) sedimentary sequences by using a coupled hydro-mechanical model. Attempts are made to relate and compare our findings with observations from the field and results of previous laboratory and analytical studies.

1.2 Motivations and objectives:

Fluid driven opening mode fracturing is a prevalent and important deformation process in the Earth's crust. Natural examples of hydrofractures appear in various forms including magmatic dykes and sills, many joints and veins, especially those that indicate the crack-seal mechanism. Natural hydrofractures that control the effective permeability and fluid flow appear to have significant implications of practical interest in various fields e.g., oil and gas reservoir assessment (hydrofractures facilitate primary and secondary migration of hydrocarbons from source and reservoirs), geothermal heat production, hydrothermal circulation and the associated ore genesis, in-situ stress measurement, risk assessment corresponding to volcanic and fault reactivation seismicity and in mining, subsurface remediation works and storage of CO_2 and waste disposal as well as long-term isolation of high-level and toxic radioactive waste. Moreover, since the mid of the 19^{th} century engineered techniques of hydraulic fracturing have also been employed widely in the oil and gas industry to enhance reservoir production. Likewise, these techniques have positive

feedbacks to fields of geothermal heat extraction, in-situ stress measurements, and mining for coal degasification.

Owing to many applications, hydrofracturing has been a subject of active research in many fields of Geoscience to elucidate the coupled mechanism of fluid-rock interaction (thermal, chemical and mechanical). This thesis centers on the fluid-solid mechanical dynamic interaction which has a profound impact on the developing geometry of hydrofractures. Being constrained to large-scale time and depth conditions, a direct observation of the natural process of hydrofracturing is hard and often inferred by indirect passive means e.g., monitoring of acoustic waves and fluid flow in geophysical studies during seismic events [17, 18], thin section studies of cored samples of source and cap rocks [19], and near-surface leak-off pressure test studies of petroleum reservoirs [20]. This has led to the necessity of appropriate model studies to get adequate physical insights into the mechanics of this complex phenomenon.

The overall goal of this thesis is to advance our understanding of the apparent role of fluid overpressure in regard to the natural fracturing in rocks. The points taken into consideration are:

1. The role of pressure gradients in initiation and quasi-static propagation of fractures assuming Biot's compressibility, which provides real-time coupling of deformation and fluid flow.
2. The effects of the evolving pressure gradient on the effective stress field and the corresponding failure behavior e.g., in drained and undrained systems.
3. The impact of heterogeneity and anisotropy on the propagation of induced hydrofractures, its interaction with existing and isolated tectonic fractures and the development of dilation faults and the following system drainage in extensional regimes.
4. The interplay of fluid overpressure versus tectonic stresses in the development of fracture networks. In literature the term hydrofracture is somehow obscure. This makes it hard to separate hydro-driven and tectonically driven extension fractures in the field.

These points are investigated with the development and implementation of a numerical model, which exhibits the porosity effective pressure dependence of brittle deformation, the respective changes in permeability and pressure diffusion in poro-elastic rocks. The numerical scheme couples an elasto-plastic DEM model with a fluid continuum grid to represent a saturated porous medium. In the model, the effective stress is directly associated with the evolving permeability where the seepage forces generated by elevated pressure gradients are transmitted to the solid particles following Biot's consolidation effects.

1.3 Existing literature

Owing a broad range of implications, existing literature on hydrofracturing traverses a wide spectrum of approaches, which include field to laboratory scale experimental studies and theoretical and numerical analysis as well.

1.3.1 Analogue models

Several tests of hydrofracturing in rock type cohesive materials are frequently being carried out under controlled hydraulic and stress conditions.

- Using a synthetic salt specimen [21] and [22] demonstrated the stress-controlled orientation of induced hydrofractures and influence of plastic deformation on the permeability respectively. [23] showed the step-wise growth of a hydrofracture at a discontinuity under the developed high pressure gradient in heterogeneous rock specimen, whereas [24] described the direct contribution of the local pore pressure field to the fracture energy for tensile fracturing in porous limestone and sandstone. It is reported that conditions of critical fracturing pressure and fracture orientation are influenced both by differences in the local scale pore pressure in the vicinity of the crack tip and the fluid pressure gradient at large scale.
- Experiments in a two-dimensional Hele-Shaw cell also provide detailed temporal and spatial pattern development corresponding to physical granular-fluid interplay during fracture growth as a function of fluid injection [25-27].
- Moreover, leak-off tests in overpressure sediments provide real-time empirical measurements of the in-situ stress field and the critical pore pressure that is needed to cause hydrofracturing [20, 28, 29]. Results of leak-off tests prescribe the quality control of maximum pressure or mud weight required to maintain safe drilling operations.
- Sandbox experiments are also being conducted generally to investigate the role of fluid pressure on the mechanics of geological phenomena e.g., [30, 31] modeled the formation of layer detachment in thrust wedges due to high fluid pressure beneath relatively impermeable layers, and in conjunction with numerical modeling [32] demonstrated that seepage forces influence the orientation of the principal stresses and thus are case sensitive to tectonic evolution and may cause the formation of listric faulting in sedimentary sequence. It is also shown that the fault dip is dependent on the overpressure gradient.

Laboratory experiments provide physical insight into the hydro-driven rock deformation at moderate scales, however they may lack the impacts of real scaled natural features e.g., gravity and inhomogeneity which find in natural rocks at relatively larger scale. Therefore, analytical and numerical solutions are requisite for a proper understanding of the mechanics of this natural phenomenon.

1.3.2 Engineered hydraulic fractures

Early efforts on the theoretical fundamentals of fluid driven fracture mechanism were laid down in e.g., [33-35] during 1950s and were mostly industry oriented. Mathematical models were proposed for hydraulic fractures of simple geometry (1) penny-shaped radial cracks and (2) wedge-shaped vertical fractures, which were being applied intensively in studies of hydraulically induced fracturing with constant fluid pressure in homogeneous and isotropic elastic continua [36-39], and (3) elliptical vertical fractures of limited height [40, 41]. Later [42-44] introduced models for the three-dimensional analysis of hydraulic fractures. Effects of solid compressibility on hydraulic fracturing in poroelastic media were taken into account in many studies [45-47], who adapted different approaches for the respective fracture criteria and fluid flow in the coupled process. Consult [48] for a detailed review.

In practice of induced hydraulic modeling traditional theory of Linear Elastic Fracture mechanics (i.e., stress singularity criteria at the crack tip), is adapted for fracture growth, whereas the internal fluid flow is modeled by using lubrication theory, which is represented by non-linear partial differential equations and relates the fluid pressure with fracture width and height.

1.3.3 Natural hydrofractures

In geosciences, the active role of pore overpressure in tectonic processes was first evaluated by [49] who made use of Terzaghi's theory of effective stress in analyzing the mechanics of thrust faulting. Later, [50] put forward a classical model based on Hubbert's work for natural joint propagation as a function of fluid pressure to overburden weight ratio. The model provides the link between controlled hydraulic fractures and natural hydrofractures (dykes and join). [5, 51] by using general effective stress law [52] evaluated theoretically Secor's model, and through grain scale force balance criteria described that poroelastic behavior has a major effect on the conditions of critical pore pressure for initiation/propagation of cracks in saturated rocks and on the evolution of the deviatoric stress field under specified boundary conditions.

In general, two different approaches have been followed in the literature for the interpretation of natural hydrofractures: (1) Overpressured fluid is assumed as an external loading to the system of interest, models on this approach have usually been used to analyze the fluid expulsion problems from overpressure containment zones or fluid loss during leak-off tests in sedimentary basins. The system is considered to be in continuum with the prescribed fractures of simple geometry. (2) Inception of Griffith tensile failure in poroelastic media is considered to be caused by internal pore pressure generation and fluid pressure gradients within the rock mass at model scale.

Theoretical analysis of elliptical elastic crack problems (dykes and veins) filled with external fluid of constant pressure in homogeneous system are reviewed by [20, 38, 53, 54]. [55] derived the solution for stress concentration effects of layer contacts between dissimilar half-spaces on the propagating hydrofractures. In contrary [6] formulated the hydrofracture problem with linearly varying fluid overpressure in a vertically growing fracture. [56] derived a solution for local stress perturbations in association with magmatic intrusions with the fluid being confined entirely within the crack, and [57] approximated the formation and pattern development of syntectonic veins by employing both approaches of a stress singularity at the crack tip and an energy balance in an elliptical flaw model. Several boundary element models have been employed by [10, 58, 59] to explore the buoyant driven propagating pathways of vertically growing hydrofractures (dykes) and the effects of mechanical discontinuities on arrest and propagation of hydrofracture.

In addition to elasto-plastic continuum approaches, studies composed of discrete element approaches with internal production of fluid pressure have also been reported in the literature. [60] and [61] both proposed a 1D numerical model for episodic fluid expulsion by compaction induced hydrofracturing in shale rich basins. In the former the permeability is obtained from a parallel plate model with the fracture aperture being pressure dependant, whereas in the later model fracture permeability is pressure independent which retains its developed geometry even after deformation events [62, 63] used a similar approach as [61] to model hydrofracturing by introducing a maximum fracture factor, however pressure build-up as a function of porosity reduction during burial is taken as a function of the effective vertical stress in the former, while in the later it is considered to be a function of depth in sedimentary basin. A review on models for pressure build-up due to mechanical and chemical compaction in sedimentary basins is given in [63]. [64] describe a toggle-switch permeability behavior of natural hydrofractures in geopressured sediments by using a cellular automaton model. More recently, [65] analytically and numerically studied the influence of seepage forces generated by local pore pressure gradients on the behavior of rock failure and proposed five basic failure patterns with specified far field stress states.

In summary, the continuum and discrete coupled fluid-solid modeling approaches though give insights into the physics of fracture mechanics in specific problems, however these models still lack the intimate coupling between the fracturing and interstitial fluid pressure. In particular, continuum approaches ignore filtration of fluid from fracture to rock matrix and vice versa and the corresponding inherent poroelastic potential response of rock deformation to fluid pressure, thus oversimplify the problem. Since the fluid balances its internal pressure distribution immediately after a change in porosity or in volume occurs static models are unable to describe the full dynamics of the system after the initiation of the fracturing. These models are further restricted only to mechanical discontinuities of simple configuration ahead of a propagating hydrofracture and do not take into account the role of hydraulic discontinuities on fluid pressure field and the stress field and their role in the dynamic propagation of tensile fractures. Natural rocks are seldom simple and often exhibit

heterogeneity and anisotropy in terms of layering of contrastive mechanical properties, variation in grain size and mineral content, planes of low strength or they contain pre-existing cracks, into which pressurizing fluid can penetrate and contribute to the stress intensity at the crack tip prior to fracturing. The conventional models also face restrictions regarding prescribed fracture and evolving fluid pathways in specific problems of interest. These hindrances prevent the attempt of appropriate constitutive relationships between representative parameters for real geological systems. Many of the discrete element models are composed of redundant and complicated formulation of hydro-mechanical parameters, which come to be computationally expensive.

Nevertheless, some hybrid numerical tools [3] provide good discrete-continuum constitutive approaches with a focus on real time Biot's poroelastic effects and exhibit the generic effects of fluid diffusion on fracture dynamics. The models demonstrate that fluid over pressure diffuses crucially by the formation and propagation of fractures. By adapting the same approach [66] proposed a coupled discrete element model for the evolution of horizontal sills by pressurized non-viscous magma in a prescribed plane of weaker strength, where the induced structure is generated according to the interaction between fluid pressure in a sill and the overburden weight. In this thesis, a new approach is utilized to acquire the dynamic aspects of hydrofracturing in geopressured sediments with the inspiration from the work of [3]. The employed numerical scheme is partly based on the work of [67] who with the least involvement of hydrodynamic parameters demonstrated the hydro-physics of the problems pertaining to fluidized granular media.

1.4 This work

This study is aimed to replicate the process of hydrofracture dynamics as function of changes in effective permeability and the consequent fracture growth along pressure gradients, where fluid-solid mechanical interaction is of central importance. The constitutive behavior is implemented by a coupled numerical code which is based on the unification of a Lagrangian based two dimensional discrete model of elastic solid giving the mechanical response of the system, with an Eulerian based continuum grid for the evolution of fluid pressure.

The simulations are conducted in the software Latte, which was architected by Koehn [68, 69] and [70, 71] as part of the microstructural modeling environment Elle [72], for the simulation of multi-scale geological processes in deformed rocks e.g., rifting, brittle and viscoelastic fracturing, solid-solid and fluid-solid interaction, and grooves on stressed crystals. The primitive configuration of the Latte model is assembled by coupling a two dimensional lattice of linear elastic springs arranged in triangular network with a particle model in a way that disc-shape particles superpose the nodes of the triangular network. The particle entity describes the discrete nature and time dependant dynamics of the system based

on Newton's second law, whereas the spring network following Hook's law of interaction inherits the micro-mechanical physics through the communication of stress and strain patterns within the system which arise from the translational movement of the discrete particles.

In order to employ hydrodynamics, a special solution of Darcy based Navier Stoke's equation which treats the local mass to momentum conservation is approximated on a separate static square grid. Dimensions of continuum grid are taken to be same but of relevantly larger lattice constant as that of elastic lattice. The lattice-particle model is then blanketed over the continuum grid in physical space, a graphical demonstration of this coupled setup is given in Fig. 4.2. The two respective entities interact with each other with the introduction of an interpolation kernel function, which exploits the local void spaces in the overlying discrete particle model to evaluate the pore pressure evolution on the nodes of continuum grid through the use of the Kozney- Carman relation. The Kozeny-Carman porosity-permeability relationship provides a two-way interplay between permeability evolution and pressure diffusion. The same kernel function is also used for the calculation of seepages forces on the individual discrete solid particles, which leads to the evolution of local effective stress states within the elastic medium. The numerical scheme thus permits the simulation of constitutive dynamic behavior of hydrofracturing with two dimensional fluid flow in the rock matrix by taking into account the pore-scale interaction and kinematics of the pressure field and the solid discrete constituents in a poroelastic medium. The method stems from Biot's theory of poroelasticity while the system is refrained to a linear elastic regime before the onset of fracturing.

A distinctive feature of the presented scheme is that it can deal with both scenarios: a) uniformly overpressure sediments provided that the pores are interconnected and localized overpressure zones develop as well with b) effects of local pressures sources in existing failure planes which tend to equilibrate the abnormal pressure in the immediate vicinity of a fracture. Another advantage is that the scheme incorporates the likely influence of porosity change on hydraulic features of the poroelastic system with respect to explicit changes in particle size in order to depict natural hydraulic heterogeneity and anisotropy in the system.

In this contribution we will use the term hydrofractures only for fractures that are produced actively by high fluid pressure. This scenario is only an extreme end-member case, what really leads to rock failure is seepage forces generated by pressure gradients and the respective poro-elastic response upon fracturing. Fluid will infiltrate the rock and depending on the rock's permeability pressure gradients may vary. The strongest gradients develop when the rock is impermeable and the gradients decay when the rock is more permeable and/or cracks develop. This effect leads to a feedback between the creation of fractures due to high fluid pressure gradients and the increase in permeability due to fracture development. This feedback is complex and does also depend on the fracture geometry and orientation with respect to the pressure source.

1.5 Organization of the thesis

The thesis is organized into three main parts (Chapters 3, 4, 5), which are archived in a consistent order from description of the theory to implementation of the proposed numerical scheme for homogeneous and heterogeneous real geological systems. It should be noticed that chapters (4, 5) are organized to serve as self-contained studies, each containing an abstract, introduction, methodology, simulation examples, discussion and conclusion section.

In the following chapter 2, a relatively brief description of the mechanical and geological concepts pertaining to rock failure at depth in the Earth's crust is given and the corresponding critical conditions of pore fluid pressure to the formation of extension fractures is discussed.

Chapter 3 provides the fundamentals of the numerical scheme which include the constitutive formulation of representative parameters related to hydrodynamics and elasto-plastic deformation. The basic configuration characteristics of the employed coupled model and the two-way hydro-mechanical interaction are explained.

Chapter 4 reports the derivation and verification aspects of the employed scheme as well as its implementation on some basic test cases of geological interest. Shortcomings and assumptions of the numerical scheme are outlined. Different perspectives of effects of high pore pressure gradients versus gravity and external tectonic loadings are discussed. In addition the influence of the background porosity on the dynamic evolution of hydrofractures and in turn the permeability in homogeneous sedimentary environment are discussed. The results are found to be consistent with previous analogue and numerical studies. The work performed in this chapter is published in Journal of Pure and Applied Geophysics.

Chapter 5 represents a further implementation of the numerical scheme to investigate the dynamic development of hydrofractures in heterogeneous media as analogues to geopressured geological problems. Heterogeneity in the system can affect both the mechanical and hydraulic properties of layers. The influence of the increase in pore pressure on the local stress field and the corresponding reorientation of propagating hydrofractures are analyzed according to total stress theory of Engelder 1990. Moreover, a transition of single layer perpendicular fracturing to large scale normal faulting and the associated system drainage is discussed. The results of the different tested cases are compared with relevant field examples from a carbonate sequence in the Oman Mountains. The investigations presented in this chapter will be submitted to the Journal Tectonophysics.

Chapter 6 concludes the thesis with the main findings and summary of the modeled examples. In addition, some possible research directions are suggested for further extension of the scope of the proposed scheme to characterize some more general geological cases e.g., vein growth and mineralization.

1.6 References

1. Jamtveit, B., et al., *Hydrothermal vent complexes associated with sill intrusions in sedimentary basins.* Geological Society, London, Special Publications, 2004. 234(1): p. 233-241.
2. Osborne, M.J. and R.E. Swarbrick, *Mechanisms for generating overpressure in sedimentary basins; a reevaluation.* AAPG Bulletin, 1997. 81(6): p. 1023-1041.
3. Flekkøy, E.G., A. Malthe-Sorenssen, and B. Jamtveit, *Modeling Hydrofracture.* Journal of Geophysical Research-Solid Earth, 2002. 107(B8).
4. Fischer, M.P., et al., *Heterogeneous hydrofracture development and accretionary fault dynamics: Comment and Reply.* Geology, 1994. 22(11): p. 1052-1054.
5. Engelder, T. and A. Lacazette, *Natural hydraulic fracturing*, in *Rock Joints: Proceedings of the international symposium on rock joints*, N.B.a.O. Stephansson, Editor. 1990, A.A. Balkema, Rotterdam: Loen, Norway. p. 35-44.
6. Gudmundsson, A., I. Fjeldskaar, and S.L. Brenner, *Propagation pathways and fluid transport of hydrofractures in jointed and layered rocks in geothermal fields.* Journal of Volcanology and Geothermal Research, 2002. 116(3-4): p. 257-278.
7. Acocella, V., A. Gudmundsson, and R. Funiciello, *Interaction and linkage of extension fractures and normal faults: examples from the rift zone of Iceland.* Journal of Structural Geology, 2000. 22(9): p. 1233-1246.
8. Cappa, F., Y. Guglielmi, and J. Virieux, *Stress and fluid transfer in a fault zone due to overpressures in the seismogenic crust.* Geophysical Research Letters, 2007. 34(5): p. L05301.
9. Sibson, R.H., *Fluid involvement in normal faulting.* Journal of Geodynamics, 2000. 29(3–5): p. 469-499.
10. Gudmundsson, A., *Rock Fractures in Geological Processes*. 2011: Cambridge University Press.
11. Faybishenko, B., P.A. Witherspoon, and S. Benson, *Dynamics of Fluids in Fractured Rock*. Geophys. Monogr. Ser., ed. B. Faybishenko, P.A. Witherspoon, and S.M. Benson. Vol. 122. 2000, Washington, DC: AGU. 400.
12. Antonellini, M. and A. Aydin, *Effect of faulting on fluid flow in porous sandstones; petrophysical properties.* AAPG Bulletin, 1994. 78(3): p. 355-377.
13. Haneberg, W.C., *Faults and Subsurface Fluid Flow in the Shallow Crust*. Geophys. Monogr. Ser., ed. W.C. Haneberg, et al. Vol. 113. 1999, Washington, DC: AGU. 222.
14. Scholz, C.H., *The mechanics of earthquakes and faulting*. 2002: Cambridge University Press.
15. Sheldon, H.A. and A. Ord, *Evolution of porosity, permeability and fluid pressure in dilatant faults post-failure: implications for fluid flow and mineralization.* Geofluids, 2005. 5(4): p. 272-288.
16. Tenthorey, E. and S.F. Cox, *Cohesive strengthening of fault zones during the interseismic period: An experimental study.* Journal of Geophysical Research: Solid Earth, 2006. 111(B9): p. B09202.
17. Zhao, D., et al., *Tomography of the Source Area of the 1995 Kobe Earthquake: Evidence for Fluids at the Hypocenter?* Science, 1996. 274(5294): p. 1891-1894.
18. Husen, S., E. Kissling, and E.R. Flueh, *Local earthquake tomography of shallow subduction in north Chile: A combined onshore and offshore study.* Journal of Geophysical Research: Solid Earth, 2000. 105(B12): p. 28183-28198.
19. Capuano, R.M., *Evidence of fluid flow in microfractures in geopressured shales.* AAPG Bulletin, 1993. 77(8): p. 1303-1314.
20. Valkó, P. and M.J. Economides, *Hydraulic Fracture Mechanics*. 1995: Wiley.
21. Doe, T.W. and G. Boyce, *Orientation of hydraulic fractures in salt under hydrostatic and non-hydrostatic stresses.* International Journal of Rock Mechanics and Mining Sciences & Geomechanics Abstracts, 1989. 26(6): p. 605-611.

22. Peach, C.J. and C.J. Spiers, *Influence of crystal plastic deformation on dilatancy and permeability development in synthetic salt rock.* Tectonophysics, 1996. 256(1–4): p. 101-128.
23. Blair, S.C., et al., *Laboratory observations of the effect of geologic discontinuities on hydrofracture propagation*. 1989, A. A. Balkema, Rotterdam. Permission to Distribute - American Rock Mechanics Association.
24. Bruno, M.S. and F.M. Nakagawa, *Pore pressure influence on tensile fracture propagation in sedimentary rock.* International Journal of Rock Mechanics and Mining Sciences & Geomechanics Abstracts, 1991. 28(4): p. 261-273.
25. Johnsen, et al., *Pattern formation during air injection into granular materials confined in a circular Hele-Shaw cell.* Physical Review E, 2006. 74(1): p. 011301.
26. Lemaire, E., et al., *From viscous fingering to viscoelastic fracturing in colloidal fluids.* Physical Review Letters, 1991. 67(15): p. 2009-2012.
27. Lemaire, E., *Pattern formation in noncohesive and cohesive granular media.* Fractals [Complex Geometry, Patterns, and Scaling in Nature and Society], 1993. 1(4): p. 968.
28. Caillet, G., *The caprock of the Snorre Field, Norway: a possible leakage by hydraulic fracturing.* Marine and Petroleum Geology, 1993. 10(1): p. 42-50.
29. Heum, O.R., *A fluid dynamic classification of hydrocarbon entrapment.* Petroleum Geoscience, 1996. 2(2): p. 145-158.
30. Cobbold, P.R. and L. Castro, *Fluid pressure and effective stress in sandbox models.* Tectonophysics, 1999. 301(1–2): p. 1-19.
31. Cobbold, P.R., S. Durand, and R. Mourgues, *Sandbox modelling of thrust wedges with fluid-assisted detachments.* Tectonophysics, 2001. 334(3–4): p. 245-258.
32. Mourgues, R. and P.R. Cobbold, *Some tectonic consequences of fluid overpressures and seepage forces as demonstrated by sandbox modelling.* Tectonophysics, 2003. 376(1–2): p. 75-97.
33. Cleary, J.M., *Hydraulic Fracture Theory*. Circular (Illinois State Geological Survey). 1958, Urbana: State of Illinois, Dept. of Registration and Education, Division of the State Geological Survey.
34. Harrison, E., W.F.K. Jr., and W.J. McGuire, *The mechanics of fracture induction and extension*. 1954.
35. Hubbert, M.K. and D.G. Willis, *Mechanics of hydraulic fracturing* Petroleum Transactions, AIME, 1957. 210: p. 153-168.
36. Daneshy, A.A., *On the design of vertical hydraulic fractures.* Journal of Petroleum Technology, 1973. 25(1): p. 83-97.
37. Geertsma, J. and F.d. Klerk, *A rapid method of predicting width and extent of hydraulically induced fractures*. 1969.
38. Howard, G.C. and C.R. Fast, *Hydraulic Fracturing*. 1970: Henry L. Doherty Memorial Fund of AIME, Society of Petroleum Engineers of AIME.
39. Khristianovic, S.A. and Y.P. Zheltov. *Formation of vertical fractures by means of highly viscous liquid*. in *In: Proceedings of the 4th World Petroleum Congress*. 1955. Rome: World Petroleum Congress.
40. Nordgren, R.P., *Propagation of a vertical hydraulic fracture.* Society of Petroleum Engineers Journal, 1972. 12(4): p. 306-314.
41. Perkins, T.K. and L.R. Kern, *Widths of Hydraulic Fractures*. 1961.
42. Meyer, B.R., *Design formulae for 2-D and 3-D vertical hydraulic fractures: model comparison and parametric studies*, in *SPE Unconventional Gas Technology Symposium*. 1986, 1986 Copyright 1986 Society of Petroleum Engineers, Inc.: Louisville, Kentucky.
43. Palmer, I.D. and H.B. Carroll Jr., *Three-dimensional hydraulic fracture propagation in the presence of stress variations.* Society of Petroleum Engineers Journal, 1983. 23(6): p. 870-878.

44. Settari, A. and M.P. Cleary, *Development and testing of a pseudo-three-dimensional model of hydraulic fracture geometry.* SPE Production Engineering, 1986. 1(6): p. 449-466.
45. Boone, T.J. and A.R. Ingraffea, *A numerical procedure for simulation of hydraulically-driven fracture propagation in poroelastic media.* International Journal for Numerical and Analytical Methods in Geomechanics, 1990. 14(1): p. 27-47.
46. Detournay, E., A.H.-D. Cheng, and J.D. McLennan, *A poroelastic PKN hydraulic fracture model based on an explicit moving mesh algorithm.* Journal of Energy Resources Technology, 1990. 112(4): p. 224-230.
47. Gordeyev, Y.N., *Growth of a crack produced by hydraulic fracture in a poroelastic medium.* International Journal of Rock Mechanics and Mining Sciences & Geomechanics Abstracts, 1993. 30(3): p. 233-238.
48. Adachi, J., et al., *Computer simulation of hydraulic fractures.* International Journal of Rock Mechanics and Mining Sciences, 2007. 44(5): p. 739-757.
49. Hubbert, M.K. and W.W. Rubey, *Role of fluid pressure in mechanics of overthrust faulting: I. mechanics of fluid-filled porous solids and Its application to overthrust faulting.* Geological Society of America Bulletin, 1959. 70(2): p. 115-166.
50. Secor, D.T., *Role of fluid pressure in jointing.* American Journal of Science, 1965. 263(8): p. 633-646.
51. Fyfe, W.S., N.J. Price, and A.B. Thompson, *Fluids in the Earth's Crust: Their Significance in Metamorphic, Tectonic, and Chemical Transport Processes*. 1978: Elsevier Scientific Pub. Co.
52. Nur, A. and J.D. Byerlee, *An exact effective stress law for elastic deformation of rock with fluids.* Journal of Geophysical Research, 1971. 76(26): p. 6414-6419.
53. Maugis, D., *Contact, Adhesion and Rupture of Elastic Solids*. 2000: Springer.
54. Sneddon, I.N. and M. Lowengrub, *Crack problems in the classical theory of elasticity*. 1969: Wiley.
55. Bonafede, M. and E. Rivalta, *The tensile dislocation problem in a layered elastic medium.* Geophysical Journal International, 1999. 136(2): p. 341-356.
56. Pollard, D.D., *Derivation and evaluation of a mechanical model for sheet intrusions.* Tectonophysics, 1973. 19(3): p. 233-269.
57. Beach, A., *Numerical models of hydraulic fracturing and the interpretation of syntectonic veins.* Journal of Structural Geology, 1980. 2(4): p. 425-438.
58. Dahm, T., *Numerical simulations of the propagation path and the arrest of fluid-filled fractures in the Earth.* Geophysical Journal International, 2000. 141(3): p. 623-638.
59. Maccaferri, F., M. Bonafede, and E. Rivalta, *A numerical model of dyke propagation in layered elastic media.* Geophysical Journal International, 2010. 180(3): p. 1107-1123.
60. Roberts, S.J. and J.A. Nunn, *Episodic fluid expulsion from geopressured sediments.* Marine and Petroleum Geology, 1995. 12(2): p. 195-204.
61. Wang, C.-y. and X. Xinong, *Hydrofracturing and episodic fluid flow in shale-rich basins; a numerical study.* AAPG Bulletin, 1998. 82(10): p. 1857-1869.
62. L'Heureux, I. and A.D. Fowler, *A simple model of flow patterns in overpressured sedimentary basins with heat transport and fracturing.* Journal of Geophysical Research: Solid Earth, 2000. 105(B10): p. 23741-23752.
63. Wangen, M., *Effective Permeability of Hydrofractured Sedimentary Rocks*, in *Norwegian Petroleum Society Special Publications*, G.K. Andreas and H. Robert, Editors. 2002, Elsevier. p. 61-74.
64. Miller, S.A. and A. Nur, *Permeability as a toggle switch in fluid-controlled crustal processes.* Earth and Planetary Science Letters, 2000. 183(1–2): p. 133-146.
65. Rozhko, A.Y., Y.Y. Podladchikov, and F. Renard, *Failure Patterns Caused by Localized Rise in Pore-Fluid Overpressure and Effective Strength of Rocks.* Geophys. Res. Lett., 2007. 34(22): p. L22304.

66. Malthe-Sørenssen, A., et al., *Formation of saucer-shaped sills.* Geological Society, London, Special Publications, 2004. 234(1): p. 215-227.
67. McNamara, S., E.G. Flekkøy, and K.J. Måløy, *Grains and Gas Flow: Molecular Dynamics with Hydrodynamic Interactions.* Physical Review E, 2000. 61(4): p. 4054-4059.
68. Koehn, D., et al., *Instabilities in Stress Corrosion and the Transition to Brittle Failure.* American Journal of Science, 2003. 303(10): p. 956-971.
69. Koehn, D., J. Arnold, and C.W. Passchier, *Fracture and Vein Patterns as Indicators of Deformation History: A Numerical Study.* Geological Society, London, Special Publications, 2005. 243(1): p. 11-24.
70. Sachau, T., *Computer simulations of microstructures related to the olivine-spinal transition*, in *Instute of Geoscience*. 2008, Johannes Gutenberg-Universität Mainz: Mainz.
71. Sachau, T. and D. Koehn, *Faulting of the lithosphere during extension and related rift-flank uplift: a numerical study.* International Journal of Earth Sciences, 2010. 99(7): p. 1619-1632.
72. Jessell, M., et al., *Elle: the numerical simulation of metamorphic and deformation microstructures.* Computers & Geosciences, 2001. 27(1): p. 17-30.

2. Mechanics of rock fracture

Natural rocks contain a large number of randomly oriented micro flaws (grain-boundaries or discontinuities of low strength) which behave as likely planes of potential failure. These flaws are usually modeled as cracks in rock mechanics. The growth and linkage of these cracks turn up into mesoscale fractures when remote stresses on the rocks meet the ultimate toughness of the cracks.

2.1 Rock failure modes

There are three end-member fracture modes in naturally deformed rocks, based on the relative displacement orientation to the plane of the initial crack [1].

- Mode-I or opening mode representing a pure tensile failure, in which the crack wall displacements are normal to the plane of the crack.
- Mode-II is in-plane shear or sliding mode, in which the crack surfaces slide on one another and the displacements are parallel to the plane of the crack but normal to the leading edge.
- Mode-III is the out-of-plane shear or tearing mode failure, in which the crack walls move relative to one another but perpendicular to the propagation direction of the crack.

In geology, mode-II and mode-III fractures are general classified as shear fractures, while mode-I is termed an extensional fracture. Fractures that display both extensive and shear modes are termed as hybrid or transitional fractures [2, 3].

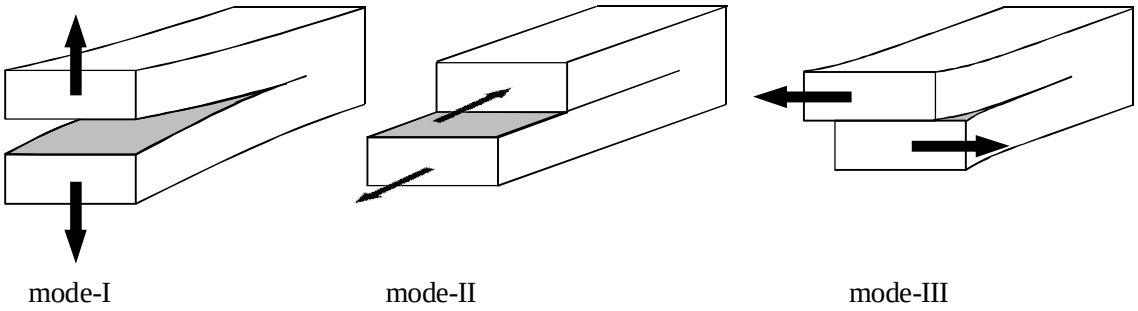

Figure 2.1 Typical modes of rock failure (left) model-I extension fracture, (centre) mode-II in plane shearing, and (right) mode-III out of plane tearing.

Many natural joints and veins are typically a result of mode-I or hybrid mode I-II or I-III, which hold a low sheared displacement followed by hydro-driven extensional fracturing. Mode-I failure leads to straight propagation paths. The hybrid mode fractures reflect the local reorientation of stresses in response to local shearing tractions and impart distinct surface morphologies. Hybrid mode I-II failure results in tilting or curving propagation paths [4], as the growing crack tip curls uniformly about an axis in the crack plane but normal to the propagation plane. In contrast, a combined mode I-III failure will cause the crack plane to twist as the crack is segmented by rotation about an axis in the crack plane but parallel to the direction of formation [5].

The surface morphology of joints records a rupture event including nucleation, propagation and arrest. Joints fracture in the form of crack-seal veins, joint zones, or intermittent growth of a single joint. Whereas, the process of shear fracturing is reflected in braded shear fractures, extensional shear fractures, en echelon cracks and pinnate joints next to the shear fracture [6].

2.2 Hydrofracture

Hydrofractures are opening mode fractures which are generated either solely by elevated fluid pressure or by a combination of both fluid overpressure and tectonic loadings, where the fluids can be of any crustal origin such as intrusive magma, oil, gas, geothermal water, hydrothermal water or supernormal formation pore pressure. Hydrofractures initiate when the internal fluid pressure in the initial cracks or formation pore pressure (in excess of the minimum principal compressive stress) transects the fracture strength of the rock.

2.2.1 Stress Intensity Factor and Subcritical Crack Growth

Having roots in Griffith theory of energy balance, linear elastic fracture mechanics is an approach that provides an effective framework for the solution to general problems of fracture propagation. It consists of stress intensity analysis around a crack in a linear elastic medium and formulates the fracture critera based on certain critical parameters i.e., loading, fracture geometry and material properties [7] which characterize the stress and strain intensity near the crack tip. The stress intensity factor K_{i} (where i is the respective failure mode) is a measure of the stress singularity at the crack tip that gives the real forces on the crack tip needed to drive its propagation.

On the micro-scale an ideal crack is generally considered to be penny-shaped (planar) opening with its long dimensions less than or equal to the diameter of individual grains within the host rock. The internal fluid overpressure P_o necessary to initiate crack extension is referred to as effective pressure and defined as

$$P_o = P_f - \sigma_n \tag{2.1}$$

where P_f is the total fluid pressure acting inside the crack and σ_n is the normal stress acting perpendicular to the crack plane (compression assumed positive). It has generally been perceived that for hydrofracture propagation such as in case of igneous dyke intrusions in saturated sedimentary basins $P_f > P_p$ is a prerequisite, where P_p is hydrostatic pore fluid pressure. However, [8] suggested that mechanism of natural hydrofracturing may also operate at $P_f = P_p$ provided that over a long period of time formation pressures build up uniformly in the interconnected pores and in the inherited micro cracks.

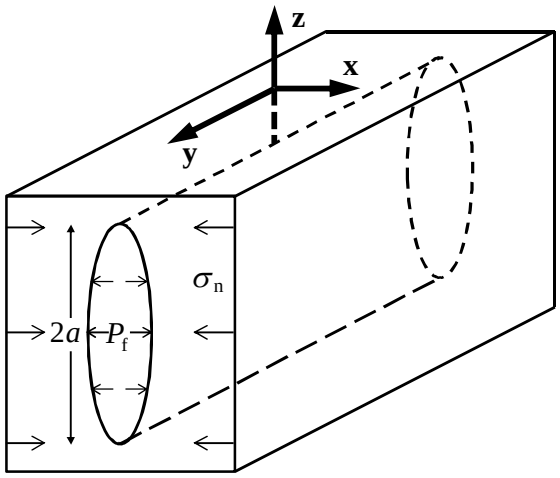

Figure 2.2 Delineation of a plane strain elliptical fracture with orientation relative to local coordinates. Driving stress σ_I for mode-I fracture opening and growth is a function of the internal fluid pressure and the stress normal to the fracture plane. (after [9])

The magnitude of the mode-I stress intensity factor for an isolated, uniformly loaded, vertical fluid filled crack under two-dimensional (2D) plane strain conditions can be written as [10]

$$K_I = \sigma_I \sqrt{\pi a} \tag{2.2}$$

where $\sigma_I = P_o$ is mode-I driving stress and a is the half length of the discrete crack in the plane of analysis (x-z plane, Fig. 2.2).

Hydrofractures are extension fractures i.e., they typically propagate in a direction perpendicular to the least compressive principal stress σ_3, and if the propagation is considered to be vertical it implies that $\sigma_n = \sigma_3 = \sigma_h$ in equation (2.1).

Crack propagation can be categorized as critical or subcritical crack growth based on the relative magnitude of the stress intensity factor K_I and fracture toughness K_{IC}. In contrast to critical propagation of tensile fractures under tectonic loading in dry rocks, hydrofracture propagation is assumed to be subcritical with a stress intensity factor that is lower than the fracture toughness $K_I < K_{IC}$. The internal fluid pressure through the law of effective stress reduces the fracture strength of the rock material and leads to relatively smaller threshold values of the stress intensity factor (termed K_{IC}^*) which is required for the subcritical quasi-static fracture propagation [9].

Subcritical fracture growth [11-13] is proposed to be the likely mechanism for the development of many joint and vein networks. It is followed that fractures propagate under the condition of subcritical growth when a threshold value of the stress intensity factor is reached or exceeded leading to the stress intensity factor in equation (2.2) as $K_I = K_{IC}^*$. On rearranging, the mode-I driving stress required to initiate the propagation of an isolated fracture is

$$\sigma_{\mathrm{I}} = \frac{K_{IC}^*}{\sqrt{\pi a}} \tag{2.3}$$

2.2.2 Pore pressure conditions for vertical hydrofracturing in a poroelastic medium

In the presence of triaxial compressive state of stress with depths in the brittle Earth's crust, the condition $P_p > \sigma_h$ must be true for the initiation of vertically oriented hydro-driven opening-mode joints and veins in the buried rocks. For a simple case of fluid-saturated (ignoring any thermal and chemical effect), porous elastic medium under plane strain conditions the total horizontal stress can be given as a function of gravity loading and pore pressure P_p [8]

$$\sigma_{\mathrm{h}} = \left(\frac{\upsilon}{1-\upsilon}\right)\sigma_{\mathrm{v}} + \left(\frac{1-2\upsilon}{1-\upsilon}\right)\alpha P_{\mathrm{p}} \tag{2.4}$$

where σ_{v} is the total vertical stress, υ is Poisson's ratio under drained condition, and α the Biot's poroelastic constant of effective stress which is <1 for more lithified rocks. When

equation 2.4 is combined with the fracture mechanics equation it produces a relationship between the pore pressure required to generate opening mode fractures and the overburden loading.

By combining equations (2.1) and (2.3), and setting $\sigma_n = \sigma_h$, $P_f = P_p$ one can find the pore pressure required for the propagation of vertical fractures

$$P_p = \sigma_h + \frac{K_{IC}^*}{\sqrt{\pi a}} \tag{2.5}$$

Substituting σ_h from equation (2.4) and solving for pore pressure gives a poroelastic based LEFM expression for the conditions of opening-mode vertical fracture growth

$$P_p = \frac{1-\upsilon}{(1-\upsilon)-(1-2\upsilon)\alpha}\left[\frac{\upsilon}{1-\upsilon}\sigma_v + \frac{K_{IC}^*}{\sqrt{\pi a}}\right] \tag{2.6}$$

Normalizing both sides of the equation (2.6) by the vertical stress σ_v, gives the pore-fluid factor λ_v as a ratio of pore pressure to vertical stress for fracture propagation

$$\lambda_v = \frac{P_p}{\sigma_V} = \frac{\upsilon}{(1-\upsilon)-(1-2\upsilon)\alpha} + \frac{1}{\alpha}\cdot\frac{\upsilon}{(1-\upsilon)-(1-2\upsilon)\alpha}\cdot\frac{K_{IC}^*}{\sqrt{\pi a}} \tag{2.7}$$

With the approximation that the subcritical stress-intensity threshold term in equation (2.7) is smaller than the vertical stress and thus of secondary interest a simpler expression emerges for estimating the order of magnitude of pore pressure required for opening-mode fracturing in saturated poroelastic medium as

$$\lambda_v = \frac{P_p}{\sigma_V} \cong \frac{\upsilon}{(1-\upsilon)-(1-2\upsilon)\alpha} \tag{2.8}$$

It is apparent from equation (2.8) that λ_v becomes independent of the Poisson's ratio and will always be 1 for $\alpha = 1$. Depending on the poroelastic factor α (0 – 1 for most rocks) and the Poisson ratio υ of the underlying rock, pore pressures required for hydraulic extensional fracturing is termed as hydrostatic if ($\lambda_v < 0.4$) occurs in near surface extensional regime, superhydrostatic ($0.4 < \lambda_v < 1.0$) in low permeable and well cemented rocks and superlithostatic pressure when ($\lambda_v \geq 1.0$) usually encounter in compressional

regimes at greater depths [14]. It is conceived that the better the cement and the lower the porosity in the rock, the lower its poroelastic constant is expected to be.

2.3 References

1. Pollard, D. and S. D., *Theoretical displacements and stresses near fractures in rocks: with application to faults, joints, veins, dikes and solution surfaces.*, in *Fracture Mechanics of Rocks*. 1987, Academic Press, London. p. 277-349.
2. Engelder, T., *Transitional–tensile fracture propagation: a status report.* Journal of Structural Geology, 1999. 21(8-9): p. 1049-1055.
3. Ramsey, J.M. and F.M. Chester, *Hybrid fracture and the transition from extension fracture to shear fracture.* Nature, 2004. 428(6978): p. 63-66.
4. Olson, J. and D.D. Pollard, *Inferring paleostresses from natural fracture patterns: A new method.* Geology, 1989. 17(4): p. 345-348.
5. Pollard, D.D., P. Segall, and P.T. Delaney, *Formation and interpretation of dilatant echelon cracks.* Geological Society of America Bulletin, 1982. 93(12): p. 1291-1303.
6. Atkinson, B.K., *Fracture mechanics of rock*. 1987: Academic Press.
7. Lawn, B., *Fracture of Brittle Solids*. 1993: Cambridge University Press.
8. Engelder, T. and A. Lacazette, *Natural hydraulic fracturing*, in *Rock Joints: Proceedings of the international symposium on rock joints*, N.B.a.O. Stephansson, Editor. 1990, A.A. Balkema, Rotterdam: Loen, Norway. p. 35-44.
9. Olson, J.E., S.E. Laubach, and R.H. Lander, *Natural Fracture Characterization in Tight Gas Sandstones: Integrating Mechanics and Diagenesis.* AAPG Bulletin, 2009. 93(11): p. 1535-1549.
10. Flekkøy, E.G., A. Malthe-Sorenssen, and B. Jamtveit, *Modeling Hydrofracture.* Journal of Geophysical Research-Solid Earth, 2002. 107(B8).
11. Atkinson, B.K., *Subcritical crack growth in geological materials.* Journal of Geophysical Research: Solid Earth, 1984. 89(B6): p. 4077-4114.
12. Segall, P., *Formation and growth of extensional fracture sets.* Geological Society of America Bulletin, 1984. 95(4): p. 454-462.
13. Olson, J.E., *Joint pattern development: Effects of subcritical crack growth and mechanical crack interaction.* Journal of Geophysical Research: Solid Earth, 1993. 98(B7): p. 12251-12265.
14. Sibson, R.H. and J. Scott, *Stress/fault controls on the containment and release of overpressured fluids: Examples from gold-quartz vein systems in Juneau, Alaska; Victoria, Australia and Otago, New Zealand.* Ore Geology Reviews, 1998. 13(1-5): p. 293-306.

3. Theory and Model Workflow

The basics of the numerical scheme used in this study deal with irreversible poro-elasto-plastic deformation problems in a coupled two-phase system consistent of a granular rock matrix with a fluid filled complementary pore network. The general setup of the model is a square box, which imparts the pertinent features of both the constituents by employing a discrete poroelastic description of the granular solid and a continuum description of the hydrodynamic part.

The solid phase is acquired by a two dimensional deformable material representation, which assembles a coupled setup of a lattice model (triangular interconnection of normal elastic springs) with a discrete element network (disc-shaped particle model), based on the work of [1] and implemented by [2]. This coupled system thus exhibits both the linear elastic behavior in terms of full description of the stress and strain fields and the discrete description of the material properties (mechanical dynamics) due to particle movements.

The hydrodynamic part is taken from the work of [3, 4] and later extended by [5-7], which was originally formulated for loosely packed fluid filled granular material problems with the consideration of both compressible and incompressible fluid pressure evolution in response to matrix deformation. The same approach has been adopted by [8] for analyzing granular Rayleigh-Taylor instabilites. The solid phase is interacting with the Continuum fluid through the granular velocity u_s and the local permeability K, where the fluid flow is evaluated in terms of fluid pressure $P(x, y)$ for the particle setup by using conservation of mass and Darcy's law. The non-hydrostatic part of the pressure field i.e., pressure gradient contributes to the net force on a unit volume element dV, which according to Newton's second law of motion is equilibrated by the coincident displacement of the particle and the pore fluid in this element.

The particle position $r(x, y)$ and velocity u_s in the elasto-plastic network are used to be the state variables for discretisation of the local solid fraction ρ and pressure gradient on a continuum square lattice that has grid constants twice as large than the particle diameter. Seepage forces generated by pressure gradients tend to displace the particles and contribute to the evolution of local stress and strain fields in the elastic lattice, of which the equilibrium configuration is then found using a successive over relaxation algorithm [9].

3.1 Hydrodynamics – mass conservation and darcy flow

With the application of the Darcy law for fluid flow in a porous media and the continuity equation assuming mass conservation of fluid and solid a macroscopic pressure diffusion equation for the continuum phase is derived. To get a fully consistent natural picture the fluid adiabatic compressibility is fused into the continuity equation by approximating fluid mass density as proportional to the pressure that ends up to a diffusion equation

$$\phi\left[\partial_{\mathrm{t}} P + u_{\mathrm{s}} \cdot \nabla P\right] = \nabla \cdot \left[\bar{P} \frac{K}{\mu} \nabla P \right] - \bar{P} \nabla \cdot u_{\mathrm{s}} \tag{3.1}$$

where ϕ is the porosity, u_{s} the particle velocity, K the local permeability and μ the viscosity of the fluid. $\bar{P} = P + 1/\beta$, where $\beta = 1/K_{\mathrm{T}}$ stands for fluid compressibility and K_{T} is the bulk modulus of the fluid. The fluid pressure $P = P_{\circ} + \rho_{\mathrm{f}} g z$, corresponds to non-hydrostatic pressure $P_{\circ}$, ρ_{f} the fluid density, g the gravitational constant and z the depth.

Left hand side of equation (3.1) displays the evolution dependence of the local fluid pressure field on the velocity of the particles according to $u_{\mathrm{s}} \cdot \nabla P$. The first term in the right side accounts for the Darcy diffusion of the fluid pressure relative to particles whereas the second term is distinguished as source term. The source term facilitates a pressure change as a function of a change in the particle solid fraction if particles move apart in the local reference scale of Darcy flow. The displaced particle volume is replaced by the volume of the fluid. The equation leads to a two-way interaction of the fluid and solid, where for each displaced particle it provides an evaluation of the changes in local porosity and pressure as well as simultaneously evaluates the positions and the velocity of the displaced particles for each continuum grid node.

The permeability K is considered to be an explicit local outcome of particle displacement and is calculated by the Kozney-Carman porosity-permeability relation

$$K = \frac{d^2 (1-\rho)^3}{180 \rho^2} \tag{3.2}$$

where d is the particle radius and $\rho = 1 - \phi$ the local solid fraction. For an incompressible fluid $\beta = 0$ the equation (3.1) becomes Poisson in nature, which simply states the mass balance between the solid and fluid phases as

$$\nabla \cdot \left(\frac{K}{\mu} \nabla P \right) - \nabla \cdot u_{\mathrm{s}} = 0 \tag{3.3}$$

3.2 Particle Dynamics – Newton's second law

If we consider a unit element of volume dV as a composite of particle and fluid masses, the total force it bears both from particle and fluid dynamics is equal to the total stresses integrated over its surface dA as shown in Fig. 3.1.

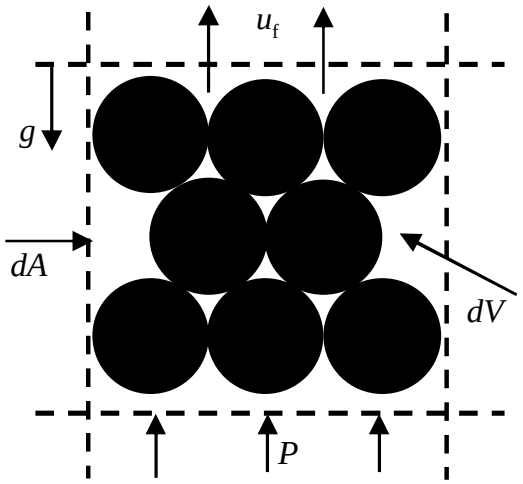

Figure 3.1 Active surface stress and pressure on a unit volume dV .

$$\rho_{\mathrm{s}}(1-\phi)V\frac{du_{\mathrm{s}}}{dt} + \rho_{\mathrm{f}}\phi V\frac{du_{\mathrm{f}}}{dt} = \sum F_I - \int \nabla P\, dA + \rho_{\mathrm{s}}(1-\phi)Vg + \rho_{\mathrm{f}}\phi Vg \tag{3.4}$$

where $\rho_{\mathrm{s}}(1-\phi)V$ and $\rho_{\mathrm{f}}\phi V$ are the respective total masses of particle and fluid in the unit volume. F_{I} is the inter-particle interaction force (elastic) and the second term on the right hand side gives normal pressure forces on the surface of the volume element. After some simplification we get

$$\rho_{\mathrm{s}}(1-\phi)V\frac{du_{\mathrm{s}}}{dt} + \rho_{\mathrm{f}}\phi V\frac{du_{\mathrm{f}}}{dt} = \sum F_I - \int_{\mathrm{v}} \nabla P\, dV + \rho_{\mathrm{eff}}(1-\phi)Vg \tag{3.5}$$

where $\rho_{\mathrm{eff}} = \rho_{\mathrm{s}} - \rho_{\mathrm{f}}$ is effective mass density. If the fluid mass density is assumed to be comparatively lower than the mass density of the particles, this leads to the simplification form of the equation by dismissing the second term on the right hand side. However, for the

approximation of fluid inertia close to the mass density of the solid particle the force balance equation will result in

$$\left[\rho_s(1-\phi)+\rho_f\phi\right]\frac{du_s}{dt}V=\sum F_I-\nabla P\cdot V+\rho_{\text{eff}}(1-\phi)Vg \tag{3.6}$$

Considering cylinder particles of mass $m_s=\rho_s V_s$, volume $V_s=\pi r^2 h$ with $h=1$ (unit third dimension) and base area $A_s=\pi r^2$ and particle number density $\rho_n=(1-\phi)/V_s$, the force balance equation for each single particle is derived as

$$\left[m_s+\frac{\rho_f\phi}{\rho_n}\right]\frac{du_s}{dt}=\sum F_I-\frac{\nabla P}{\rho_n}+\rho_{\text{eff}}V_s g\ . \tag{3.7}$$

This is the translational equation of each individual particle dragged with velocity u_s in the absence of any frictional and tangential effects. The mass m_s in the term on the left hand side accounts for the summation of fluid mass to each individual solid particle as a function of the local porosity to particle number density ratio. This accounts for the particle mass as being fluid coated and thus incorporates the fluid inertia into the model.

3.3 Implementation – Fluid-Solid Interaction

On the square grid of the continuum phase, the generalized diffusion equation is solved for the case of a compressible fluid with the Alternative Direction Implicit scheme. The size ($\Delta x, \Delta y$) of the grid unit cell is taken to be twice as large as the lattice constant of the triangular elastic lattice or the average particle diameter. An area weight smoothing function is employed for the estimation of the local solid fraction ρ and the velocity u_s of the particles according to their positions corresponding to the four nearest nodes of the continuum grid. The weight function is defined as

$$s(r-r_o)=\begin{cases}\left(1-\dfrac{w_1}{\Delta x}\right)\left(1-\dfrac{w_2}{\Delta y}\right) & \text{if } w_1<\Delta x,\ w_2<\Delta y\\ 0 & \text{otherwise}\end{cases} \tag{3.8}$$

where $w_1=|x-x_\circ|$ and $w_2=|y-y_\circ|$. The function assigns the proportional ($s(r-r_\circ)$ times) average area of a particle at position $r(x,y)$ to the grid node at position $r_\circ(x_\circ,y_\circ)$ and exhibits a proportionally higher contribution the closer the particle gets to the respective node position. A graphical demonstration of the weight area contribution is given in (Fig. 4.3,

5.4c). The same weight function is used for the calculation of pressure forces at individual particles from the nearest four grid nodes.

For each displaced particle the function provides an evaluation of the changes in local porosity and pressure as well as simultaneously evaluates the positions and the velocities of the displaced particles for each continuum grid node. In order to acquire a fully 3D consistency of a closely packed fluid filled granular material (a prerequisite for 3D Kozney-Carman permeability) in the experiments, a fraction 3/2 of the calculated 2D solid fraction is used in the simulations. The factor 3/2 is the solid fraction ration between a randomly packed packing of solid cylinders to the randomly packed solid spheres. Likewise, a lower minimum threshold value of the solid fraction $\rho_{\min} = 0.15$ is set in equation (3.2), since the Kozney-Carman porosity permeability relation is not valid below this solid fraction.

3.4 Brittle Deformation and Physical Features of the Coupled Model

As derived in equation (3.7), the particle dynamics follows Newton's second law of motion in the hybrid fluid-solid model. The general work flow of the hybrid model is as follows: Using the ADI scheme pressure gradient evolves in the model. The discrete particles which act as a substrate over the elastic lattice tend to move on the application of the seepage forces which are being generated by the non-hydrostatic part of the evolved pressure field. This consequently derives the local perturbation of the effective stress and strain field in the solid. This movement also causes local changes in the pore size and accordingly the fluid pore pressure. The equilibrium configuration of the two dimensional triangular elastic lattice is then obtained by using a successive over relation algorithm [9]. If any elastic spring exceeds its breaking threshold, the spring breaks depicting discrete tensile fracturing and a new equilibrium configuration is arrived for the solid forces. Once the system is fully relaxed new values of the discrete solid fraction for the evolved pressure field are calculated and the process is echoed until both the fluid and the solid elastic field arrive at a full equilibrium state.

The coupled model also works well for simulations of tectonically deformed poro-elastic materials with the likely influence of pore fluid overpressure on the behavior of rock failure. The model can exhibit a number of failure routines as a result of external strains imposed on initially undeformed material either individually or in a combination of the following ways: (1) uniaxial/biaxial compression in the x- and y- directions (2) simple shear along the x-axis or (3) lateral dilation. Through this setting all major types of deformation can be achieved. Depending on the required deformation type only the upper and the right boundary walls of the elastic lattice are moveable at constant rate with the fixed left and the lower boundary walls. The deformation mechanism is performed in such a way that the total area of the model remains constant throughout the experimental run, provided the basics that the applied strains on the moveable boundaries do not affect the relaxation process.

Two different boundary conditions are taken for the elastic-particle solid lattice and the continuum grid. The elastic solid has fixed boundary coordinates that are set by moveable lattice boundaries which are subjected to an externally applied strain. In the case of applied gravity the upper boundary is free. A weight corresponding to the density of overlying sediments and their height is applied to the upper boundary and particles within the box are given an additional body force to account for differential gravitational forces within the simulation box The fluid has Dirichlet or Neumann boundary condition representing undrained and drained fluid conditions. In addition, wrapping boundaries can also be employed on lateral walls in the elastic lattice in order to diminish boundary effects that usually affect the problems of simple shear.

The simulated material may be either a homogeneous or heterogeneous system. Heterogeneity in the model can be introduced both in the elastic lattice and in the continuum pressure field through a Gauss normal distribution on the mechanical properties of the spring networks and hydraulic particle sizes in order to simulate inherent disorder. Introduction of hydraulic particle size distribution provides an epoxy to inherent porosity and permeability heterogeneity in the continuum pressure field. Anisotropy can be distributed with the induction of layered segments of different Young's modulus related to real materials taken in the model, where the Young's modulus is related to internally derived stress tensors by a scaling factor to determine the real stresses.

3.5 References

1. Malthe-Sørenssen, A., et al., *Simulation of Extensional Clay Fractures.* Physical Review E, 1998b. 58(5): p. 5548-5564.
2. Koehn, D., et al., *Instabilities in Stress Corrosion and the Transition to Brittle Failure.* American Journal of Science, 2003. 303(10): p. 956-971.
3. McNamara, S., E.G. Flekkøy, and K.J. Måløy, *Grains and Gas Flow: Molecular Dynamics with Hydrodynamic Interactions.* Physical Review E, 2000. 61(4): p. 4054-4059.
4. Anghel, D.-V., et al., *Erratum: Grains and gas flow: Molecular dynamics with hydrodynamic interactions [phys. rev. e [bold 61], 4054 (2000)].* Physical Review E (Statistical, Nonlinear, and Soft Matter Physics), 2006. 74(2).
5. Goren, L., et al., *Pore Pressure Evolution in Deforming Granular Material: A General Formulation and the Infinitely Stiff Approximation.* J. Geophys. Res., 2010. 115(B9): p. B09216.
6. Johnsen, et al., *Pattern formation during air injection into granular materials confined in a circular Hele-Shaw cell.* Physical Review E, 2006. 74(1): p. 011301.
7. Vinningland, J.L., et al., *Experiments and simulations of a gravitational granular flow instability.* Physical Review E, 2007a. 76(5): p. 051306.
8. Niebling, M., *Sedimentation instability : A numerical and experimental study*, in *Department of Physics*. 2009, University of Oslo, Norway.
9. Allen, D.N.G., *Relaxation methods*. 1954: McGraw-Hill.

4. Dynamic Development of Hydrofracture

Abstract:

Many natural examples of complex joint and vein networks in layered sedimentary rocks are hydro-fractures that form by a combination of pore fluid overpressure and tectonic stresses. In this paper, a two-dimensional hybrid hydro-mechanical formulation is proposed to model the dynamic development of natural hydrofractures. The numerical scheme combines a Discrete Element Model (DEM) framework that represents a porous solid medium with a supplementary Darcy based pore-pressure diffusion as continuum description for the fluid. This combination yields a porosity controlled coupling between an evolving fracture network and the associated hydraulic field. The model is tested on some basic cases of hydro-driven fracturing commonly found in nature i.e., fracturing due to local fluid overpressure in rocks subjected to hydrostatic and nonhydrostatic tectonic loadings. In our models we find that seepage forces created by hydraulic pressure gradients together with poroelastic feedback upon discrete fracturing play a significant role in subsurface rock deformation. These forces manipulate the growth and geometry of hydrofractures in addition to tectonic stresses and the mechanical properties of the porous rocks. Our results show characteristic failure patterns that reflect different tectonic and lithological conditions and are qualitatively consistent with existing analogue and numerical studies as well as field observations. The applied scheme is numerically efficient, can be applied at various scales and is computational cost effective with the least involvement of sophisticated mathematical computation of hydrodynamic flow between the solid grains.

4.1 Introduction:

Brittle deformation of rocks in association with over pressured fluid plays an important role in the geophysical, geochemical and structural mechanics of the Earth's crust in a wide variety of geological settings [1]. A number of fluid expansion mechanisms e.g., burial compaction, clay dehydration, organic matter decomposition and aquathermal expansion as well as impermeable rock units which behave as barrier to subterraneous fluid flow render the pore fluid overpressure, which if in excess of the least principal stress ($P_f > \sigma_3$) may lead to load parallel or load oblique tension fracturing (Fig. 4.1) in depths of the Earth's crust.

The mechanism of hydrofracturing has great implications in the interpretation of field observations and for the prediction of natural or industrial problems in a broad range of research disciplines. After pioneering work of [2, 3] which explored pore fluid pressure as an important factor for small scale hydrofracturing in tectonic processes, significant efforts have been made in the development of theoretical fundamentals [4-8]. Apart from theoretical aspects, a significant amount of analytical and numerical solutions have also been put forward by many investigators to address this coupled process in a qualitative and quantitative manner [9-14].

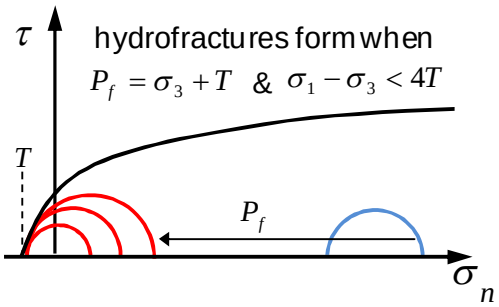

Figure 4.1 Mohr diagram of tensile failure due to fluid overpressure. The blue Mohr circle represents the initial state of stress. The Mohr circle moves towards the left hand side (red circles) as a function of increase in fluid pressure, which results n extension or hybrid extension-shear failure.

Most of the previous numerical tools are built on continuum approaches and consider fluid flow in fractures of simple geometry (penny-shaped elliptical or vertical cracks) using the theory of linear elasticity. Much of these approaches however, lack the constitutive relationship of explicit coupling between the solid and fluid being considered separately and makes strong approximations upon complex flow and deformation interaction arising from brittle failure, material disorder and inhomogeneity present at various scales in geo-pressurized problems. Some porosity controlled models [10, 15-18] revealed that the potential response of inherent poroelastic mechanics is an important parameter in hydro-driven rock failure, where the seepage forces caused by pore pressure gradients [19-21] in porous rocks affect the driving stress for fracture initiation and growth. Regardless of the underlying driving agent hydrofracturing is a complex process which incorporates the dynamic coupling of at least three sub-processes [22]; 1) Restructuring of rock skeleton upon elastic/in-elastic strain. 2) Corresponding alteration of both the permeability and the interstitial fluid pressure. 3) Further mechanical deformation leading to fracture propagation with concurrent variation in the pore or fracture filled fluid pressure.

Inspired by [10] we extended the work of [23] to a hybrid discrete-continuum constitutive modeling approach. The scheme emphasizes the evolution of rock failure in light of the underlying synergistic evolution of rock permeability upon fracture growth and the consequent change in interstitial pore pressure. The hypothesis is that porosity effective pore

pressure diffusion along the pressure gradient is critical for the formation of discrete opening mode fractures and thus may influence the propagation of hydrofractures at large scale in porous rocks under controlled strain conditions.

The present paper evaluates the theoretical aspects of the numerical scheme for some basic configurations to which analogue and analytical studies are present i.e., hydrofracturing in homogeneous porous media under hydrostatic and non-hydrostatic conditions. In the following section we give details of the fluid-solid two-way coupling scenario of the scheme. In section 3 the validation of the solution is given and in section 4 implementation of the method is illustrated by means of simulation examples related to simple geometrical problems. Finally, results from this study are pointed out in section 5. The Alternative Direction Implicit procedure for the solution of the continuum diffusion is given in the Appendix-A.

4.2 Formulation

The simulations implemented in this study constitute of a special solution of the Darcy based Navier Stoke's equation and its coupling with a discrete poroelastic medium. The basic assumption is that the poroelastic feedback is behaving according to Biot's poroelastic theory within a linear elastic regime. This connects pore-scale force balanced hydro-physics with the evolution of the effective stress gradient in a porous rock. Once a fracture initiates, the overall behavior of the model becomes plastic and Biot's compressibility is no longer applicable [10]. The numerical scheme can encounter the displacement of discrete particles or deformation of a solid matrix directly. In this way the hydrodynamics evolve intrinsically with irreversible micro deformation in a solid matrix through the use of the Kozeny-Carman porosity-permeability relation.

The solution procedure adopted for this coupled problem is based on the same basic principles that were successfully used in simulations to model instabilities in fluid filled granular media [24-27]. The same type of hybrid models was also used to model gravitational instabilities in Rayleigh-Taylor like situations with grains falling in a gas [28-32] or a fluid [33-35], and in situations of aerofracturing, i.e. injection of gas in granular media [36, 37]. It was shown to reproduce lubrication in sheared fault gouges due to the presence of an interstitial fluid [38, 39] and a variant of two fluid models is used to model fluidizes beds [40] and saturated landslides [41, 42]. In the following subsections we outline the idealizations employed to set up the hybrid model and describe the model components along with the formulation of constitutive equations. Then we turn to the solution of the fluid-solid interaction, deformation mechanism and finally the assumptions made in this study.

4.2.1 Methodology

The numerical scheme is built on a 2D hybrid Particle-Lattice model of unit dimension that utilizes a small-scale triangular discrete spring network code inherited from the software 'Latte' (part of the modeling environment 'Elle', [23, 43]) as a deformation isotropic porous material. The discrete lattice is then coupled with a continuum fluid phase presented by a stationary square grid of equivalent or larger dimension (Fig. 4.2).

The computation is governed by a set of two differential equations, one deals with the translation (elastic deformation) of solid particles and the second solves the time dependent diffusion of fluid pressure according to local strain rates through a poro-elasto-plastic relationship. For a given configuration of the pressure field and the solid particles, the respective constitutive equations are approximated separately by two different numerical procedures. The elastic media is relaxed by a standard over-relaxation algorithm containing kinematic boundary conditions ($n \cdot u = 0$) for boundary particles, while the Pressure ADI routine is used for the solution of the pressure diffusion in a continuum grid (Appendix-A).

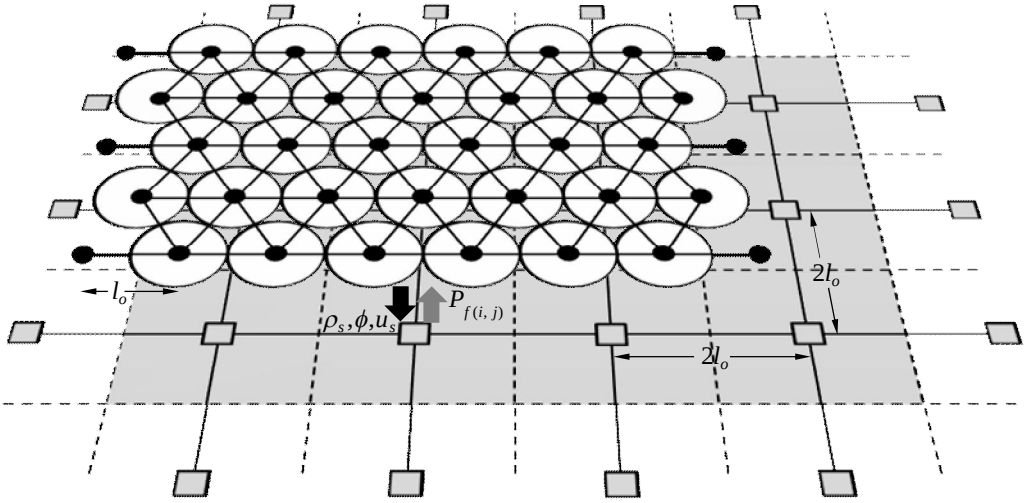

Figure 4.2 Schematic diagram of the hybrid hydro-elastic model, illustrates overlapping regions in physical space comprising the DEM lattice and the continuum grid.

With a local mass to momentum conservation, the scheme embodies coupling between the solid and the Darcy continuum description. The porosity dependent evolution of the pressure gradient imparts fluid drag forces at the particles of the discrete model. Permeability is treated as an implicit fluid flow property and is an output of the discrete model as a function of change in local porosity where the change in porosity is determined by the translational movement of mass centers of the particles.

4.2.2 Discrete elastic model

The 2D DEM model is assembled by coupling a triangular network of volume-less linear elastic springs with a particle model where disk shaped particles of constant radius superpose the nodes of the triangular structure. The particle model has its genesis from molecular dynamic models and represents the discrete quantities of the solid material, whereas following Hook's law of interaction the spring lattice model inherits the micro-mechanical physics between the nodes. This setup thus mimics isotropic elastic behavior of solid materials and can be used to model deformation problems in systems described by linear elastic theory. The intrinsic stiffness constant k of linear springs is related to macro-scale elastic material-parameters (E, v) through the consistency measures of strain energy between the 2-D elastic lattice of the triangular network and solid continua [10].

$$k = \frac{\sqrt{3}}{2} El \tag{4.1}$$

where l corresponds to the thickness of the 2D particle-lattice model.

The model produces plain strain deformation and a large-scale average stress tensor can be determined from the local deformations of elastic springs for each time step Δt. Springs can break when a prescribed tensile stress threshold is overcome to exhibit discrete mode-1 fractures in the material. Broken springs are removed from the elastic network, whereas the respective particles still retain repulsive forces to accommodate the successive tension. The breaking strength of springs is related to the mode-I stress intensity factor K_I, a key parameter that gives stress singularities at crack tips and does depend on the size of micro cracks in the material [10].

$$K_I = \sigma_I \sqrt{\pi a} \tag{4.2}$$

where σ_I is the critical mode-I driving stress for the relative displacement of fracture walls and a is the length of micro cracks in an isotropic medium. The porous model is assumed to be homogeneous corresponding to its elastic properties on large scale, however inherent disorder ubiquitous in natural media can be quenched through characteristic distributions of material properties on particles or annealed disorder (Griffith's micro cracks and other defects at grain scale) can be introduced by modifying the elastic properties of mechanical springs. It has been indicated that fracture patterns observed both in field and laboratory studies can be replicated by implying the realistic normal distribution of strength threshold in DEM models [44-46].

To avoid rigid body translation the elastic system is confined (closed system) by elastic walls at the boundaries. The walls behave as linear elastic springs and exercise a force

on the confronted particles proportional to their distance. For instance, the force by a lateral wall on particle i contacted at $x = x_w$ is

$$f_i = \begin{cases} -k_w(x_i + r_i - x_w)n_i & \text{if } x_i + r_i - x_w > 0 \\ 0 & \text{else} \end{cases} \tag{4.3}$$

where r_i is the particle radius, n_i is a unit vector normal to the wall and k_w is a spring constant for particle wall interaction.

4.2.3 2D Pressure diffusion field

With negligible fluid inertia, a time dependent macroscopic diffusion equation is derived that contains mass and momentum conservation in the bulk simulation of particle and continuum dynamics. The output is an interstitial fluid flow expressed in terms of a porosity dependent pressure gradient, which makes the computation simple and efficient. We start with the continuity equations (both for solid and fluid) at the characteristic scale of a grain diameter.

$$\partial_t\left[(1-\phi)\rho_s\right] + \nabla\cdot\left[(1-\phi)\rho_s u_s\right] = 0 \tag{4.4}$$

$$\partial_t(\phi\rho_f) + \nabla\cdot(\phi\rho_f u_f) = 0 \tag{4.5}$$

where ρ_s, ρ_f are the densities and u_s, u_f the velocities of the solid particles and fluid respectively and ϕ is the local porosity. The Darcy equation for the segregation of fluid and solid gives a local fluid seepage u_f for a pressure drop described by the local permeability on a unit area that is larger than the grain diameter.

$$\phi(u_f - u_s) = -\frac{K}{\mu}\nabla P \tag{4.6}$$

where μ and P stand for the fluid viscosity and pressure, whereas the local permeability K is expressed as a function of the local solid fraction ρ according to the empirical Kozeny-Carman relation for a Darcy like regime.

$$K(\rho) = \frac{d^2(1-\rho)^3}{180\rho^2} \tag{4.7}$$

where d is the particle diameter and 1/180 is an empirical constant valid for packing of spheres. Similar to the quenched noise in elastic material constants, a distribution of

hydraulic particle size can be treated as an epoxy to intrinsic hydraulic heterogeneity (solid fraction, permeability) in the continuum routine. In general, a larger particle area will result in low permeability and high pressure gradient and eventually an overall larger fluid drag force at the local fixed scale of reference and vise versa. To get a fully consistent picture, the fluid adiabatic compressibility β is included into the continuity equation according to the fluid state equation i.e., proportional approximation of the fluid density to pressure

$$\rho_f = \rho_o(1+\beta P) \ , \tag{4.8}$$

where ρ_o denotes the fluid density at some reference pressure. Substituting ρ_f and u_f into equation (4.5) and eliminate $\partial_t \phi$ from the subsequent equation we end up with the following diffusion equation for the non-hydrostatic pressure P, with an approximation of finite solid compressibility relative to fluid.

$$\phi\beta(\partial_t P + u_s \nabla \cdot P) = \nabla \cdot \left[(1+\beta P)\frac{K}{\mu}\nabla P \right] - (1+\beta P)\nabla \cdot u_s \ . \tag{4.9}$$

The left hand side of equation (4.9) is the Lagrangian derivative of pore pressure, the first term on the right hand side describes the Darcy diffusion of the fluid pressure relative to particles and the third term in the equation is distinguished as source term. The source term facilitates a pressure change as a function of a change in the particle solid fraction if particles move apart in the local reference scale of Darcy flow. For a detailed dimensional and non-dimensional derivation of the continuum equation presented above see the reference [38, 39, 47].

The assumption of omitted fluid inertia is evident in equation (4.9), where the fluid flow is described by the pressure field $P(x, y)$ only. This diffusive-advective description of the fluid flow is valid when the Reynold's number $\mathrm{Re} = u_f d \, {}^{\rho_f}\!/_{\mu}$ is small, where μ is dynamic viscosity of the fluid, d the particle size (diameter). The Reynold's number will be small if particles are small as is in the considered cases of dense models. Assuming the validity of the current approach a priori, one can also evaluate the condition of $\mathrm{Re} < 1$ using Darcy's law i.e., $\mathrm{Re} = -(Kd \, {}^{\rho_f}\!/_{\mu^2})\nabla P$ in the simulations (which is true for all the cases subjected here). As far as the particle movement (fracture aperture) is comparable to the diameter of particles, the above assumption of negligible fluid inertia is valid. However, if the fracture aperture becomes broader (sub-particle scale) the fluid inertia becomes important. This not only affects the particle-fluid coupling but also the fluid dynamics and in this case an equation describing the flow of fluid momentum, like the Navier-Stokes equation is required [27]. Nevertheless, this approach is also valid for flow fields at large Reynold's numbers [48].

4.2.4 Two way solid-continuum interaction

The DEM lattice is blanketed over the continuum grid in a way that the boundaries of the two parallelized lattices coincide with each other. With the lattice constant of the continuum grid set to be twice as large as that of the discrete lattice, this setup incorporates the "cloud in a cell" method (Fig. 4.3) to facilitate the two-way interaction between the porous matrix and the hydrodynamic phase. The particle density ρ and velocity u are estimated locally on the continuum grid in each iteration as a function of the local mean particle density specified by a linear tent weight function upon four nearest grid nodes.

$$\rho(r_o) = \sum_i^n s(r_i - r_o) \tag{4.10}$$

$$u(r_o) = \sum_i^n u_i s(r_i - r_o) \tag{4.11}$$

where subscript i stands for particle number and the smoothing function $s(r - r_o)$ satisfies the weighted distribution of particle mass relative to its position.

$$s(r - r_o) = \begin{cases} \left(1 - \frac{w_1}{\Delta x}\right)\left(1 - \frac{w_2}{\Delta y}\right) & \text{if } w_1 < \Delta x,\ w_2 < \Delta y \\ 0 & \text{otherwise} \end{cases} \tag{4.12}$$

where $r(x, y)$ and $r_o(x_o, y_o)$ are the positions of the particle and the continuum node respectively, $w_1 = |x - x_o|$ and $w_2 = |y - y_o|$ are the relative distances.

With this configuration, the fluid drag force f_p on each particle encountered by a fluid continuum cell can also be deduced by averaging the pressure gradient at the respective continuum node.

$$f_p = -\sum_k s(r_i - r_k)\left(\frac{\nabla P}{\rho_n}\right)_k \tag{4.13}$$

where k runs over four nearest grid nodes. This definition guarantees the mutual and balanced attribution of the pressure force f_p to solid particles from the continuum grid and the density/momentum contribution of the grains to the respective continuum unit cell as determined by equation (4.20) below.

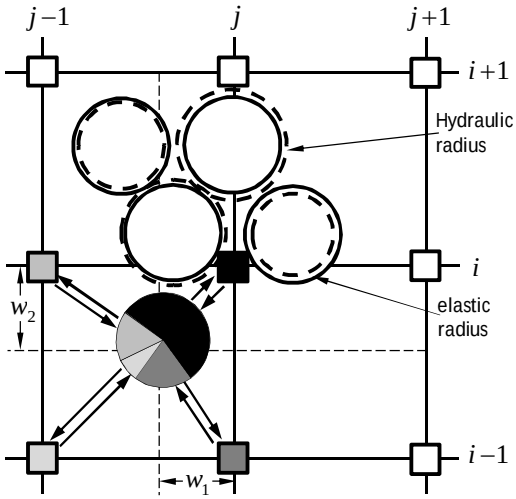

Figure 4.3 General overview of the twofold function of the numerical setup. Polar arrows illustrate the linear interpolation of particle area weight (grayish color code) to surrounding grid nodes and in turn the time dependent drag force from grid nodes to encountered particles.

In the coupled scheme, fluid pressure gradients that are approximated between fixed continuum nodes produce effective stresses at the particles of the DEM lattice. This steers the particles to displace and leads to stretching of the connected elastic springs, which ultimately break and be demonstrated as explicit fracturing when the imposed effective stress exceeds a given tensile stress threshold. Upon the formation of discrete cracks, rearrangement of the particles in the elastic medium (i.e., fracture opening) devise local changes in the background void space of the system, which in turn affects the permeability to be used in the successive step to determine the fluid pore pressure field. This evolution of fluid pore pressure again provides feedback to the stress field in the system and leads to fracture propagation or opening as a function of the particle dynamics. The procedure is repeated until both the continuity equation and the discrete grains are relaxed. The flowchart for one complete cycle of the algorithmic scheme is given in Fig 4.4.

4.2.5 Deformation mechanics

The translation motion of the initially relaxed solid particles (solid-solid interaction) is managed by the momentum exchange between solid and fluid phases in a unit volume cell dV (with unit third dimension) of the coupled system on account of-the inter-particle contact force f_e (either connected with a spring or repulsive force), fluid force f_p and gravity loading f_g.

$$m\frac{dV}{dt} = f_e + f_p + f_g \tag{4.14}$$

where the forces f_e being aligned along the connected elastic springs are characterized by spring constant k_{ij} times the actual distance between the centroid of the particles minus the equilibrium distance a_{ij}.

$$f_e = \sum_j k_{ij} \left(|a_{ij}| - (x_i - x_j) \right) \cdot \hat{n}_{ij} \tag{4.15}$$

where x_i and x_j are the positions of the connected particles, $\hat{n}_{ij}$ is unit vector pointing from the centroid of particle i to particle j and the sum runs over all the connected neighbors j. The fluid force f_p that acts on the surface normal dA of the unit cell is a result of the fluid flow due to the pressure gradient and is given as:

$$f_p = -\int P dA \tag{4.16}$$

where P is the local fluid pressure, which is the sum of the hydrostatic pressure $\rho_f gz$ and extraneous pressure P_o. The term gravitational force f_g incorporates the gravity effects of both the fluid and solid masses where the former together with the hydrostatic part of pressure determines the effective stress $\sigma_{eff} = (\rho_s - \rho_f) gz$ on the solid particles.

$$f_g = \rho_s \cdot \rho dV \cdot g + \rho_f \cdot \phi dV \cdot g \tag{4.17}$$

In the geological realm a transient hydrofracturing is likely to take place by a pore pressure P in excess to σ_{eff}. However, for the considered linear elastic model that exhibits deformation in a quasi-static fashion we only need to assume pore pressure deviations from the lithostatic pressure. This has been achieved by introducing the effect of gravity in form of lithostatic stress and results in the calculated stresses minus the lithostatic pressure. The inferred gravity force on a single cylindrical particle i of volume $V_s = \pi r^2 h$ with base area $A_s = \pi r^2$, where $h = 1$ is the thickness in the third dimension is:

$$f_i^g = \rho_s \pi R_i^2 gs \tag{4.18}$$

with

$$s = \frac{2}{3} \frac{E_m}{E_R} \frac{A_m}{A_R} \tag{4.19}$$

where ρ_s is the material mass density, $R_i = r_i \times S$ with S the dimension of the real system. E_m, E_R and A_m, A_R stand for the Young's Moduli and areas of particles in the model and

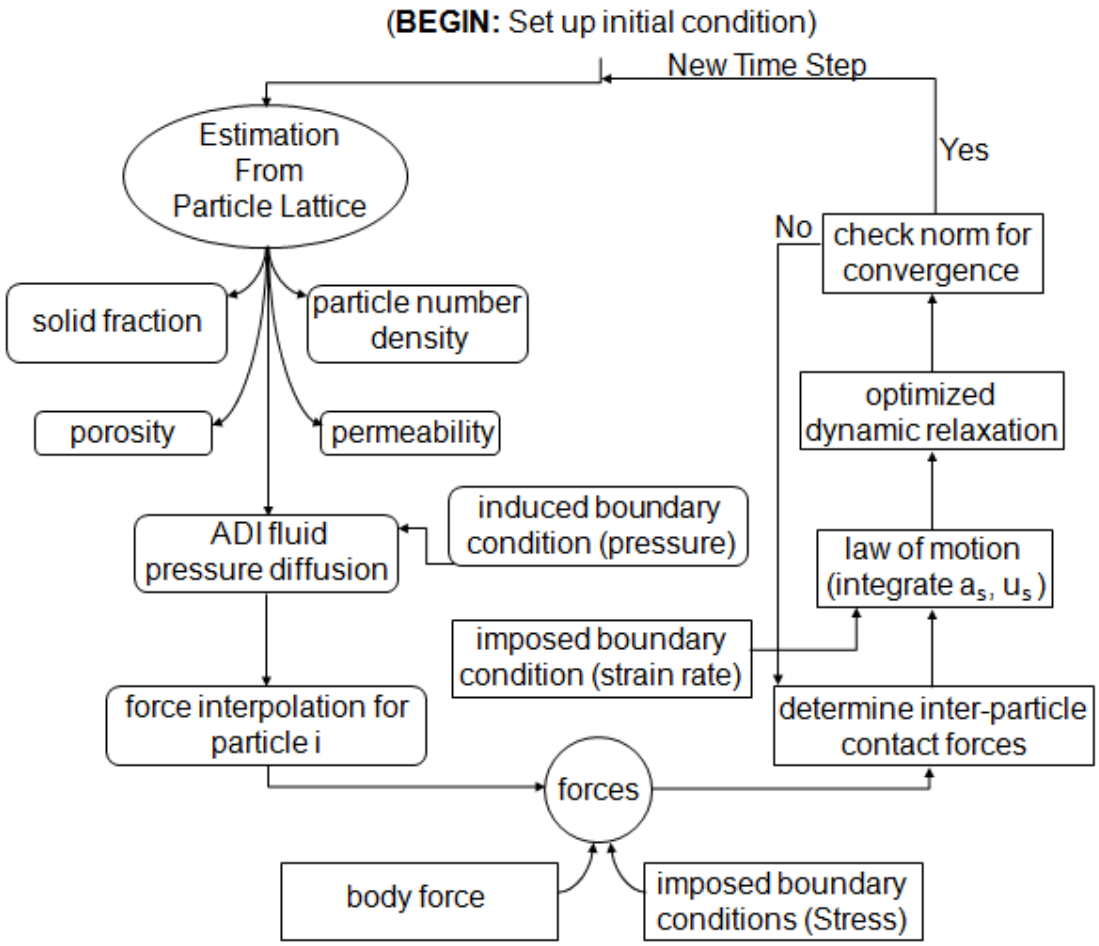

Figure 4.4 Flowchart for the complete cycle of the algorithmic scheme.

in real system respectively. The factor 2/3 in equation (4.19) is derived using the expedient strain-stress relation ($\sigma_{\mathrm{v}} = \frac{E\upsilon}{(1+\upsilon)(1-2\upsilon)}\varepsilon_h + \frac{E(1-\upsilon)}{(1+\upsilon)(1-2\upsilon)}\varepsilon_{\mathrm{v}}$) from the generalization of Hooke's law for a 2D plane strain problem assuming $\upsilon = 1/3$ and zero lateral deformation. This is essential in order to acquire a compatible one dimensional lithostatic stress $\sigma_{\mathrm{v}} = \rho g h$ for the isotropic 2D linear elastic solid.

By considering the local fluid velocity a rival of the local particle velocity i.e., high viscous fluid and substituting the respective constitutive force terms in equation (4.14) one can derive the following force-balance equation, which exhibits an explicit coupling between granular motion and fluid flow in the unit cell ($dV = 1/\rho_n$).

$$m_s\left[1+\frac{\rho_f\phi}{\rho_s(1-\phi)}\right]\frac{du_s}{dt} = F_i - \frac{\nabla P}{\rho_n} + \rho_{eff}V_s g \ , \tag{4.20}$$

where ρ_n is the particle number density, $\rho_{eff} = \rho_s - \rho_f$ is the effective mass density and g the gravity. This is the translational equation of each individual particle dragged with velocity u_s in the absence of any frictional and tangential effects. The mass m_s in the left term accounts for the summation of fluid mass to each individual solid particle as a function of the local porosity to particle number density ratio.

4.2.6 Assumptions

The assumptions made in order to keep the proposed scheme amenable are:

- The fluid-solid friction force at the surface of the solid particles is not considered, therefore the pressure gradient ΔP is the only agent that produces a drag force (in the direction of fluid flow) on particles.
- The fluid is considered to be purely viscous and therefore any effect like thermal evolution of the fluid (a pivotal factor in the development of subsurface overpressure e.g., dehydration of sediments in intrusive zones in particular) is not taken into account.
- The locally interpolated solid fraction on the 2D continuum grid is multiplied by 2/3. With this factor we obtain a good mapping of the 2D porosity on the corresponding 3D equivalent (prerequisite for the 3D Kozeny-Carman permeability) with a match between closed packed configurations and the empty configurations [27]. Without this correction the qualitative behavior is comparable but quantities like fracture speed, propagation or the flux for certain pressure gradients can change by a prefactor, roughly up to a factor 2.
- Analytically the Kozeny-Carman relation works as long as the solid fraction is greater than zero, but a solid fraction of 0.15 or less presents a solid-fluid composite mainly as a fluid and is thus inconsistent with the Kozeny-Carman relation (originally

established for dense granular media). We thus chose to apply a threshold to the permeability of the medium with a solid fraction of 0.15 (e.g., in a broader fracture aperture). The main purpose of limiting the solid fraction and hence permeability to this upper value is to allow larger time steps and improve the speed of the model. Effectively, the zones of the model where the permeability is equal to large values correspond to almost homogeneous pressure zones. The exact value of this cutoff does not affect the pattern formation significantly, as different values of the cutoff have been tested (between 0.25 and 0.05) without any significant changes [24, 28].

4.3 Model verification

We first test the linearity of the porosity controlled Darcy flow field and the associated pressure forces on each particle. If we consider compressible water as fluid in the pore space, the evolution of seepage forces in the simulations (Fig 4.5) validates the theoretical aspects of the scheme. A reference model of unit dimension is taken as a porous rock where the solid skeleton is composed of 11500 disc-shaped adhesive particles. The system is confined mechanically at all boundaries whereas hydraulically it is restrained only at the side boundaries. Neglecting any gravitational loading a hydraulic gradient i is established in the system by setting the bottom boundary at a constant pressure input (normalized $P = 1.0$) and fixing the top boundary at 0.0 pressure respectively. The pressure input value is kept suitably low in order not to produce fractures.

Two series of simulations are conducted to test the model by considering a homogeneous (Fig. 4.5a) and a heterogeneous (Fig. 4.5b) porous rock respectively. In the heterogeneous case a seal is inserted in the model. The seal is represented by a horizontal layer of low permeability with a thickness of 0.1 with lower boundary at 0.2 unit and upper boundary at 0.3 unit on the ordinate axis. In the test simulations, initially a high pressure gradient is concentrated in the vicinity of the source boundary, therefore only the intimate particles are subject to resultant seepage forces and consolidate along the direction of the pressure drop. However, after 5000 time steps the pressure gradient becomes linear and the fluid approaches a steady state flow condition in the homogeneous model. Whereas, in the heterogeneous medium a strong pressure drop develops across the layer of relative low permeability. Two linear regimes develop, one below the seal with a relatively steep gradient and one above the seal with a relatively gentle gradient. Consequently vertical seepage forces of high contrast in magnitude are measured at the seal boundaries (Fig. 4.6).

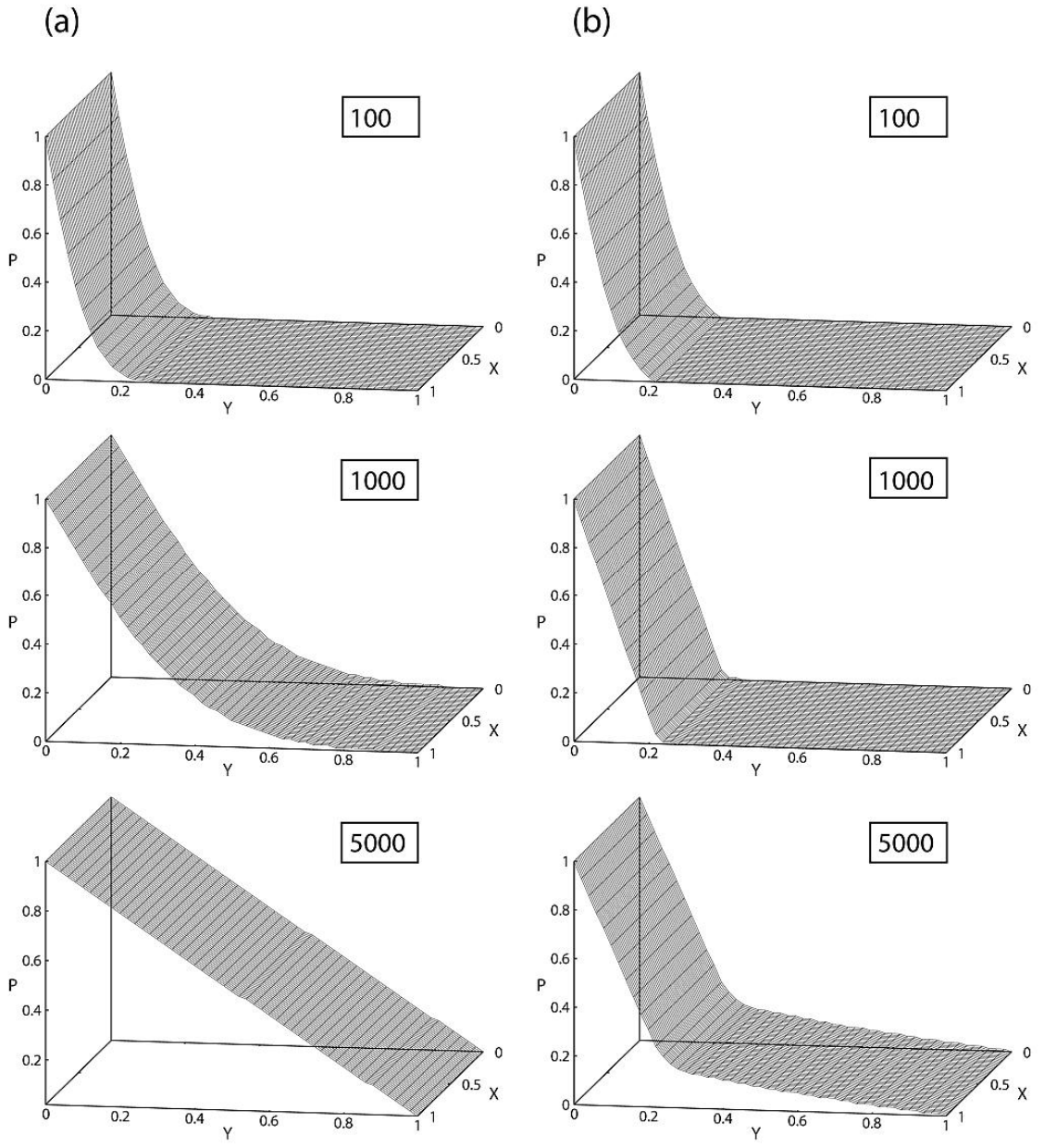

Figure 4.5 Normalized pore pressure profiles at different time steps, (a) in a homogeneous porous medium, (b) in a heterogeneous porous medium accompanying a horizontal seal of low porosity at position $0.2-0.3$ on the y-axis (vertical axis).

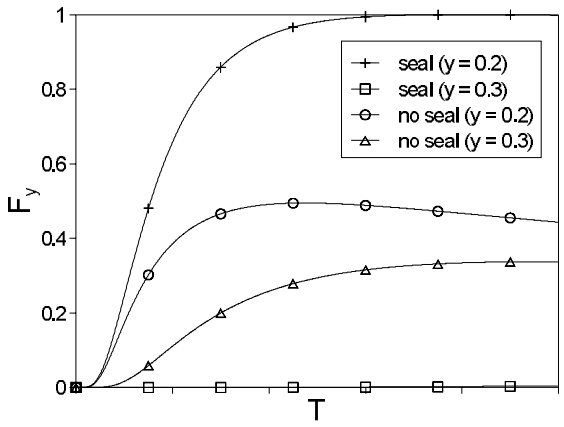

Figure 4.6 Overall evolution of the vertical seepage forces as a function of time ($T:1000$) for a homogeneous system and at the lower and upper boundary contacts of the seal in a heterogeneous system. The forces display a sharp contrast in magnitude in the heterogeneous case, whereas in the homogeneous medium the forces show a gradual increase in pressure force. Both the heterogeneous and homogeneous cases reach a steady state condition.

4.4 Model implementation

In the following sections we show two different test cases to illustrate the development of hydro-fractures in the model.

- Foremost, we discuss fracturing in a homogeneous medium where fractures develop around a point source (fluid is injected locally) in the absence of external deformation. We investigate the fracture pattern that develops as a function of fluid pressure gradients under isotropic diffusion of the fluid pressure. In addition we analyze the influence of changes in background porosity and study the state of stress during fracturing in detail. Later, the likely influence of background non-hydrostatic stress states (i.e., uniaxial vertical loading and pure shear deformation) on the growth of hydrofracture is also examined.
- In the second set of two simulations, we advance to simulate fracture patterns due to local pressure sources in the presence of gravity and tectonic strains. In these cases we use examples where seepage forces develop due to a local increase in pore pressure and caused local perturbation in the background non-hydrostatic stress state. In this case the tectonic strain conditions will control the different fracture patterns.

In each test the model starts from a fully relaxed state and is loaded in small steps afterwards. According to the boundary conditions loading includes increase of fluid pressure in the fluid lattice, vertical loading due to gravity or horizontal loading due to tectonic strains by moving the boundary walls. The mechanical and hydraulic boundary conditions vary accordingly with respect to the underlying problem to imitate laboratory and field conditions.

4.4.1 Point source in a homogeneous porous medium

In these simulations the fluid pressure is increased at a point source with a constant rate ($P/\Delta t$) at the centre of a homogeneous and isotropic poro-elastic domain. The model is mechanically confined and bears no-flow boundary conditions. In these simulations the hydrofracturing process shows two stages, fracture initiation and episodic fracture growth until the system reaches a steady state (Fig. 4.7, 4.8a).

The accumulation of fluid pressure at the point source generates an isotropic pressure gradient in the surrounding which contributes to the evolution of the effective stresses and deforms the porous rock elastically as a function of Biot's poro-elastic coefficient. The rock experiences micro fracturing from the concentration of stress on relatively weak rock elements. The discrete fractures nucleate at the source location and tend to propagate into the undisturbed region (Fig. 4.7). At this stage, tension cracking accommodates the strain in the system and results in stress relief and a potential local change in porosity when particles are pushed away by the pressure force and fractures open. This cycle is repeated following the two-way temporal and spatial feedback between hydraulic pressure field and elastic field on account of induced fracturing in the porous matrix until a steady state condition is acquired and fracturing ceases. The symmetry of the developing fracture pattern at the point of injection is a function of a circular extension around the fluid source. The symmetric pattern validates the homogeneous existence of pore pressure in the rock matrix. The seepage forces that develop due to the pressure diffusion modify the force balance in the porous rock sample, which deterministically drives the discrete tensile crack growth along the pressure gradient and results in a regular fracture geometry.

Fig. 4.8a shows the evolution of the effective mean stress in the model (positive mean stress is extensional) as a function of time and the growth of broken bonds with time for the simulation shown in Fig. 4.7. In the first steps of the model the effective mean stress increases in a non-linear fashion due to the diffusive nature of the pore fluid pressure. Once the tensile strength of the material is reached the rock fractures instantly and bears significant stress drops. Induction of discrete fractures impacts also the integrated rock strength which is shown by the subsequent failure events even at relatively lower order of stress magnitudes. Finally fracture growth ceases and the mean stress reaches a steady state. Because the shown stress is an average of a larger area in the model the fracturing continues locally even though the mean stress has already reached equilibrium.

Under the same fluid injection rate a quantitative comparison of the mean stresses in rock samples with different background porosities is given in Fig. 4.8b. The graphs in show the evolution of the effective mean stress field and the fracturing behavior of the rock as a function of porosity. Rocks that inherit low porosity entail the production of high seepage forces to drive tensile failure at comparable low average tensile stress. A low average stress illustrates that the stress in a low porosity rock will be very localized around the point source.

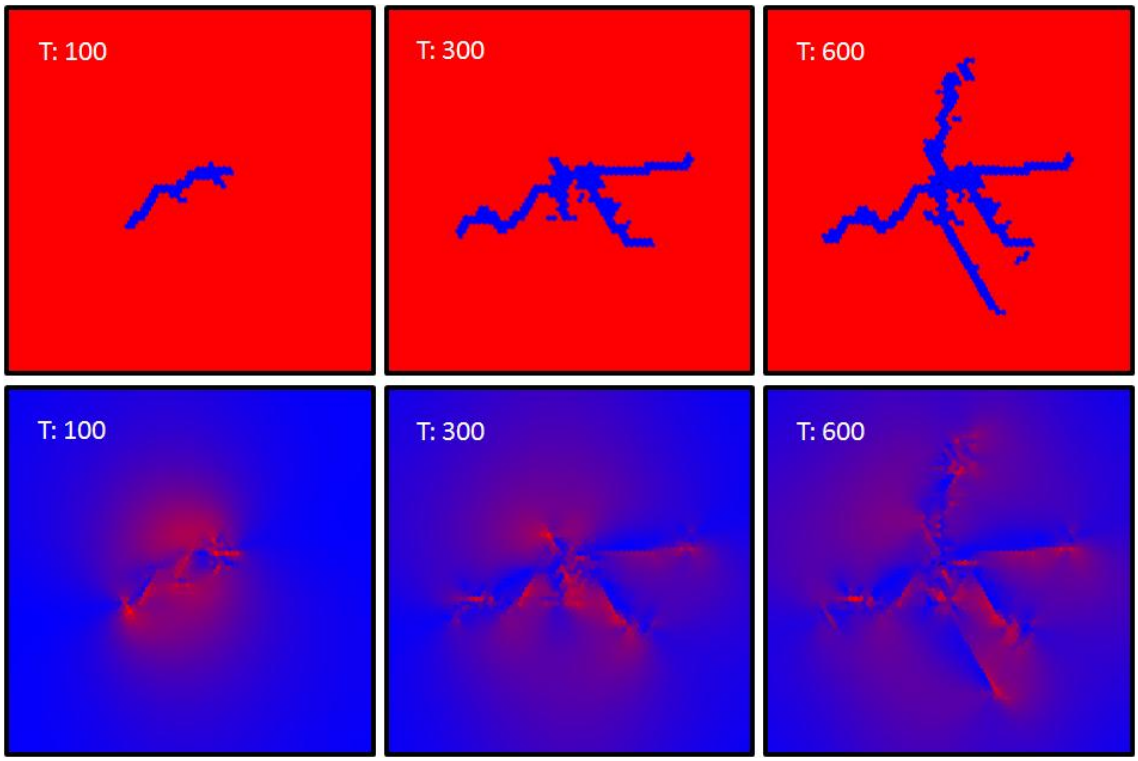

Figure 4.7 The figures above with red background show the development of circular hydro-fractures (T= model time, blue particles have broken bonds) by a point source overpressure. The figures below with blue background show the same simulations and illustrate the associated differential stress states in the model at the respective failure stages (red=high; blue=low differential stress). The time step runs from left to right direction.

The stress drop associated with failure of the material will be relatively large. In addition the state of stress may become asymmetric in these low porosity rocks due to friction along developing fractures (solid-solid coupling), where the overall stress regime may become compressive. Subsequently small isolated shear or hybrid extension-shear fractures can develop near the tip of the primary dilational fractures when fracturing happens relatively early in low porosity rocks. When the porosity becomes larger the initial loading of the system due to the fluid input becomes successively more non-linear (Fig. 4.8b) up to a point where the pressure just diffuses out of the system without the creation of fractures.

We also simulated a number of examples (Appendix-B, Appendix-C) with the similar hydraulic setup but different external boundary conditions. The developing fracture patterns closely resemble the results observed experimentally by [49, 50] in rock type material. The simulations manifest the effective influence of pore pressure on the likelihood of tensile failure and the corresponding fracture propagation under non-hydrostatic stress conditions in homogenous sedimentary rocks.

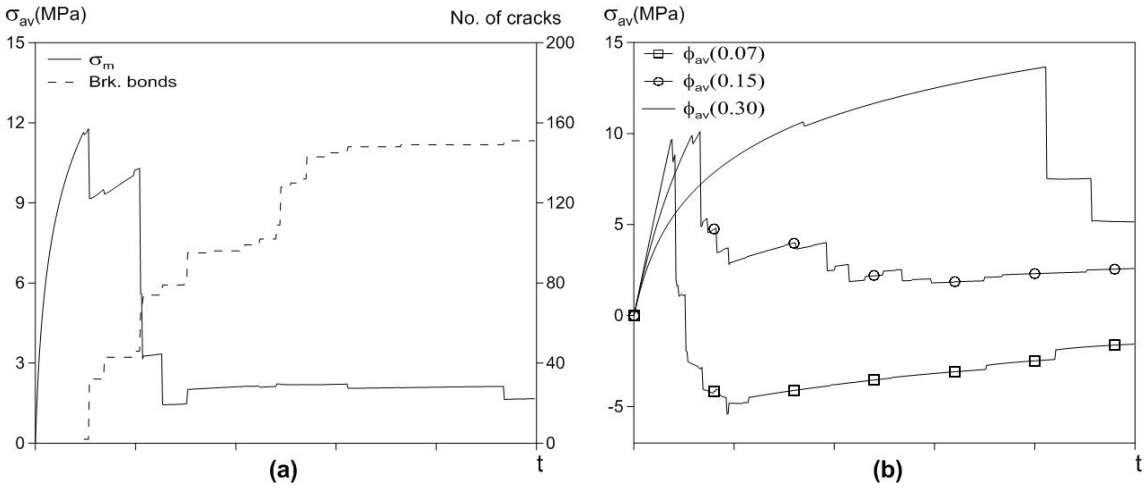

Figure 4.8 (a) Graph shows oscillations in effective mean stress and associated number of broken bonds in the model associated with simulations in Fig. 4.7. The stress shows the episodic evolution of the fluid pressure. Positive effective mean stress in the model is defined as extensional stress. **(b)** Mean stress as a function of background rock porosity, where an increase in porosity results in a lower driving force because the pressure can diffuse faster. Note: –ve sign in the model is annotated for compressive stress and +ve sign for extensional stress.

4.4.2 Hydrofracturing in a homogeneous medium under gravity loading

In the second set of simulations, we reproduce the patterns of hydrofracturing caused by a local pore fluid overpressure under non-hydrostatic tectonic loadings of gravity and lateral stresses and found the results consistent with [20]. The problem is analogous to various geological systems (magmatic intrusions, hydrothermal venting, volcanoes etc.), which yield a local perturbation in the effective stress field with the induction of localized pore overpressure.

Fig. 4.9 and 4.10 show simulations with a local point source at the bottom of the model, where the former sustains a stress regime of horizontal extension and the later horizontal compression. The model material is homogeneous and the gravitational loading is followed by equation (4.18). In order to incorporate the effect of gravitational loading, the model is subjected to a two-stage deformation in both cases. First, the model is let to settle under uniaxial gravitational loading assuming the model is 1 km in depth from the Earth surface with fixed side walls, a rock density of 2.5 kg/m^3, Young modulus of 80GPa and Poisson ratio of 1/3. This setup yields a global stress anisotropy where vertical and horizontal stresses differ due to Poisson effects. Secondly, we apply a lateral extension or compression with a relative small horizontal strain rate in order to have a fluid dominated effective state of stress in the rock. A hydraulic anisotropy is produced in the simulations by inducing a pressure drop with a zero assigned pressure at the upper boundary and no flow boundary conditions at the side-walls.

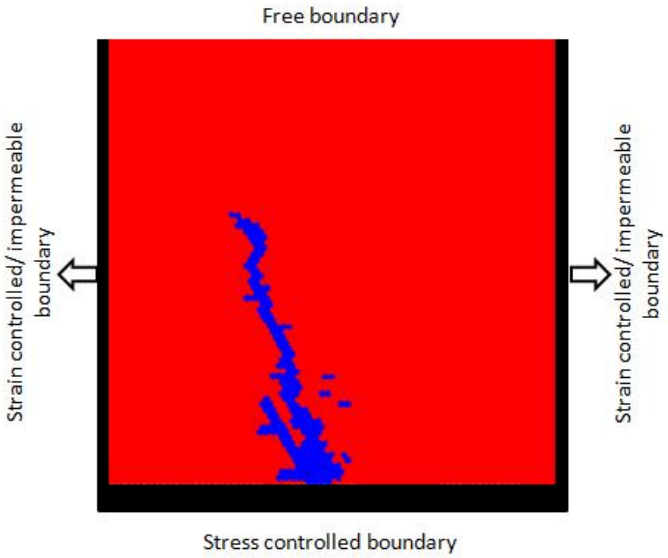

Figure 4.9 Vertical hydrofracture in a rock model subjected to lateral extensional strain. A vertical gravitational load is applied to the system and fluid is injected at a point source in the middle of the system at the lower boundary.

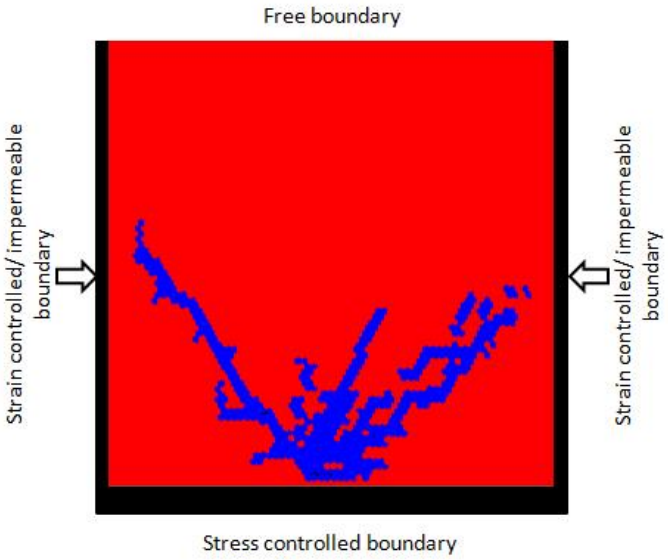

Figure 4.10 Conjugate shear fractures under compressive state of stress. A vertical gravitational load is applied to the system and fluid is injected at a point source in the middle of the system at the lower boundary.

The system that is loaded with a gravitational body force experiences buoyancy forces i.e., $P = (\rho_s - \rho_f)gz$ in equation (4.9) with the reduction in effective stresses due to an increase in local pore pressure. This gradient may lead to a quasi-static fracture propagation through parts of the model. The failure patterns illustrated in Fig. 4.9 and 4.10 are consistent

with the different forces that are applied. Fracturing nucleates in the areas where fluid pressures are high (point source at the bottom of the models). The fractures propagate upwards reflecting the gravitational loading of the system. The horizontal tectonic forces produce almost vertical extensional mode I crack like failure when the system is extending (Fig. 4.9) and conjugate shear failure when the system is under compression (Fig. 4.10). Even though the source of the fracturing is a high fluid pressure in both cases the pattern that develops is strongly influenced by the heterogeneous stress field due to gravity and tectonic loading. This is clearly illustrated when Fig. 4.7 is compared, since Fig. 4.7 has the same fluid boundary condition with a point source as Fig. 4.9 and 4.10 but the fracture pattern is very different in the later cases due to the external stress field.

4.5 Discussion and conclusion

Discrete fractures or instant opening of existing cracks as a function of fluid overpressure drive perturbations in permeability, change the state of stress and the corresponding release of strain energy on the scale of pores. In this contribution we present a hybrid numerical solution based on first principles rather than on empirical constitutive relationship with ad hoc fitting parameters to model natural examples of hydrofractures. First principles constitute the equation of state separately for the fluid and the solid and the pore scaled forces balance to describe interactions. The scheme thus combines the pertinent features of both continuum and DEM descriptions, and examines the dynamic coupling between porous flow and diagenetic process through fracture mechanics as a response to an applied pressure gradient across the system.

It appears likely that the interplay between the temporal and spatial evolution of the pore pressure and tectonic/gravitational stresses manipulate hydro-fracturing and the corresponding permeability changes. Our model shows an evolution of the deformation dependent permeability illustrating that in hydro-mechanical systems permeability is a nonlinear and time dependent parameter where fracturing localization is very important. The system reacts to forcing and produces the permeability that it needs to allow the fluid pressure to diffuse. It has manifested that small-scale diagenetic events can have adequate impact on the pressure field and in turn the fracture geometry. In our model this effect is achieved by the idealized hydro-mechanical constitutive relation of Kozeny-Carman permeability through a weighted interpolated function. In this relation even small displacements of particles can lead to significant changes in the local solid density and thus the Darcy fluid flow.

It has been perceived that several key features (flow rate upon compaction, yield surface, strain softening and hardening etc.) of critical soil mechanics (CSSM) are consistent with the observed porosity and pressure dependent deformation behavior of porous rocks [51-55]. Therefore, the use of Kozeny-Carman relation (originally developed for soils) for the

evolution of the permeability field in the presented model is justified. However, concerns may rise where porosity-permeability relations deviate from the trend of the basic equation [56] e.g., fracturing in subsurface impermeable rocks causes enhancement in the permeability in contrast to permeable rocks which bear a reduction in permeability. In this case one can pursue either of the following two ways:

1. Use different modified forms of the permeability dependence on the porosity both for ductile and brittle dominated deformation zones using the assumption of linearity between porosity and log permeability with defined parametric values from experimental data [57].

2. When approximating the local dimension of induced fracture (aperture), a modified form of the porosity-permeability relationship can be derived from the cubic law of fluid flow in fractures [58].

The simulated results validate the generality of the scheme implying that linear Darcy flow has an effective factor in the process of hydrofracturing, and the results are in good agreement with previously reported laboratory and field studies. The numerical scheme can qualitatively replicate some typical quasi-static field examples of hydrofractures when different modeling approaches are applied. Representative example problems constitute fracturing in homogeneous and heterogeneous porous rocks analogous to hydraulic fracturing in pressurize boreholes and natural fracture patterns due to local fluid overpressure. Simulation results illustrate that the diffusion of fluid pressure is a crucial mechanism that interacts with the effective stress field under different geological conditions and produces fracture geometries like branching fractures at point sources, vertical and shear hydrofractures under tensional/compressional tectonic settings.

The presented routine defines a fast approach both for qualitative and quantitative estimation of hydro-driven deformation problems at micro scale. The method can also be used to analysis large scale problems with the suitable selection of none dimensional parameters. In general, gravity loading and the associated non-hydrostatic stress fields along with mechanical heterogeneity in the lithology can have a vital influence over the evolution of buoyant effective forces and thus the hydrofracture patterns. Therefore future work will attempt to integrate these physical parameters in order to determine the appropriate geological conditions when analyzing natural vein and joint networks in real reservoirs.

The presented scheme is also capable to model 3D hydrofracturing, which may have more significant advantages in understanding the complex growth of fractures under the influence of 3D heterogeneity and non-hydrostatic conditions. The only change required is the interpolation of local mass density and velocity over a cubical unit volume of a 3D continuum grid using the same assigned tent function. In the future we intend to couple the derived continuum code with a newly developed 3D next-nearest particle lattice code “Melange” [59].

4.6 Appendices

4.6.1 Appendix-A: ADI – 2D Pressure Diffusion

The ADI method is time implicit. With symmetric discretization in time i.e., between a forward and backward step, this methods is unconditionally stable and the precision is better than with a purely forward in time implicit method [60]. The two-dimensional pressure diffusion equation (9) can be rewritten as

$$\frac{\partial P(\vec{r},t)}{\partial t} = \left(1+\beta P\right)\frac{K(\vec{r},t)}{\beta\mu\phi(\vec{r},t)}\left[\frac{\partial^2 P(\vec{r},t)}{\partial x^2}+\frac{\partial^2 P(\vec{r},t)}{\partial y^2}\right]-\frac{1}{\beta\phi(\vec{r},t)}g(\vec{r},t) \qquad \text{(A1)}$$

where $g(\vec{r},t)$ is the source term and $\vec{r}$ stands for position in space. This is a second-order parabolic partial differential equation. Corresponding to the time and space discretization of the 2D pressure continuum using forward difference with time on the left-hand side and central difference with space on the right hand side of equation (A1).

$$\frac{P_{i,j}^{n+1/2}-P_{i,j}^{n}}{\Delta t} = (1+\beta P)\frac{k_{i,j}}{\beta\mu\phi_{i,j}}\left[\frac{P_{i+1,j}-2P_{i,j}+P_{i-1,j}}{(\Delta x)^2}+\frac{P_{i,j+1}-2P_{i,j}+P_{i,j-1}}{(\Delta y)^2}\right]-\frac{1}{\phi\beta}g_{i,j} \qquad \text{(A2)}$$

where suffixes i, j and n are the indices in the x, y, and t directions respectively.

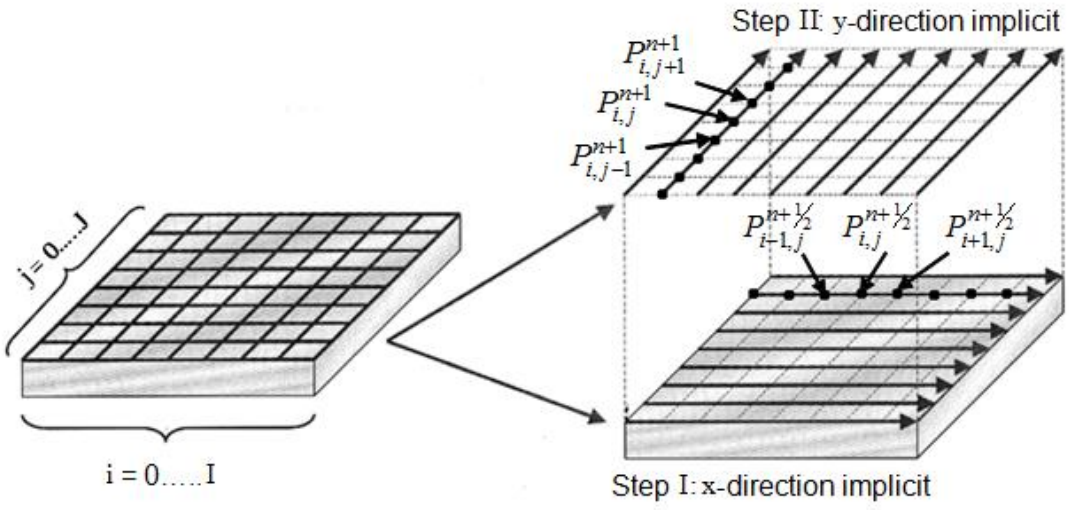

Figure 4.11 Schematic diagram of ADI solution of Finite-difference pressure continuum, after [61].

The main idea of the ADI method is to reduce the 2-D problem into a succession of two one-dimensional problems by proceeding one time step from n to $n+1$ in two sub-time

steps (Fig. 4.11). The first half-step (n to $n+½$) is taken implicitly in the x-direction and explicitly in the y-direction followed by the second half-step ($n+½$ to $n+1$) that is taken implicitly in the y-direction and explicitly in the x-direction.

Detailed differential equations in stage-1 for each j at marched time $n+½$ and the corresponding tridiagonal system of equations for the respective one-dimensional problem can be derived in form of matrix equation of dimension I:

$$-\alpha_{i,j}P_{i+1,j}^{n+½}+(1+2\alpha_{i,j})P_{i,j}^{n+½}-\alpha_{i,j}P_{i-1,j}^{n+½}=\gamma_{i,j}P_{i,j+1}^{n}+(1-2\gamma_{i,j})P_{i,j}^{n}+\gamma_{i,j}P_{i,j-1}^{n}-\frac{\Delta t}{2\phi\beta}g_{i,j} \quad \text{(A3)}$$

$$\begin{bmatrix} 1 & 0 & 0 & ... & ... & 0 \\ -\alpha_{i,j} & 1+2\alpha_{i,j} & -\alpha_{i,j} & 0 & ... & ... \\ 0 & ... & ... & ... & ... & 0 \\ ... & ... & 0 & -\alpha_{i,j} & 1+2\alpha_{i,j} & -\alpha_{i,j} \\ 0 & ... & ... & 0 & 0 & 1 \end{bmatrix}\begin{bmatrix} P_{0,j}^{n+½} \\ P_{1,j}^{n+½} \\ ... \\ ... \\ P_{I,j}^{n+½} \end{bmatrix}=$$

$$\begin{bmatrix} 1 & 0 & 0 & ... & ... & 0 \\ \gamma_{i,j} & 1-2\gamma_{i,j} & \gamma_{i,j} & 0 & ... & ... \\ 0 & ... & ... & ... & ... & 0 \\ ... & ... & 0 & \gamma_{i,j} & 1-2\gamma_{1,j} & \gamma_{i,j} \\ 0 & ... & ... & 0 & 0 & 1 \end{bmatrix}\begin{bmatrix} P_{i,0}^{n} \\ P_{i,1}^{n} \\ ... \\ ... \\ P_{i,J}^{n} \end{bmatrix}-\frac{\Delta t}{2\phi\beta}g_{i,j} \quad \text{(A4)}$$

$i=0,1,.....,I;\ j=0,1,.....,J$

where

$$\alpha_{i,j}=(1+\beta P)\frac{K_{i,j}\Delta t}{2\mu\beta\phi_{i,j}(\Delta x)^2} \quad \text{and} \quad \gamma_{i,j}=(1+\beta P)\frac{K_{i,j}\Delta t}{2\mu\beta\phi_{i,j}(\Delta y)^2}$$

By analogy, stage-II of the ADI method for each i at time $n+1$, is expressed in tridiagonal system of dimension J:

$$-\gamma_{i,j}P_{i,j+1}^{n+½}+(1+2\gamma_{i,j})P_{i,j}^{n+½}-\gamma_{i,j}P_{i,j-1}^{n+½}=\alpha_{i,j}P_{i+1,j}^{n}+(1-2\alpha_{i,j})P_{i,j}^{n}+\alpha_{i,j}P_{i-1,j}^{n}-\frac{\Delta t}{2\phi\beta}g_{i,j} \quad \text{(A5)}$$

$$\begin{bmatrix} 1 & 0 & 0 & \dots & \dots & 0 \\ -\gamma_{i,j} & 1+2\gamma_{i,j} & -\gamma_{i,j} & 0 & \dots & \dots \\ 0 & \dots & \dots & \dots & \dots & 0 \\ \dots & \dots & 0 & -\gamma_{i,j} & 1+2\gamma_{i,j} & -\gamma_{i,j} \\ 0 & \dots & \dots & 0 & 0 & 1 \end{bmatrix} \begin{bmatrix} P_{i,0}^{n+1} \\ P_{i,1}^{n+1} \\ \dots \\ \dots \\ P_{i,J}^{n+1} \end{bmatrix} =$$

$$\begin{bmatrix} 1 & 0 & 0 & \dots & \dots & 0 \\ \alpha_{i,j} & 1-2\alpha_{i,j} & \alpha_{i,j} & 0 & \dots & \dots \\ 0 & \dots & \dots & \dots & \dots & 0 \\ \dots & \dots & 0 & \alpha_{i,j} & 1-2\alpha_{i,j} & \alpha_{i,j} \\ 0 & \dots & \dots & 0 & 0 & 1 \end{bmatrix} \begin{bmatrix} P_{0,j}^{n+1/2} \\ P_{1,j}^{n+1/2} \\ \dots \\ \dots \\ P_{I,j}^{n+1/2} \end{bmatrix} - \frac{\Delta t}{2\phi\beta} g_{i,j} \qquad \text{(A6)}$$

$i = 0,1,\dots..,I;\ j = 0,1,\dots..,J$

Implementing the Gauss-algorithm with a Dirichlet boundary condition, the derived tridiagonal system of equation (A4) is solved J times and equation (A6) by I times.

4.6.2 Appendix-B: Hydrofracture patterns as function of the ratio of external stresses

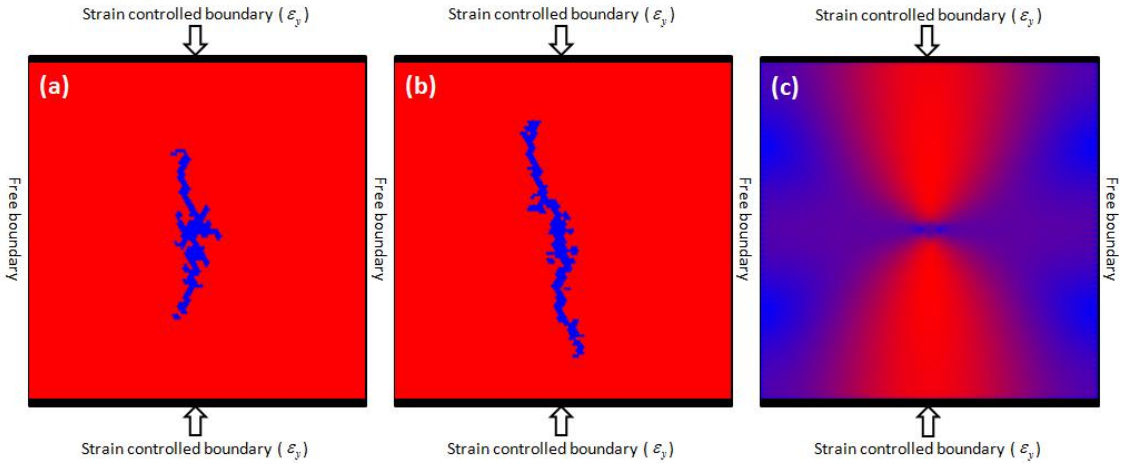

Figure 4.12 Different patterns of hydro-fractures in a situation where a constant point source is injected in a homogeneous media under different remote stresses: (a) with relative smaller σ_y, the results show the initial development of circular fracturing at the source location (centre) with elongated fractures oriented parallel to the axis of the applied stress. In contrast to the pattern shown in (a), in (b) a larger σ_y dominates the overall pattern and results only in sub-vertical oriented fractures parallel to the main stress axis and through the source location (central). (c) The figure shows the state of stress field at the onset of fracturing, where the red color code represents high differential stress and blue low differential stress.

4.6.3 Appendix-B: Hydrofracturing in pure shear stress field

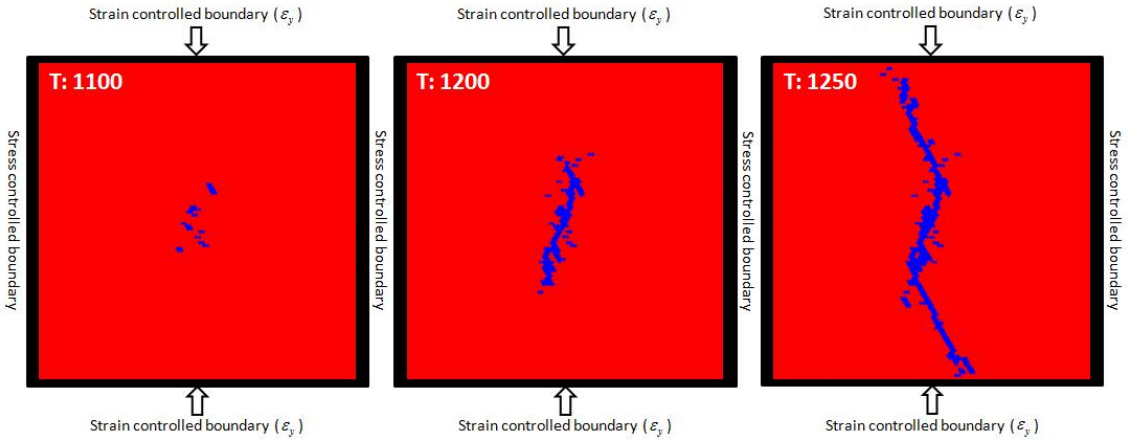

Figure 4.13 This figure shows a time series illustrating the influence of the local pore overpressure on brittle failure in a pure shear stress regime. In this case the extension fractures develop at the source location (centre) and link up with shear fractures towards the edges of the simulation box (time steps T increase from left to right).

4.7 References

1. Fyfe, W.S., N.J. Price, and A.B. Thompson, *Fluids in the Earth's Crust: Their Significance in Metamorphic, Tectonic, and Chemical Transport Processes*. 1978: Elsevier Scientific Pub. Co.
2. Hubbert, M.K. and D.G. Willis, *Mechanics of hydraulic fracturing* Petroleum Transactions, AIME, 1957. 210: p. 153-168.
3. Hubbert, M.K. and W.W. Rubey, *Role of fluid pressure in mechanics of overthrust faulting: I. mechanics of fluid-filled porous solids and Its application to overthrust faulting.* Geological Society of America Bulletin, 1959. 70(2): p. 115-166.
4. Biot, M.A., L. Masse, and W.L. Medlin, *A Two-Dimensional Theory of Fracture Propagation.* SPE Production Engineering, 1986. 1(1): p. 17-30.
5. Cleary, J.M., *Hydraulic Fracture Theory*. Circular (Illinois State Geological Survey). 1958, Urbana: State of Illinois, Dept. of Registration and Education, Division of the State Geological Survey.
6. Daneshy, A.A., *On the Design of Vertical Hydraulic Fractures.* SPE Journal of Petroleum Technology, 1973. 25(1): p. 83-97.
7. Secor, D.T., *Role of fluid pressure in jointing.* American Journal of Science, 1965. 263(8): p. 633-646.
8. Valkó, P. and M.J. Economides, *Hydraulic Fracture Mechanics*. 1995: Wiley.
9. Cleary, M.P. and S.K. Wong, *Numerical Simulation of Unsteady Fluid Flow and Propagation of a Circular Hydraulic Fracture.* International Journal for Numerical and Analytical Methods in Geomechanics, 1985. 9(1): p. 1-14.
10. Flekkøy, E.G., A. Malthe-Sorenssen, and B. Jamtveit, *Modeling Hydrofracture.* Journal of Geophysical Research-Solid Earth, 2002. 107(B8).
11. Gordeyev, Y.N. and A.F. Zazovsky, *Self-similar solution for deep-penetrating hydraulic fracture propagation.* Transport in Porous Media, 1992. 7(3): p. 283-304.

12. Meyer, B.R., *Design formulae for 2-D and 3-D vertical hydraulic fractures: model comparison and parametric studies*, in *SPE Unconventional Gas Technology Symposium*. 1986, 1986 Copyright 1986 Society of Petroleum Engineers, Inc.: Louisville, Kentucky.
13. Tzschichholz, F., et al., *Beam Model for Hydraulic Fracturing.* Physical Review B, 1994. 49(10): p. 7056-7059.
14. Gordeyev, Y.N., *Growth of a crack produced by hydraulic fracture in a poroelastic medium.* International Journal of Rock Mechanics and Mining Sciences & Geomechanics Abstracts, 1993. 30(3): p. 233-238.
15. Boone, T.J. and A.R. Ingraffea, *A numerical procedure for simulation of hydraulically-driven fracture propagation in poroelastic media.* International Journal for Numerical and Analytical Methods in Geomechanics, 1990. 14(1): p. 27-47.
16. Mourgues, R. and P.R. Cobbold, *Some tectonic consequences of fluid overpressures and seepage forces as demonstrated by sandbox modelling.* Tectonophysics, 2003. 376(1–2): p. 75-97.
17. Olson, J.E., S.E. Laubach, and R.H. Lander, *Natural Fracture Characterization in Tight Gas Sandstones: Integrating Mechanics and Diagenesis.* AAPG Bulletin, 2009. 93(11): p. 1535-1549.
18. Wangen, M., *Effective Permeability of Hydrofractured Sedimentary Rocks*, in *Norwegian Petroleum Society Special Publications*, G.K. Andreas and H. Robert, Editors. 2002, Elsevier. p. 61-74.
19. Engelder, T. and A. Lacazette, *Natural hydraulic fracturing*, in *Rock Joints: Proceedings of the international symposium on rock joints*, N.B.a.O. Stephansson, Editor. 1990, A.A. Balkema, Rotterdam: Loen, Norway. p. 35-44.
20. Rozhko, A.Y., Y.Y. Podladchikov, and F. Renard, *Failure Patterns Caused by Localized Rise in Pore-Fluid Overpressure and Effective Strength of Rocks.* Geophys. Res. Lett., 2007. 34(22): p. L22304.
21. Rozhko, A.Y., *Role of Seepage Forces on Seismicity Triggering.* Journal of Geophysical Research-Solid Earth, 2010. 115.
22. Adachi, J., et al., *Computer simulation of hydraulic fractures.* International Journal of Rock Mechanics and Mining Sciences, 2007. 44(5): p. 739-757.
23. Koehn, D., J. Arnold, and C.W. Passchier, *Fracture and Vein Patterns as Indicators of Deformation History: A Numerical Study.* Geological Society, London, Special Publications, 2005. 243(1): p. 11-24.
24. Johnsen, et al., *Pattern formation during air injection into granular materials confined in a circular Hele-Shaw cell.* Physical Review E, 2006. 74(1): p. 011301.
25. Johnsen, et al., *Coupled air/granular flow in a linear Hele-Shaw cell.* Physical Review E, 2007. 77(1): p. 011301.
26. Johnsen, et al., *Decompaction and fluidization of a saturated and confined granular medium by injection of a viscous liquid or gas.* Phys Rev E Stat Nonlin Soft Matter Phys, 2008. 78(5 Pt 1): p. 6.
27. McNamara, S., E.G. Flekkøy, and K.J. Måløy, *Grains and Gas Flow: Molecular Dynamics with Hydrodynamic Interactions.* Physical Review E, 2000. 61(4): p. 4054-4059.
28. Vinningland, J.L., et al., *Experiments and simulations of a gravitational granular flow instability.* Physical Review E, 2007a. 76(5): p. 051306.
29. Vinningland, J.L., et al., *Granular Rayleigh-Taylor instability: experiments and simulations.* Physical Review Letters, 2007b. 99(4): p. 048001.
30. Vinningland, J.L., et al., *Size invariance of the granular Rayleigh-Taylor instability.* Physical Review E, 2010. 81(4): p. 041308.
31. Vinningland, J.L., et al. *Granular Rayleigh-Taylor instability*. in *6th international conference on micromechanics of granular media, powder and grains*. 2009a: AIP.

32. Vinningland, J.L., et al. *Granular Rayleigh-Taylor instability*. in *Traffic and Granular Flow conference 2007*. 2009b. Orsay, 2009.
33. Niebling, M.J., et al., *Mixing of a Granular Layer Falling Through a Fluid.* Phys Rev E Stat Nonlin Soft Matter Phys, 2010a. 82(1 Pt 1): p. 7.
34. Niebling, M.J., et al., *Sedimentation Instabilities: Impact of the Fluid Compressibility and Viscosity.* Physical Review E, 2010b. 82(5): p. 051302.
35. Vinningland, J.L., et al., *Family-Vicsek Scaling of Detachment Fronts in Granular Rayleigh-Taylor Instabilities during Sedimentating Granular/Fluid Flows.* The European Physical Journal - Special Topics, 2012. 204(1): p. 27-40.
36. Niebling, M.J., et al., *Dynamic Aerofracture of Dense Granular Packings.* Physical Review E (accepted), 2012a.
37. Niebling, M.J., et al., *Estudios Numéricos de Aerofractures en Medios Poros / Numerical Studies of Aerofractures in Porous Media.* Revista Cubana de Fysica, 2012b. 29(1E): p. 66.
38. Goren, L., et al., *Pore Pressure Evolution in Deforming Granular Material: A General Formulation and the Infinitely Stiff Approximation.* J. Geophys. Res., 2010. 115(B9): p. B09216.
39. Goren, L., et al., *The Mechanical Coupling of Fluid-Filled Granular Material Under Shear.* Pure and Applied Geophysics, 2011. 168(12): p. 2289-2323.
40. Jackson, R., *The Dynamics of Fluidized Particles*. 2000: Cambridge University Press.
41. Denlinger, R.P. and R.M. Iverson, *Flow of Variably Fluidized Granular Masses across Three-Dimensional Terrain 2. Numerical Predictions and Experimental Tests.* J. Geophys. Res., 2001. 106(B1): p. 553-566.
42. Spickermann, A., et al., *A Grain-Fluid Mixture Model to Characterize the Dynamics of Active Lanslides in Fine-Grained Soils.* Journal of Geophysical Research-Solid Earth, 2012.
43. Bons, P.D., D. Koehn, and M.W. Jessell, *Microdynamics Simulation*. 2007: Springer.
44. Malthe-Sørenssen, A., et al., *Modeling and Characterization of Fracture Patterns in the Vatnajökull Glacier.* Geology, 1998a. 26(10): p. 931-934.
45. Malthe-Sørenssen, A., et al., *Simulation of Extensional Clay Fractures.* Physical Review E, 1998b. 58(5): p. 5548-5564.
46. Walmann, T., et al., *Scaling Relations for the Lengths and Widths of Fractures.* Physical Review Letters, 1996. 77(27): p. 5393-5396.
47. Gidaspow, D., *Multiphase Flow and Fluidization: Continuum and Kinetic Theory Descriptions*. 1994: Academic Press.
48. Beetstra, R., M.A. van der Hoef, and J.A.M. Kuipers, *Drag Force of Intermediate Reynolds Number Flow Past Mono- and Bidisperse Arrays of Spheres.* AIChE Journal, 2007. 53(2): p. 489-501.
49. Bruno, M.S. and F.M. Nakagawa, *Pore pressure influence on tensile fracture propagation in sedimentary rock.* International Journal of Rock Mechanics and Mining Sciences & Geomechanics Abstracts, 1991. 28(4): p. 261-273.
50. Doe, T.W. and G. Boyce, *Orientation of hydraulic fractures in salt under hydrostatic and non-hydrostatic stresses.* International Journal of Rock Mechanics and Mining Sciences & Geomechanics Abstracts, 1989. 26(6): p. 605-611.
51. Cuss, R.J., E.H. Rutter, and R.F. Holloway, *The Application of Critical State Soil Mechanics to the Mechanical Behaviour of Porous Sandstones.* International Journal of Rock Mechanics and Mining Sciences, 2003. 40(6): p. 847-862.
52. Wong, T.-f., C. David, and W. Zhu, *The Transition from Brittle Faulting to Cataclastic Flow in Porous Sandstones: Mechanical Deformation.* J. Geophys. Res., 1997. 102(B2): p. 3009-3025.
53. Wong, T.-f., H. Szeto, and J. Zhang, *Effect of Loading Path and Porosity on the Failure Mode of Porous Rocks.* Applied Mechanics Reviews, 1992. 45(8): p. 281-293.

54. Ling, H., et al., *Anisotropic Elastoplastic Bounding Surface Model for Cohesive Soils.* Journal of Engineering Mechanics, 2002. 128(7): p. 748-758.
55. Gerogiannopoulos, N.G. and E.T. Brown, *The Critical State Concept Applied to Rock.* International Journal of Rock Mechanics and Mining Sciences & Geomechanics Abstracts, 1978. 15(1): p. 1-10.
56. Zhu, W. and T.-f. Wong, *The Transition from Brittle Faulting to Cataclastic Flow: Permeability Evolution.* J. Geophys. Res., 1997. 102(B2): p. 3027-3041.
57. Sheldon, H.A., A.C. Barnicoat, and A. Ord, *Numerical Modelling of Faulting and Fluid Flow in Porous Rocks: An Approach Based on Critical State Soil Mechanics.* Journal of Structural Geology, 2006. 28(8): p. 1468-1482.
58. Steefel, C.I. and A.C. Lasaga, *A Coupled Model for Transport of Multiple Chemical Species and Kinetic Precipitation/Dissolution Reactions with Application to Reactive Flow in Single Phase Hydrothermal Systems.* American Journal of Science, 1994. 294(5): p. 529-592.
59. Sachau, T. and D. Koehn, *Melange: A viscoelastic lattice-particle model applicable to the lithosphere.* Geochemistry, Geophysics, Geosystems, 2012. 13(12): p. Q12009.
60. Press, W.H., *Numerical Recipes in C: The Art of Scientific Computing*. 1992: Cambridge University Press.
61. Wang, T.-Y. and C.C.-P. Chen, *Thermal-Adi: A Linear-Time Chip-Level Dynamic Thermal Simulation Algorithm Based on Alternating-Direction-Implicit (ADI) Method*, in *Proceedings of the 2001 international symposium on Physical design*. 2001, ACM: Sonoma, California, United States. p. 238-243.

5. Dynamics of hydrofracturing and permeability evolution in layered reservoirs

Abstract

A coupled hydro-mechanical model is presented to model fluid driven fracturing in a porous material that is structured as layered reservoir. In the model the solid elastic continuum is described by a hybrid lattice-particle model based on a discrete element approach coupled with a fluid continuum grid that is used to solve Darcy pressure diffusion. The model assumes poro-elastic effects and yields real time dynamic aspects of the fracturing and effective stress evolution under the influence of excess fluid pressure gradients. The model is used to study the formation of different fracture patterns in heterogeneous geological settings. We show that the formation and propagation of hydrofractures is highly sensitive to different mechanical and tectonic conditions. In cases where fluid pressure is the driving force, sealing layers induce permutation between the principal directions of the local stress tensors, which regulates the growth of vertical fractures and may result in irregular pattern formation or sub-horizontal failure below the seal. Stiffer layers tend to concentrate differential stresses and lead to vertical fracture growth, whereas the layer-contact tends to fracture if the strength of the neighboring rock is high. The stress field at the onset of fracturing becomes anisotropic, which eventually leads to the development of large-scale failure in the system by linking isolated tensile fractures. If the model is under extension for a long time, large-scale hydrofractures develop by linking up confined tensile fractures in competent layers. This leads to the formation of large-scale normal faults in the layered systems, so that subsequently the effective permeability is highly variable over time and the faults drain the system. The simulation results are well consistent with some of the field observations carried out in the Oman Mountains, where abnormal fluid pressure is reported to be a crucial factor in the development of several generations of regional fracture and fault sets, including bedding-normal and bedding-parallel fracturing.

5.1 Introduction

Fluid overpressure in the Earth's crust is an important physical characteristics and a major controlling factor for the mechanics of fracturing and faulting in a variety of geological settings [1, 2]. Overpressure yields a negative feedback on the integrated stress regime at depths in the crust and enhances the potential brittle deformation of rocks [3, 4] where

existing fractures and joints open and the frictional resistance in faults is reduced at a variety of scales (from grain to fault scales).

Regardless of the source origin (i.e. injection of extraneous fluid or internal yield), fluid assisted formation of load parallel or load oblique fractures are traditionally termed hydrofracturing. For instance, engineered hydrofracturing in petroleum engineering is a paradigmatic case. However, for natural systems, which are spatially and temporally subject to multisource stresses, this definition is not necessarily clear. Several authors tend to use the term hydrofracture for almost any extensional fracture in the Earth's crust with the argument that fluid pressure is needed to create tensile stresses and extension fractures [5, 6]. Others use the term hydrofracture explicitly for a fracture that is created by high fluid pressure and use the plain term fracture for tectonically induced cracks that may also have experienced fluid pressures [7-12]. Currently, the literature lacks a distinctive definition of what a fracture is termed that is dominantly produced by high fluid pressure in contrast to fractures that are produced due to a combination of tectonic stresses and fluid pressure. In this contribution we use the term hydrofracture to describe a fracture that forms solely due to fluid overpressure e.g., fluid production in a tectonically stable sedimentary basin and term fluid assisted fractures those that result from a combination of increase of active tectonic stresses and fluid pressures.

Mineral veins are the most abundant indicators of fluid assisted fracturing in the Earth's upper crust since they are often associated with extensional dilational sites in overpressured environments [13-15]]. Field observations typically show orthogonal vein sets that arrest or divert at layer interfaces [9, 16, 17]. The shape and orientation of these structures can provide information on the temporal and spatial evolution of the regional stress-strain fields, deformation kinematics as well as paleo-hydrogeology of sedimentary basins [18-20].

In general stress fields within the Earth's crust can change as a function of fluid pressure, tectonic stresses or material heterogeneities. In confined sedimentary basins (impermeable faults zones and cap rocks) as well as regions of low-grade metamorphism, high fluid pressure near to lithostatic pressure develops and eventually trigger fluid assisted fracturing or real hydrofracturing (Fig. 5.1). This phenomenon may also result in the permutation of the local stress tensor so that induced fractures become horizontal, a process that is sensitive to tectonic diagenesis and may trigger small scale seismic events and fault reactivation [21-25] Leclere et al. 2012]. In addition, [26] indicated that heterogeneity and contrasting mechanical properties in rocks can also induce changes in the order of magnitude of principal stresses and intrusive bodies e.g., horizontal dykes and sills may also render the process of stress permutation at least at the local scale [27, 28].

The mechanism of hydrofracturing is a highly dynamic process and comprises at least a two way feedback between the hydraulic and mechanical domains of a geological system

[29]. In porous rocks porosity is often related to the strength of the solid material and following poroelasticity is one of the governing factors for the permeability. Pressure oriented local stress perturbation and fracturing influences the primary porosity and increases the bulk permeability of the host rock. Hydrofracture propagation facilitates the development of permeable pathways, which significantly enhance flow rates. It has an impact on fluid migration, reservoir quality distribution [30-32], episodic expulsion and entrapment of ore-forming fluids [33] as well as the activation of geothermal circulation/venting with the induction of pressure and temperature anomalies [28, 34]. [35] describes the "toggle switch" behavior of hydrofractures leading to permeability enhancement and reduction by an instant change between the extremely low/high to high/low value of pressure. [Kobchenko et al., 2011] images how fractures get activated and transport fluid during heating of organic-rich shales.

An analysis of the growth of hydrofractures in heterogeneous reservoirs has shown that besides fluid overpressure, hydrofracture propagation depends primarily on the mechanical properties in particular the stiffness of the constituent units of host rock [9, 36]. Layer thickness and strength of layer contacts have also been shown to exhibit strong effects on the propagation and spacing of fractures as well as change in absolute permeability in layered rocks [5, 7, 8].Most of the previous numerical tools that are used to study fracturing however do not take a look at the real time effects of material properties (e.g., stress-effective porosity evolution and vice versa due to poroelasticity) on the developing fracture patterns. This effect is complex and depends on the fracture geometry, fluid pressure diffusion and the strain field conditions.

In this paper, we analyze the dynamic influence of change in material properties under the loadings of high fluid pressure gradient, gravity and tectonic stresses on the development of different fracture patterns analogues to field scale structures. The present work is the continuation of [37] in which a 2D coupled model based on Darcy diffusion of fluid pressure is introduced and implemented to study hydrofracturing in homogeneous porous rocks. The model permits the quantitative and qualitative study of the evolution of the effective stress field in accordance with porosity-effective pressure elevation, the dynamic interaction with the initiation and growth of fractures in terms of deformation-induced permeability variations and the respective pattern formation. In the current work, we consider layered heterogeneous rock configurations to discuss the corresponding effects of material properties (e.g., Young's modulus, breaking strength) and initial noise in the system on the developing structures. In addition, we give an example of how layer-confined vertical fractures develop into normal faults and how this transition changes the permeability (fluid flow) in a multi-layer sedimentary sequence.

In the next section we discuss the role of fluid overpressure in rock deformation followed by field observations, which were carried out in the Oman Mountains. Afterwards we describe the proposed numerical scheme and present simulation results of hydrofracturing

in heterogeneous rocks and their comparison with the natural examples. Finally we end up with discussion and conclusion of the study.

5.2 Fluid association in subsurface rock deformation

Fracturing in the brittle crust mainly takes place in mode-I extensional and dominated mode-II shearing depending on the balance between the differential stress ($\sigma_1 - \sigma_3$) and rock tensile strength T [24]. Theoretically, the predominant state of triaxial compressive stress due to gravity loading [38] favors only shear failure in rocks buried at depth, therefore for extensional fractures to open under these conditions, an additional force is needed to produce tensile stresses. This additional force is thought to come from the fluid pressure that builds up in pores and integrated fractures in the rocks [39-41].

Rocks in near surface geology normally contain fluids in interconnected pores and fracture networks. Thus, fluid pressure at depth is a function of the hydraulic head, leading to hydrostatic pressure profiles for slowly deforming rocks with interconnected pore networks. In a tectonically stable sedimentary basin the least principal stress σ_3 is a function of σ_1 ($\sigma_3 = \upsilon/_{1-\upsilon} \cdot \sigma_1$), with σ_1 being set by gravity i.e., given by the weight of the overlaying rocks. The Poisson ratio is normally around 0.25 to 0.3, so that the effective σ_3 will be close to zero or slightly tensile under normal homogeneous conditions. This scenario however changes once the fluids are confined, which can happen due to compaction of the rock matrix during diagenetic and metamorphic processes that lead to loss of porosity and hence permeability. Once the fluid is confined, the fluid pressure can rise above hydrostatic which can lead to pore fluid expulsion and reverses the fluid flow from a downward to an upward direction. This commonly also happens when impermeable layers in heterogeneous basins act as barriers for the fluid below. The elevated fluid pressure acts normal to horizontal layer interfaces and builds a steep pressure gradient across the seals.

In a fluid saturated rock mass, Terzaghi's normal effective stress σ'_{ij} is given by:

$$\sigma'_{ij} = \sigma_{ij} - P_f \delta_{ij} \tag{5.1}$$

where σ_{ij} is the total normal stress, P_f the pore fluid pressure and δ_{ij} the Kronecker delta with the sign convention of positive for compressive stress. If the fluid pressure is larger than σ_3, the effective stress becomes tensile and the rock may fail under mode-I failure. A Mohr diagram is often used to illustrate the respective fracturing mode in Rock Mechanics. In Fig. 5.1b the Mohr circle represents the 2D stress state in the Earth's crust with σ_1 and σ_3 being compressive on right hand side. Excess in fluid pressure P_f offsets the normal stresses and

reduces the value of the effective stresses. This drives the Mohr's circle towards the left along the σ_n-axis from its initial compressive stress state until it transects the composite Mohr-Coulomb failure envelop in the tensile regime. Eventually hydro-extension rock failure parallel to the direction of the maximum compressive stress occurs in the Earth's crust with $\sigma_1 - \sigma_3 < 4T$.

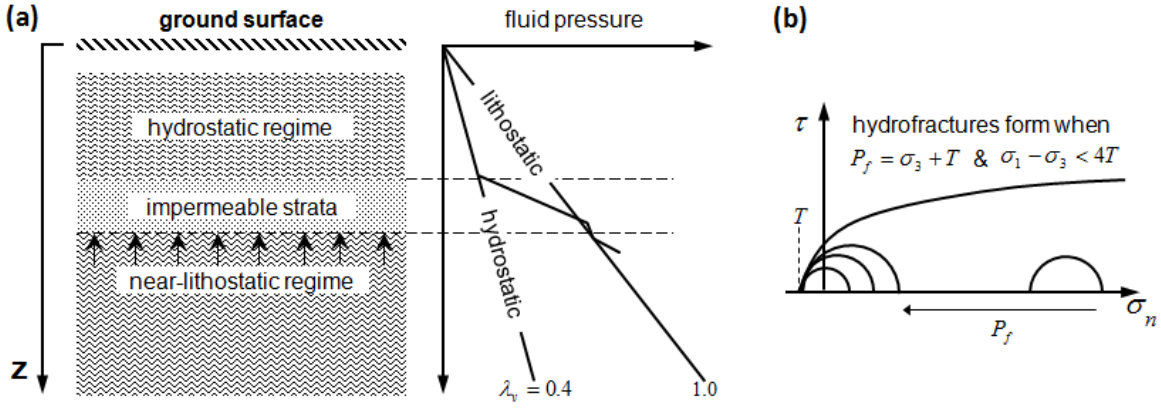

Figure 5.1 (**a**) A fluid pressure step-up from hydrostatic to order of lithostatic pressure generates a steep pressure gradient across the sub-horizontal seal layer in a heterogeneous sedimentary basin (after [24]). (**b**) Mohr circle analysis of fluid assisted rock failure. An increase in fluid pressure shifts the Mohr circle from its initial compressive stress state at the right side to left tensile regime until it transects the tensile strength of the rock or the Mohr-Coulomb failure envelope and eventually leads to extension or hybrid extension-shear fractures.

The above stated functionality of the fluid pressure is a simplification. This scenario is only an extreme end-member case, normally the rocks are porous and fluid can percolate through the rock. The actual force that acts on the walls of pores or fractures and leads to rock failure (hydrofracturing) is the fluid pressure gradient. In order to understand the effects of fluid pressure on fracturing and vice versa in heterogeneous systems one has to look at the evolution of fluid pressure gradients and the respective poroelastic response as a result of stress perturbations in the porous matrix [4, 29, 42-45]. For tensile fracturing in saturated rock the respected order of pore pressure pertaining to Biot's poroelastic response to Terzaghi's effective stress state can be approximated by the pore-fluid factor λ_v [24, 41].

$$\lambda_v = \frac{P_f}{\sigma_v} = \frac{\nu}{1-\alpha_p-(1-2\alpha_p)\nu} \tag{5.2}$$

where the pore-fluid factor is a ratio of pore fluid pressure to vertical stress . Depending on the poroelastic factor α_p (0 – 1 for most rocks) and the Poisson ratio ν of the rock, the pore pressure required for hydraulic extensional fracturing is hydrostatic if $(\lambda_v < 0.4)$ in near

surface extensional regimes, superhydrostatic $(0.4 < \lambda_v < 1.0)$ in low permeable and well cemented rocks and superlithostatic when $(\lambda_v \geq 1.0)$ in compressional regimes at depth.

In the presented numerical scheme we conceded a similar approach of poroelasticity where we model fluid flow through the rock and the buildup of effective stresses due to fluid pressure gradients explicitly to understand the influence of the fluid on the development of fracture patterns [45-47].

5.3 Field observation

In this section we present outcrop analogues of fluid filled fractures or veins observed in the Oman Mountains in Oman and discuss the contrasting driving forces, fluid pressure, gravity and tectonic stresses in forming these structures. The Oman Mountains are thought to have experienced significantly high fluid pressures [17, 48, 49] and are composed of a Permian to Cretaceous well-bedded dolomite and limestone sequence that overlies pre-Permian basement rocks. The geological history includes southwards directed overthrusting of the Oman ophiolite sequence, a large scale extensional event, the development of several strike slip systems and the final uplift of the mountains [49-52]. Especially extension and strike slip deformation were accompanied by several generations of regional fractures and faults, which are cemented with calcite and minor quartz. Bedding perpendicular vein sets often follow stress oriented anastomosing patterns with regular spacing showing single extensional or conjugate extensional shear patterns. These regularly spaced patterns seem to be overprinted by chaotic and very closely spaced veins that indicate the existence of extreme fluid pressure gradients. Fracture/vein localization seems to be influenced by the layer succession, where deformation is commonly linked to competent carbonate beds or along the layer interfaces (Fig. 5.2a). The bedding parallel veins are thought to be partly associated with the permutation of the effective stress field due to high fluid pressures. Moreover, most of the associated faults appear to act as fluid flow contributors (Fig. 5.2b) [49].

In Fig. 5.3 we show three outcrop examples of vein sets that are interpreted to be driven by different forces. Fig. 5.3a shows linear vein sets of variable spacing in a bedding plane on the very top of the sedimentary sequence in the Oman Mountains. The outcrop is situated just below a large-scale thrust where the Oman ophiolite with some exotic sedimentary units was thrust over the Permian to Cretaceous sequence. Though the veins in the layer follow several orientations they overall show a clear direction and spacing. We interpret the regularity of the pattern to reflect a heterogeneous stress field as a function of

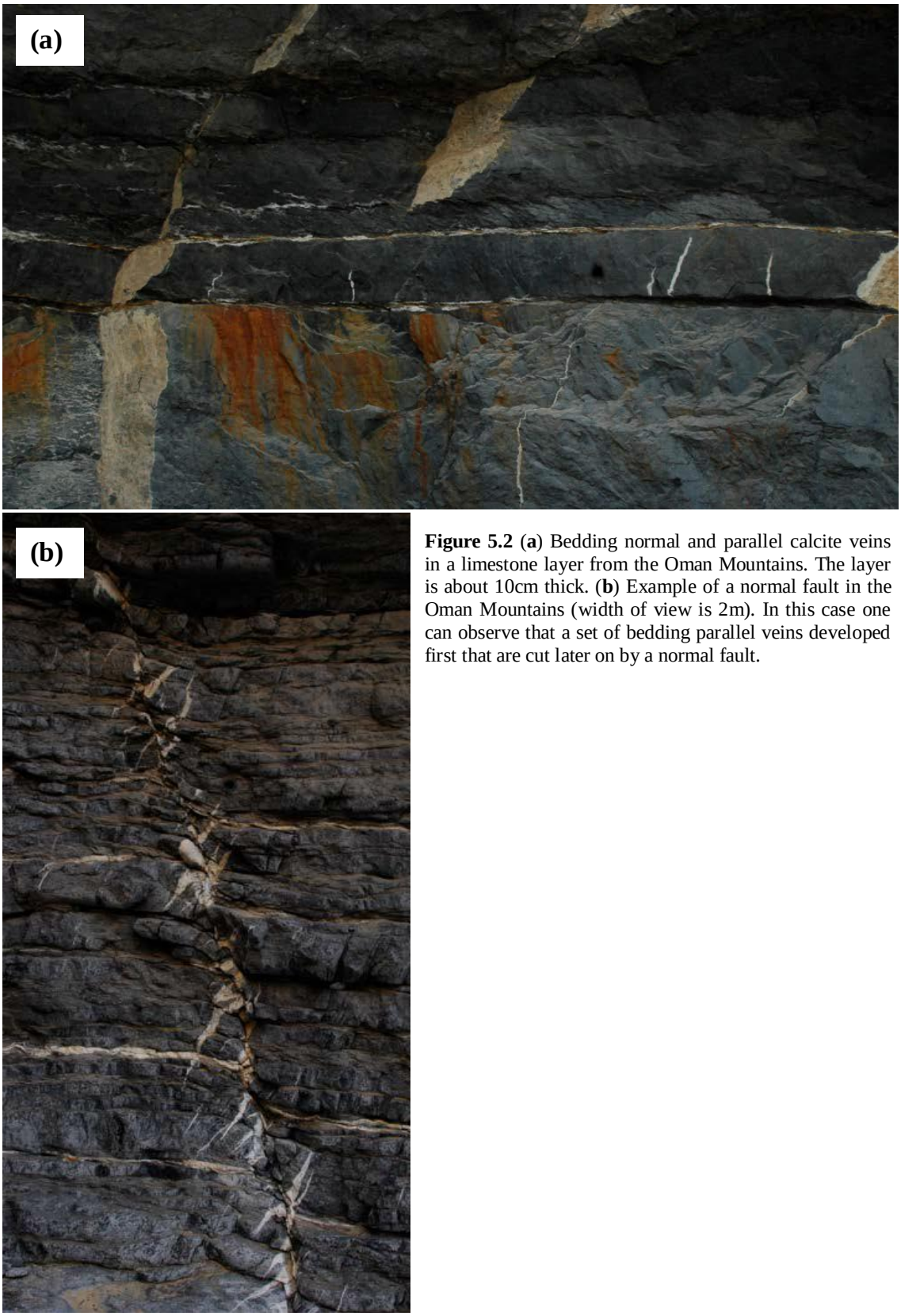

Figure 5.2 (**a**) Bedding normal and parallel calcite veins in a limestone layer from the Oman Mountains. The layer is about 10cm thick. (**b**) Example of a normal fault in the Oman Mountains (width of view is 2m). In this case one can observe that a set of bedding parallel veins developed first that are cut later on by a normal fault.


(a)


(b)

Figure 5.3 Different vein patterns in the uppermost Cretaceous carbonate units (a,b) and pre-Permian core rocks (c) of the Oman Mountains. (**a**) Well oriented and regular spaced linear vein geometries exhibit the dominant influence of tectonic stresses, (**b**) the spatial induction of immense calcite material despite the regular vein pattern portrays the mutual role of fluid pressure and tectonic stresses, and (**c**) pure hydrofracture having zigzag ascending geometry affirms the role of fluid pressure and gravity only.

tectonic stresses indicating that fluid pressure was not the dominant pattern forming force, so that they are tectonic fractures/veins. The second example in Fig. 5.3b shows veins in another locality of the same sequence as those shown in Fig. 5.3a. In this case the veins still show a systematic orientation. However, the intensity of the veins is spatially highly variable, so that some of the veins are so closely spaced that the host rock cannot be seen anymore. We argue that such a feature indicates that fluid pressure gradients may have started to play a role in the production of the veins. Therefore, in contrast to Fig. 5.3a, the veins shown in Fig. 5.3b may be termed hybrid hydro-tectonic fractures/veins since fluid pressure is important but some orientation symmetry is still present indicating an influence of tectonic stresses. Finally, the veins exposed in the basement rocks (pre-Permian) of the Oman Mountains are shown in Fig. 5.3c. These veins are found to be very thick, jagged and highly chaotic. Some of the veins are sub-horizontal while others follow a vertical zig-zag pattern. Neither spacing nor any preferred orientation are visible that may indicate any influence of tectonic stresses. In this case it is clear that high fluid pressure gradients and gravity did play the main role in pattern formation, which promotes the hypothesis that the developed veins are real hydrofractures.

5.4 Numerical model

In order to simulate the development of these structures numerically we employ a coupled two-dimensional hydro-mechanical approach to model a 2D pressurized sedimentary section in the Earth's crust. The model is explained in detail in [53]. The approach combines the continuum description of fluid pressure with a discrete description of deformable elastic solid where the later is represented by a hybrid triangular lattice-particle model and is blanketed over a stationary square grid of fluid field (larger lattice constant) such that the boundaries of the two entities coincide with each other. Accommodating local mass to momentum conservation a Darcy pressure gradient evolves for a given solid-fluid configuration according to local strain conditions through a poro-elasto-plastic relationship. The model is grounded on the same hypothesis as [45], which emphasizes the growth of hydro-driven fractures in the light of instantaneous and synergistic evolution of rock permeability and interstitial pressure diffusion in the porous elastic medium. In the following subsections we outline the constitutive elements of the coupled scheme.

5.4.1 Governing equation of fluid diffusion

It is assumed that the seepage forces on the local scale (particle scale) as a function of the evolution of fluid pressure gradients induces a localized perturbation in the effective stress field which may lead to rock deformation. Therefore, the continuum fluid phase is determined exclusively in terms of the pressure field $P(x,y)$, where (x,y) are the coordinates of the two dimensional grid space. The inertia of the fluid is not considered in the model, which is justified for a fluid flow with low Reynolds number.

Using Darcy law, the time dependent governing equation (5.3) of pressure diffusion is established from the mass conservation of fluid and solid in order to evince the seepage velocity of a compressible fluid through the porous media.

$$\phi\beta\left[\frac{\partial P}{\partial t}+u\nabla\cdot P\right]=\nabla\cdot\left[\left(1+\beta P\right)\frac{K}{\mu}\nabla P\right]-\left(1+\beta P\right)\nabla\cdot u \tag{5.3}$$

where $\phi=1-\rho$ is the porosity, β is the fluid compressibility, P is the fluid pressure and u is the solid velocity field. K and μ are the permeability and fluid viscosity respectively. The implementation of the evolution of the diffusion equation is obtained by an unconditionally stable time implicit Alternate Direction Implicit (ADI) method [54]. In the model, the pressure gradient over a given volume develops according to the permeability $K(x,y)$, which is treated as an implicit fluid flow property and is an explicit output of the discrete elastic model as a function of the variation in local porosity $\rho(x,y)$. Fluid compressibility is

assumed by considering the isothermal ideal gas law i.e., $\rho_f \propto P$ whereas the local permeability K is determined through the empirical Kozney-Carmen relation given by:

$$K(\rho, a) = \frac{r^2}{45} \frac{(1-\rho)^3}{\rho^2} \tag{5.4}$$

where r is the particle radius and 45 is an empirical constant valid for a packing of spherical beads.

5.4.2 Discrete model of elastic solid

The basis for the assigned Discrete Element Model (DEM) an elasto-plastic code is inherited from the software 'Latte' as part of software package 'Elle' [55]. The setup is a 2D hybrid lattice-particle model in which the particle model, as a discrete element material representation is agglomerated with a regular triangular lattice of volume-less linear elastic springs. With the elastic spring constant k as function of the macro-scale elastic material property E, the DEM model determines the discrete description of isotropic linear elastic continua of a real system and consequently can be used to simulate plain strain deformation problems according to linear elasticity theory [45].

$$k = \frac{\sqrt{3}}{2} El \tag{5.5}$$

where l stands for the thickness of the two dimensional configuration used in the model. In order to model heterogeneous material i.e., layered sedimentary rocks; local changes in spring constant k describe the corresponding variation in the mechanical properties (Young's modulus) of the material. A standard over-relaxation algorithm [56] is used to obtain the equilibrium configuration of the elastic system after each deformation time step (based on the net forces applied on each node). This technique uses successive relaxations close to the fracture tips as most of the deformation occurs near the tips of the fractures in a deformed system. In the plastic part of the model, springs break and imitate local mode-1 discrete failure of the material if the force acting on them exceeds a prescribed threshold (σ_c) corresponding to the local tensile strength upon the application of extraneous loadings. The average threshold of tensile strength is related to the stress intensity factor $K_I = \sigma_I \sqrt{c}$, where σ_I is the critical mode-I tensile stress for the relevant displacement of fracture walls and c is the characteristic length of micro-cracks in the material [45]. Broken springs get removed from the network and the associated particles lose cohesion but are still subject to repulsive forces when they meet, accommodating the neighboring successive tension.

Deformation mechanics of the coupled continuum-elastic model is governed by a mutual momentum exchange between the solid and fluid phases at the scale of a unit volume cell of the continuum system. The net force F_i^n acting on a particle i is composed of three components, interaction force f_e from neighboring particles either connected with spring or repulsive forces, seepage force f_p resulting from interstitial fluid pressure, and forces arising from boundary conditions i.e., gravity f_g and external tectonic force (strains) and is given as

$$F_i^n = f_e + f_p + f_g \tag{5.6}$$

5.4.3 Force pertaining to elasticity

In the elastic part of the model, each spring inherits a spring constant k and an equilibrium length a, which is identical to the sum of the initial radii of two connected particles. The inter-particle force f_e, which acts along the connected elastic springs is proportional to the given spring constant

$$f_e = \sum_j k_{ij} \left(|\vec{a}_{ij}| - |\vec{x}_i - \vec{x}_j| \right) \cdot \hat{n}_{ij} \tag{5.7}$$

where the sum is over all connected neighbor nodes j, $\vec{x}_i$ and $\vec{x}_j$ are the positions of the connected nodes, and $\hat{n}_{ij}$ is the unit vector pointing from the centroid of node i to node j.

5.4.4 Fluid seepage force

The seepage force is generated due to the gradient of the non-hydrostatic part of the pressure field and is a result of the momentum exchange between the elastic material and the viscous fluid flowing in the reservoir. Assuming negligible fluid-solid friction at the interface surface, the only coupling force is the pore pressure gradient ΔP induced by a fluid source in the reservoir. The pressure force f_p on the surface normal of a given particle configuration in the unit grid cell (Fig. 5.4c) of surface area dA is calculated by an area-weight smoothing function.

$$f_p = -\int P dA \tag{5.8}$$

where P corresponds to $P = P_o - \rho_f g z$, where P_o is the local fluid pressure in the reservoir at some reference depth z, ρ_f is the fluid density, and g the gravity constant.

5.4.5 Gravity loading

In the coupled model the term gravitational force incorporates the gravity effects of both the fluid and solid where the former together with the hydrostatic part of pore pressure determines the effective stress field $\sigma_{eff} = (\rho_s - \rho_f)gz$ in the elastic solid. The gravity force on each particle in the elastic scheme is inferred using the formulation

$$f_i^g = \rho_s \pi R_i^2 gC \tag{5.9}$$

where ρ_s is the solid mass density, $R_i = r_i \times S$ with S the dimension of the real system, g is the acceleration of gravity and C=2/3 is a scale factor derived in [37] to acquire a compatible one dimensional lithostatic stress for an isotropic 2D linear elastic solid.

5.4.6 Implementation

The two way interaction between the porous solid and the hydrodynamic phase is achieved through the use of a projection operator from the discrete space to the fluid grid space, using a smoothing function $s(r_i - r_o)$, which distributes the weight of a particle over the four neighboring fluid grid nodes as shown in Fig. 5.4c.

$$s(r_i - r_o) = \begin{cases} \left(1 - \dfrac{l_x}{\Delta x}\right)\left(1 - \dfrac{l_y}{\Delta y}\right) & \text{if } l_x < \Delta x,\ l_y < \Delta y \\ 0 & \text{otherwise} \end{cases} \tag{5.10}$$

where $r_i(x, y)$, $r_o(x, y)$ are the positions of the particle and grid node respectively, $l_x = |x_i - x_o|$ and $l_y = |y_i - y_o|$ are the relative distances and Δx, Δy are the lattice constant along the x and y coordinates. This setup is also called "cloud in cell" method which renders the translation of mass m and velocity v of individual particles into continuous local particle density $\rho(r_o) = \sum_i s(r_i - r_o)$ and velocity fields $u(r_o) = \sum_i u_i s(r_i - r_o)$, where subscript i runs over the number of particles present in a unit area associated with a particular grid node at position r_o. The same smoothing function is also used to obtain the drag force $f_p = -\sum_k s(r_i - r_o)\left(\nabla p / \rho_n\right)_k$ on a single particle due to fluid pressure, index k runs over four nearest grid nodes. The basic approximations to this approach are the multiplication of the calculated 2D solid fraction with 2/3, as well as setting of a lower cutoff of the 2D solid fraction e.g., $\rho_{\min} = 0.25$.

Two different approaches have been used in order to account for anisotropies in the model, we insert single layers and multi-layers of dissimilar material and sedimentary properties. A single horizontal layer is defined in the lower half section of the model in order to depict a sealed reservoir which inherits different stiffness values and low permeability relative to the underlying reservoir and overburden matrices (Fig. 5.4a, b). In the multi-layered model, four layers of low permeability and high stiffness are considered at regular intervals along the ordinate coordinate. According to the boundary conditions considered, loading includes an increase of fluid pressure in the fluid grid field(corresponding to phase transition, fluid source or fluid injection in this zone), a vertical loading due to gravity, or a horizontal loading due to tectonic strains by moving the lateral boundary walls. In all models, the elastic system is constrained by elastic walls at the two lateral and the bottom boundaries, whereas the upper boundary is set free in order to get the equilibrium under gravity loading. The elastic walls are described as linear elastic springs so that the force on any interacting particle from a wall is proportional to the distance that the particle is pushed into the wall. For instance, the force by a lateral wall on the particle i contacted at location $x = x_w$ is

$$f_i = \begin{cases} -k_w(x_i + r_i - x_w)n_x & \text{if } x_i + r_i - x_w > 0 \\ 0 & \text{else} \end{cases} \tag{5.11}$$

where k_w is a spring constant for wall interaction r_i is the particle radius, n_i is a unit vector along the x-axis. In the elastic domain, relaxation and plastic deformation is assumed to be instantaneous relative to the diffusion of the fluid pressure. After each time dependent diffusion step of fluid pressure, the elastic equilibrium is acquired on account of the elasto-plastic deformation in the material by the subjected seepage forces and other loadings.

The elastic constant of springs is taken as an average of the constants of the respective particles connected at their ends. This presents a gradual change of mechanical properties corresponding to models of layered sedimentary rocks, i.e., at layer interfaces. The Young's modulus, breaking strength of springs and the layer thicknesses are predefined in the models where stresses and tensile strength of the material are described as a function of local elastic constants given at the particle scale and the Young's modulus of the material. In the model, these quantities are measured in a non-dimensional coordinate system where default values of the initial elastic constant and the tensile strength of the springs are set as 1.0 and 0.00125 respectively. By using scaling relations the simulated quantities are then rescaled in order to compare the real geological scale. Most sedimentary rocks possess a Young's modulus within the range 5-80 GPa [8], therefore if we consider that an elastic constant of 1.0 in the model equals 10 GPa, the breaking strength of the springs scales to 12.5 MPa by $\sigma_\circ = E_\circ \sigma'$, where $E_\circ$ is Young's modulus of the material.

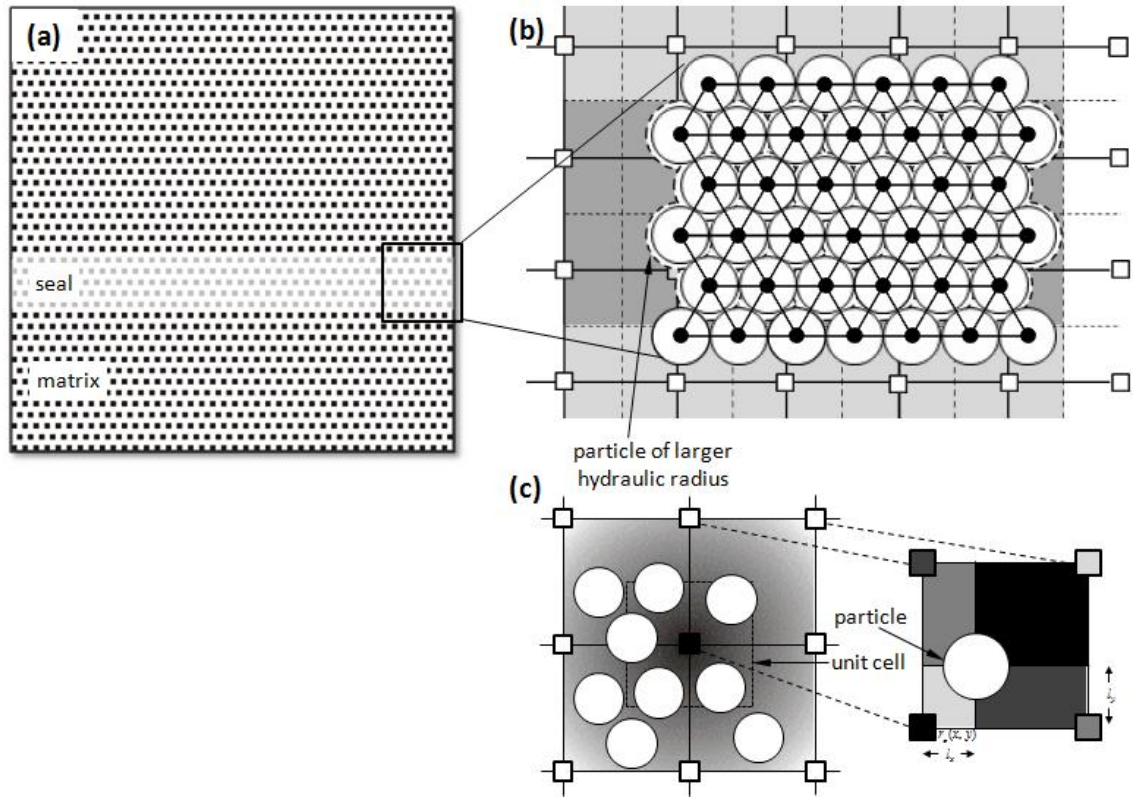

Figure 5.4 Initial model configuration and fluid-solid interaction criteria. (**a**) A single layered caprock geometry, where a sub-horizontal low permeable layer is sandwiched between permeable matrices. (**b**) Coupled particle-lattice model overlapping the pressure grid field in physical space. Linear dark grey background depicts transaction of hydrostatic to lithostatic fluid pressures due to a low permeable seal. (**c**) Fluid-solid interaction according to the smoothing function, grey background depicts the pressure gradient towards the central fluid node.

The respective constituents of the elastic system are assumed to be homogeneous corresponding to their material properties on large scale, however in order to grasp the effect of the inherited disorder of a real material, we set a pseudo-random distribution of material strength. Natural disorder in geological media corresponds to the ubiquitous presence of Griffith's micro-cracks, variation in their densities and lengths and other defects, which are present at the grain scale. It has been demonstrated that fracture patterns that are observed both in the field and laboratory can be numerically reproduced by implying realistic normal distributions of strength thresholds in DEM models [18, 57, 58]. Therefore, an algorithm is used to produce a Gaussian/Lognormal distribution of breaking strength in order to quench the natural heterogeneity in the model around the mean values on the scale of individual particles. The breaking strength of the material is sensitive to the lower values of the quenched distribution.

The subsequent model setup is thus analogous to confined reservoirs with seal layers of very low permeability. In each simulation the coupled model starts from a fully relaxed

state and is loaded in small steps afterwards. The model is subject to a random pressure source that complies a probability distribution function ($0 \leq P \leq 1$) with a maximum pressure in the middle of the lower permeable layer (below the seal). An increase in pore pressure in the source layer creates a linear pressure gradient across the impermeable seal, which ultimately develops high buoyancy forces in the surrounding matrix. This causes high concentration of stresses in the seal layer and depending on material properties of the model constituents it triggers different patterns of successive mode-1 fracture propagation at relatively weak rock elements (intrinsic flaws). The induction of the tension fractures (opening) accommodates the strain and eventually the stress relief in the elastic system following a rearrangement of particle positions. This concurrently promotes the local change in the background porosity, which by influencing the permeability results in diffusion of pore pressure in the fractured zone. The evolution of fluid pore pressure again provides feedback to the stress field in the system and leads to fracture growth along the pressure gradient and results in a regular fracture geometry. The cycle is echoed successively following the two-way temporal and spatial feedback between hydraulic pressure and strain evolution and associated fracturing in the porous matrix until both the continuity equation and the elastic lattice are relaxed and fracturing ceases.

A varying range of mechanical and hydraulic properties are used in the simulation setup in order to realistically represent the mechanism of quasi-static hydro-driven brittle deformation in heterogeneous rocks in the shallow crust. This involves a switch from sub-vertical to horizontal tensile fracturing as a function of the direction of the principal stress tensors due to high pressure gradients in high pressurized systems [24, 49] as well as in low permeability fault zones [25].

5.5 Results

We present 5 different simulations where the first four have a geometry with one horizontal low-permeable layer – similar to a cap-rock, whereas the fifth simulation contains multiple layers. Fig. 5.4a illustrates the initial configuration of the single layered models where a horizontal layer with a thickness of 10 percent of the model height is emplaced in the lower half of the simulation. We investigate the state of stresses, patterns of hydrofracture propagation and the potential system failure as a function of the mechanical properties of the impermeable seal layer relative to the surrounding matrix. Tectonic loading is not included in these models. The fifth example shows fracture formation under an extensional stress regime in addition to abnormal fluid overpressure and gravity.

In all the simulations the solid skeleton (elastic lattice) of the reference model has a resolution of 100×150 disc-shaped particles which define an area of 1:1 km, the model thus bears a linear gravitational loading of a 1km long sedimentary column in the uppermost crust with a Poisson ratio of 1/3. The mechanical parameters and other characteristics for the

respective simulation examples are given in (Table 1), a low average porosity of 6% is taken for seal layers compared to 30% of the surrounding matrix. As boundary conditions the coupled system is confined mechanically at the lateral and lower boundaries until otherwise described whereas hydraulically it is restrained only at the side boundaries. The breaking strength of springs in the model varies in order to induce a noise on the system. The distribution of breaking strength set for the different simulations are shown in Fig. 5.5. The fluid has a compressibility of $4.5e^{-10}$ Pa^{-1}, a viscosity of 0.001 Pas and one time step in the simulations is equivalent to 0.1 days. Fluid pressure at the top of the box is set to 0MPa whereas the bottom boundary is set to 10MPa (assuming hydrostatic pressures). Fluid pressure input is fast enough for fluid pressure gradients to build up.

5.5.1 Fracturing in single layer confined reservoirs

In the first simulation we attempt to model bedding parallel and bedding normal fractures in a heterogeneous medium, structures that can be found often in limestone sequences of the Oman Mountains (Fig. 5.2a). Fig. 5.6a shows the model evolution where red color code represents the matrix, darker red the stiff seal layer and blue fractures. The background dimensionless strength of the matrix varies between 0.0006 to 0.0033 with an average of 0.001. Using 35GPa as default Young's modulus of the system the strength refers to a range of 21-115 MPa with an average of 35 MPa. In the simulation the Young's modulus of the seal layer is taken to be 10 times higher than the surrounding matrix. In addition the breaking strength of springs in the horizontal seal layer are set to be 5 times lower than the strength of the matrix. The breaking strength of the whole aggregate will be controlled mainly by the lower values, between 21-28 MPa for the first case (surrounding matrix) and 4-7 MPa for the second case (seal).

The development of the fracture pattern in Fig. 5.6a shows that the layer first develops layer perpendicular fractures. These are initiated by the fluid pressure gradient, however their orientation is due to the heterogeneous stress field as a function of gravity so that the lowest stress is horizontal. During successive increase in fluid pressure the initial fractures cannot drain the system and a horizontal fracture develops at the lower contact of the seal. In the closed and confined system, seepage forces generated by the accumulated pore pressure counter the lithostatic stress component σ_v under the influence of poroelastic effects. The vertical compressive stress reduces in a non-linear fashion and gradually turns into the tensile regime (Fig. 5.6c). In the absence of any tectonic loading a subsequent increase in fluid pressure results in the directional switch of the compressive stress components, upon which the system is subjected to overburden uplift at the layer interface as well as the concentration of stresses in the low permeable seal layer (Fig. 5.6b). The simulation exhibits two patterns of hydrofracture growth due to a high Young's modulus of the seal layer. Fluid pressure gradients and a high stress concentration in the seal lead to layer perpendicular fractures. In addition as shown in graph (Fig. 5.6c), the vertical stress component reduces faster than the

horizontal component which leads to a second set of successive layer parallel fractures at the seal and source layer interface. This results in tensile/hybrid tensile shear fracturing along the layer interface and eventually leads the seal to fail horizontally. A graph showing the evolution of the stresses in the vertical (y) and the horizontal (x) directions and the corresponding trend of a Mohr diagram during the simulation run are illustrated respectively in (Fig. 5.6c, d).

Table 1 Parametric values for different numerical experiments

	Simulation 1	Simulation 2	Simulation 3	Simulation 4	Simulation 5
Model (default)					
Young's modulus E (GPa)	35	80	80	80	80
Breaking strength (MPa)	21 - 115	5 - 74	5 - 74	5 - 74	5 - 74
Av. Strength (MPa)	35	15	15	15	15
Av. Porosity (%)	30	30	30	30	30
Seal					
Relative Young modulus E (GPa)	10	1	1	1	5
Relative breaking strength	0.5	1	0.5	0.1	1
Relative porosity	0.2	0.2	0.2	0.2	0.2

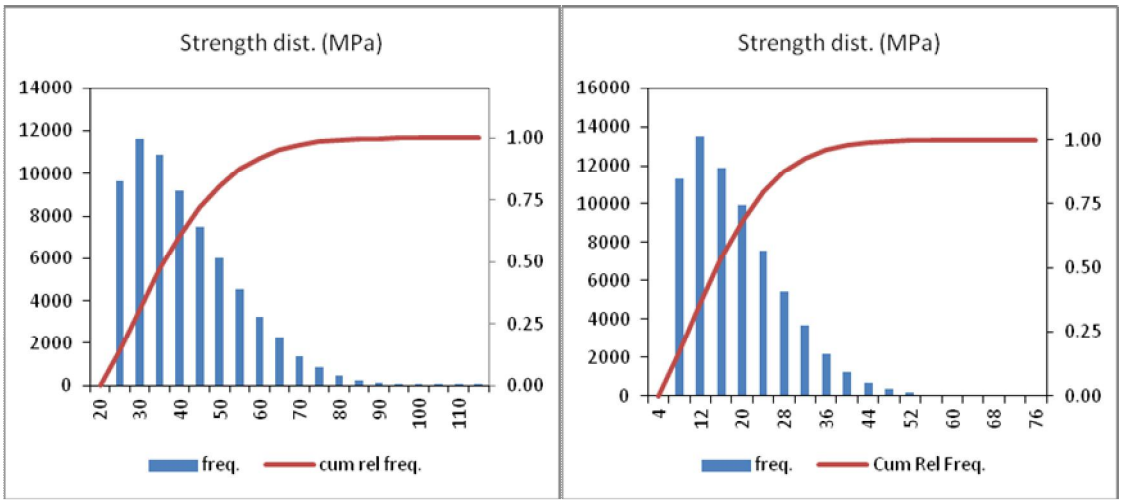

Figure 5.5 Default breaking strength distribution (scaled values) of elastic springs used for the different simulations, (**left**) in experiments 1 and (**right**) in experiments 2-5.

The presumed setup is analogous to confined reservoirs with seal rocks of low permeability. Seals in fluid filled layered reservoirs are commonly soft rocks i.e., shales, however during the evolution of sedimentary basin the mechanical compaction and other diagenetic processes may increase the stiffness of the soft seal up to a significant order of magnitude, which may change the conditions for hydrofracturing, their arrest and propagation over time [9]. If an increase in internal fluid pressure is the main forcing, it seems that a soft layer above the seal behaves as stress obstruction for fracture propagation.

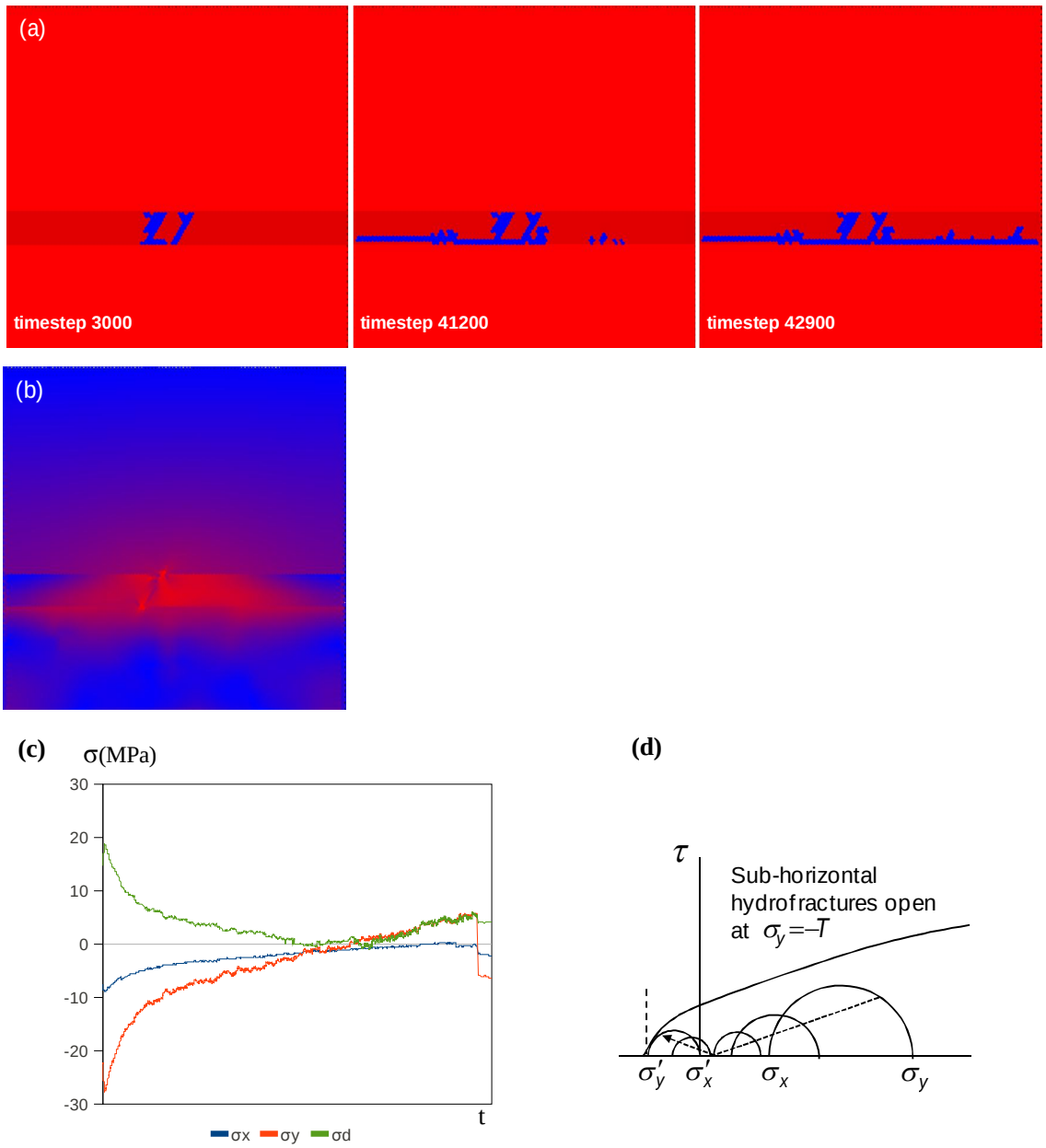

Figure 5.6 (**a**) Initial layer perpendicular hydrofracture in a stiffer impermeable seal (dark red layer) followed by final layer parallel shearing. Fluid is injected randomly in the lowest soft and permeable layer. This creates a high pressure drop across the seal and results in permeability changes through fracturing. Time T proceeds from left to right and fractures are represented by blue color. (**b**) Figure depicts the differential stress state on the onset of fracturing in the system, where the blue color represents low and the red high differential stress. The less permeable seal shows high stress concentrations whereas the layer below the seal shows low stresses due to high fluid pressures. The high differential stress that is accumulated in the stiffer seal layer is relieved with time following fracturing in the seal. (**c**) Evolution of the magnitude of the stress in the x and y direction and the differential stress in the seal. A switch from compressive to a tensile state of vertical stress is seen in the seal and at the interface due to low permeability of the seal comply the condition for layer parallel fracturing. (**d**) Mohr circle description of the stress states graphed in Fig. 5.6c.

In this case the heterogeneous system may fail in the form of layer parallel shearing at the macro scale and thus facilitate fluid migration along layer contacts. This is in agreement with field studies [6, 48], which indicate that vertically growing fractures preferentially propagate through stiff rocks rather than through soft layers. On this basis one may predict that bedding parallel veins like the one shown in Fig. 5.2a are a sign of abnormal fluid pressure.

In the next three simulations of hydrofracture development, we vary the breaking strength of the enclosed impermeable seal layer from 1.0 over 0.5 to 0.1 times less in magnitude than that of surrounding matrix, which result in a strong, medium and weak layer. A default Young's modulus of 80 GPa and a non-dimensional strength distribution of 0.00006-0.00093 with an average 0.00018 is allocated to the elastic springs in the model which scales to a range of 5-74 MPa and an average 15 MPa breaking strength in real rocks. Fig. 5.7 illustrates the evolution of resulting fracture patterns in the respective model setups where Fig. 5.7a shows simulation run with a strong seal layer, Fig. 5.7b with a medium and Fig. 5.7c with a weak seal layer. The layered heterogeneities have a great influence on the fracture propagation and derive variable pattern development. In addition, with a relatively small breaking strength of the matrix as compared with simulation in Fig. 5.6, the fluid pressure gradient at the source is high enough to fracture the weaker matrix around the pressure source. Vertical tension fractures nucleate at the source zone in the lower layer and propagate upward under the influence of gravity and the pressure gradients.

In Fig. 5.7a the growing fractures when reach the seal they are obstructed and stop to propagate vertically (Fig. 5.7a, timestep: 700) indicating the stress barrier behavior of the strong seal layer. Because the mechanical properties of matrix and seal layer are the same, the stress concentration in the seal due to buoyancy force is not high enough to promote fracture propagation across the seal. It is rather deduced that due to high permeability contrast the continuous build up of fluid pressure does re-orient the principal stresses in the source layer so that the fractures below the seal propagate sideways and the seal does not fracture (Fig. 5.7a, timestep:750).

The second and third simulations (Fig. 5.7b, 7c) show a different scenario. In Fig. 5.7b the strength of the seal is less so that a vertically growing fracture transects the whole seal layer (timestep: 600) up to its contact with upper permeable and strong layer. Most of the fracturing however still occurred in lower layer subsequent to minor fracture reorientation in later stage (timestep: 750) which shows an intermediate case of fracture patterns. On contrary, simulation in Fig. 5.7c where with the same rate of pressure build up the now weak impermeable seal (strength $1/10^{th}$ of matrix) tends to fail concurrently with the upward propagation of hydrofractures. All the fractures orientate along the pressure gradient throughout the simulation run and no second generation of horizontal fractures develop in the lower layer. In both simulations Fig. 5.7b & 7c, the developing fractures propagate from

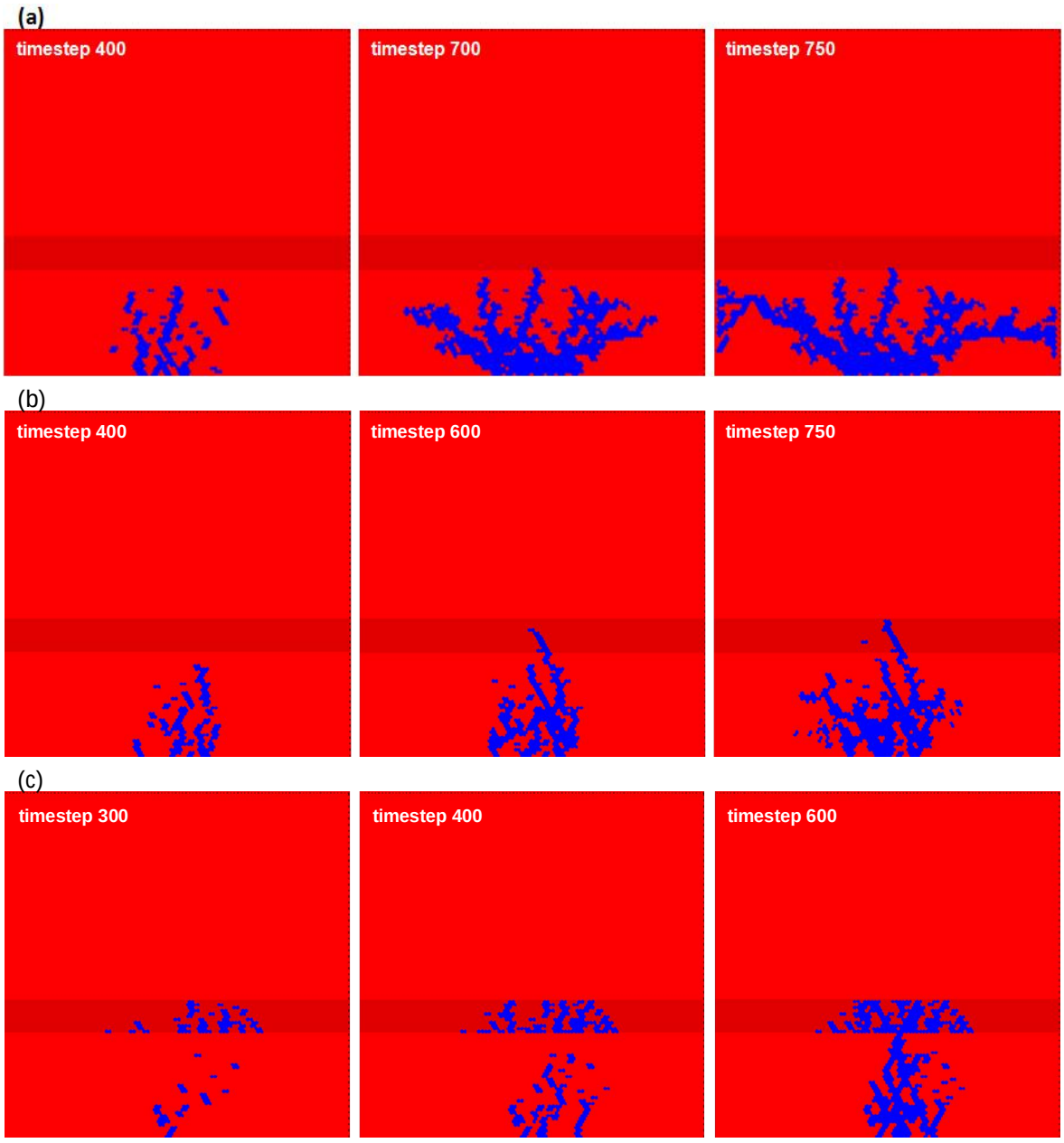

Figure 5.7 (**a**) Development of irregular hydrofractures around an elliptical source in a weaker rock unit. Due to comparative high strength of the seal the growing fractures could not propagate into the seal layer and change from a vertical to a sub-horizontal direction indicating the likely influence of the seal's impermeability to fluid pressure diffusion and stress fields. (**b**) & (**c**) illustrate the developing fracture patterns correspond to a seal layer that is 0.5 and 0.1 times weaker than the seal shown in simulation (**a**). It is shown that the seal with a lower strength has a higher probability of seal failure and of vertical propagation of hydrofracture. The vertical growing hydrofracture from the source zone links up with the fragmented parts of the much weaker seal layer.

strong to weak layers, however the propagation pass out in the reverse case and restricted mostly in the weak seal layer. It is therefore depicted that though impermeability of seal layer is prerequisite for the generation of pressure gradient beneath it, however in the only

loading of fluid pressure the fate of seal failure is highly dependent on the presence of background vertical discontinuities. Reduction in strength of the seal layer leads to vertical hydrofractures that gradually form from horizontal fractures.

The patterns of simulation 7a are similar to field example of hydrofractures as shown in Fig. 5.3c, where large veins develop in the basement of the Oman Mountains in relatively soft schist. The veins are thick and show orientations that are very similar to the hydrofractures in the simulated examples, they look like sheets and steep conjugate shear like fractures.

5.5.2 Transition from fracturing to faulting in multilayer systems

In the following simulation, we illustrate how tectonic deformation, fluid pressure gradients and gravity can influence the development of fracture networks in multilayer systems. The model setup consists of four hard layers of low permeability that are interbedded in a regular sequence with soft permeable layers. The model contains the same default values of the material parameters that are used in the last three simulations, however the Young's modulus of the impermeable layers is considered to be 5 times higher than that of the permeable layers. For the first 25000 time steps (6.8 yrs) the model was subjected to gravity and fluid pressure input in order to build up a realistic hydraulic gradient (fluid pressure rise up to lithostatic levels 25 MPa) in the system. Onward, a lateral tensile strain in form of outward movement of right boundary wall with a constant rate $\Delta\varepsilon = 1e-7$ step^{-1} was introduced to the system in order to model tectonic forcing.

Fig. 5.8 illustrates the evolution of normal faulting during four time steps corresponding to 0.36, 0.54, 0.74 and 1.9 m extension over the whole deformation system. It is shown that once tectonic strain builds up, the hard layers in the heterogeneous system start to fracture and develop a characteristic spacing, whereas the soft permeable matrix does not fracture. After time step 30400 (8.3 yrs) the fluid pressure gradients are high enough to fracture the soft matrix around the source and a larger scale fracture develops that propagates through the lower layers. After time step 32400 (8.87 yrs) the upward growing fracture runs through the whole system by interacting with the local fractures in the hard layers and eventually turns into large-scale normal fault. With progressive deformation the induced fault zone becomes highly permeable and serves as fluid pathway through the system. This observation is consistent with the field example (Fig. 5.2b) where a fault is associated with vein sets and affirms that the similar deformation sequence is responsible for some of the veins and fault sets in the Oman Mountains. The draining of the system by the permeable large-scale fault can also be observed in Fig. 5.8b, c that illustrate the development of fluid pathways through the model. Note that the local layer perpendicular fractures are not part of this large-scale fluid drain. Our model shows a behavior that is often observed in real system and can also be found in the Oman mountains. Layer perpendicular veins develop first but

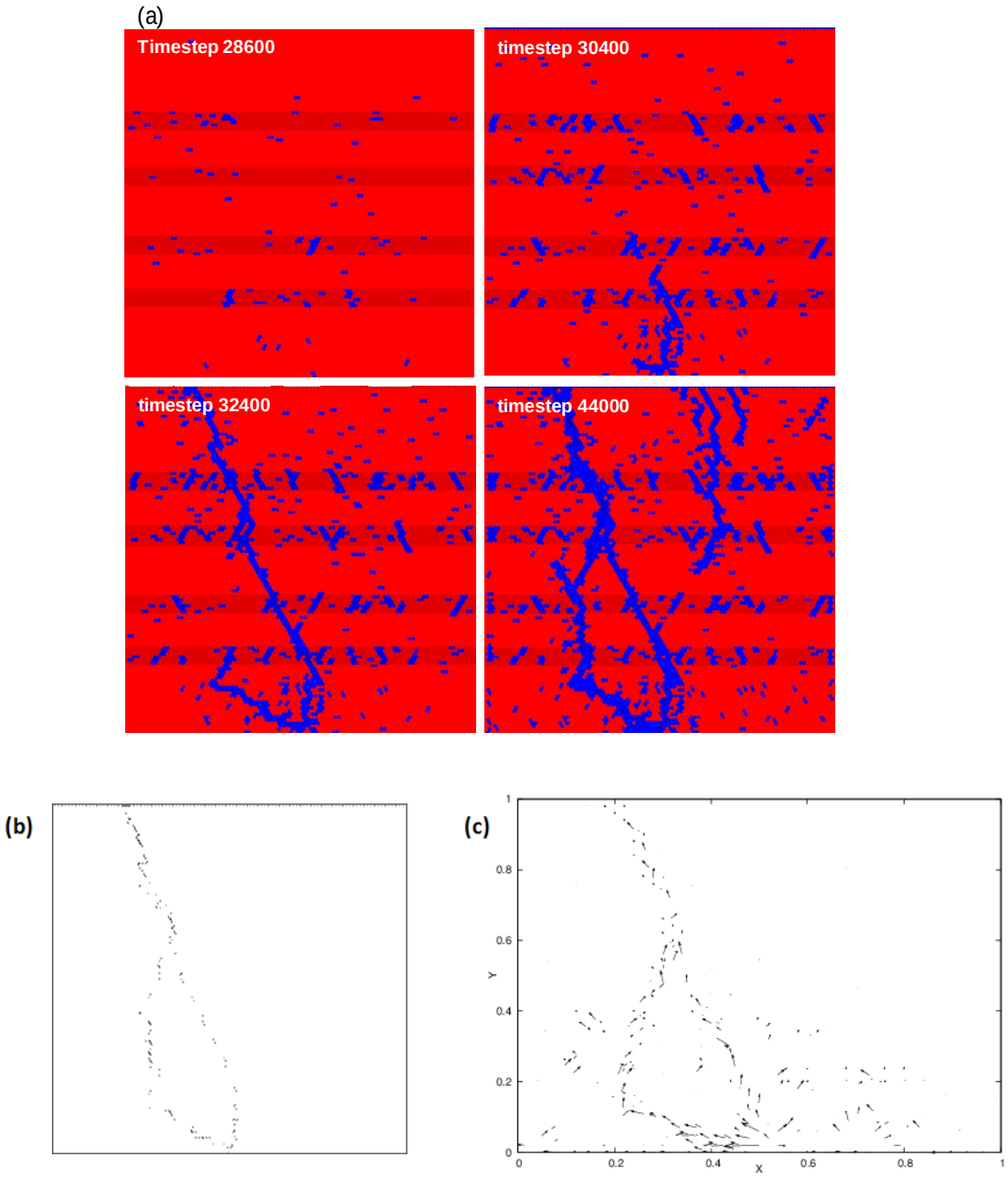

Figure 5.8 (**a**) Vertical propagating fault connecting the isolated small-scaled fractures in competent seal layers (dark red) which are caused by tectonic stresses in an extension dominated regime (timesteps correspond to lateral extension of 0.36, 0.54, 0.74 and 1.9 m respectively, where one time step is 0.1 days). This observed pattern is very similar to the field example (Fig. 5.2b). (**b**) Figure depicts the corresponding dilation of the fault plane, whereas (**c**) shows the resultant directional fluid flow field, where fluid drains through the system along the connected pathway. The simulation box is of dimension 1:1km.

they are mainly associated with local fluid flow and develop because of the mechanical properties of specific layers. If the spacing is uniform this implies that tectonic forces are the main driver for these structures. Once strain becomes larger and fluid pressures are involved,

the vein network develops into mature large-scale faults that localize fluid flow and can drain a high pressure system. This scenario may be present in the Oman mountains where layer perpendicular veins develop in hard carbonate beds and large-scale normal faults cut through the whole sequence and seem to drain deeper fluids [49].

5.6 Discussion

The proposed two-dimensional hybrid hydro-elastic model successfully reproduces realistic patterns of fractures and faults that are associated with fluid pressure gradients as well as gravity and tectonic loading. The coupled model inherits a two-way feedback between the continuum and elastic domains and imitates the evolution of field scale veins and fracture networks in a layered sedimentary system. The presence of large pressure gradients due to permeability contrasts between the seal and the surrounding layers, and the dynamic link between fluid pressure and fracture growth causes oscillations of the stress field in the adjacent rock units immediately after a fracture forms.

In the first example we compare the numerical results with bedding parallel and irregular vein sets as shown in Fig. 5.2a & 5.3c. It is observed that heterogeneity in the lithology and mechanical properties e.g., Young's modulus, breaking strength distribution influence strongly the evolution of buoyancy, fracture patterns and localization in seal and host rock layers. It is well established that hydrofractures in layered sedimentary rock sequences are more likely to develop in and propagate through stiff rather than soft layers due to concentration of stresses in the stiffer layers.

However, the layer contact is also considered to be an important parameter that represents a discontinuity in the matrix. Being a weaker zone in the solid continua layer contacts are case sensitive to the elevated effective stress gradient and tend to open up and thus influence the pattern formation of growing hydrofractures [59, 60]. In our simulation, a high contrast in mechanical and material properties between the layers causes a weak bedding contact that fails once it is subject to high fluid pressure gradients. Most cap rocks in fluid filled layered reservoirs are shales that are composed of parallel-aligned clay minerals. Compaction and other diagenetic processes during the evolution of basins may result in further reduction of the clay's permeability, an increase in stiffness or the development of mechanical weak pockets in intrinsic strength [9], which may further alter the conditions of hydrofracturing in layered reservoirs over time.

In this contribution we are simulating uniaxial strain models (gravity loading in undrained or tectonically relaxed basin), in which σ_{h} increases with increasing Pf as consequence of poroelastic effects and eventually favors the propagation of fractures in the horizontal direction, a scenario that is usually associated with accretionary wedges [40, 61]. In the presence of a free upper surface the poroelastically derived stress field faces relatively

less resistance in the vertical direction so that the system may expand vertically. If stresses are confined in the horizontal direction σ_h may become larger in magnitude than σ_v so that conditions for horizontal fracture propagation are approached. Bedding parallel veins have generally been attributed to represent local principal stress permutations as a function of basinal supra-hydrostatic fluid pressure [49]. One should however note that seal thickness is also pivotal for pattern formation and fracture spacing.

The strength distribution of the matrix is another crucial material property that can regulate the dynamics of induced hydrofractures and is commonly simplified in numerical studies. A weaker seal layer will likely fail in a vertical direction during the ascending growth of hydrofractures and will thus contribute to channeling of pressurized fluid flow across the seal to more permeable layers. Conversely a seal with a comparably high strength turns up to be a stress barrier to the vertically propagating fractures. Restriction in fracture propagation results in an increase in fluid pressure, which may cause a switch in the direction of principal effective stresses in the permeable host layer and subsequently divert the growth of the initially vertically induced fractures to near horizontal fracture sets. This situation is reached druing the emplacement of sills where fluid pressure is at or above the lithostatic [62]. This is consistent with [45], who states that in a geological context a vertical permeability variation is not enough to induce cap rock fracturing if the fluid pressure is the only driving force but that the background heterogeneity in the material properties is also important.

The developing fracture patterns in the simulations depend strongly on the fluid pressure gradient. This is inconsistent with the idea that fluid pressure in rocks only moves the Mohr circle towards the tensile regime to induce extensional fractures. This leads to the wrong prediction of patterns and does not separate a fracture that is produce by fluid pressure gradients from a fracture that is produced by tectonic stresses. The simple approach does not treat fluid pressure gradients or its interaction with tectonic and gravity loadings as such to yield effective stress gradients, a prerequisite for the generation of buoyancy suffice to growth of vertical hydrofractures in particular. Our model shows that fluid pressure gradients can be extremely important in pattern formation. In the presence of the respective loadings i.e., pressure gradient, gravity and tectonic stresses, it is observed that a whole set of fracture patterns can develop depending on the dominant driving force in the system. Fractures that are produced by fluid pressure gradients only can look fundamentally different to tectonically induced fractures.

It is also evident that permeability as such is a dynamic property that changes simultaneously with the deformation of an overpressure system. Fracture networks in Fig. 5.8 show that there is a strong correlation between layer perpendicular fracturing and faulting. Layered systems that are subjected to non-hydrostatic tectonic stresses in the presence of high fluid pressure gradients along anisotropies undergo a transition from layer fracturing to large scale shearing [63]. Fracturing in the model takes place on the local scale whereas faulting seems to drain the whole system and forms a large-scale connectivity. Vertical fractures in

stiff layers accommodate the additional strain locally with only a minor increase in stress, however under the prevailing conditions of fluid overpressure the differential stress can increase up to a critical limit leading to the development of large scale faults. The stress drops significantly when the whole system fails along large-scale normal faults and high fluid pressure gradients along the fault may weaken the fault plane [64]. This has strong correlation with fluid drain where the growing fractures and the fluid pressure in the system strongly influence each other depending on effective permeability of the interconnected fracture networks. This behavior is similar to what is observed in the Oman Mountains, where veins and faults correlate and stable isotopes seems to indicate that faults drain the system [49, 65]. After their formation the faults usually behave as plastic systems and deter any further stress accumulation unless they are fully healed by the mineralization of the fracturing fluid. This phenomenon has strong influences on the strength of the fault planes and the subsequent earthquake events which may sometime turn into catastrophic failure [18].

The process of hydrofracturing has direct applications in many fields e.g., Geothermal reservoirs or normal oil and gas reservoirs, or CO2 sequestration, where formation fluid pressure gradients play a role in cap-rock failure or permeability creation for the transport of pressurized fluid. We believe that our model can form a basis for better understanding of the influence of fluid pressure gradients and tectonic stresses on the development of natural fractures in reservoirs.

5.7 Conclusion

In conclusion, our coupled numerical model can simulate the dynamic evolution of hydrofracturing. The model can reproduce realistic geometries of the field scale fracture and vein networks and demonstrated how the pattern changes depending on the material properties (i.e., stiffness and breaking strength distribution) and the applied external forces e.g., high fluid pressure gradient, gravity and lateral tectonic forces. Results of the model indicate that layers of low permeability may result in the local perturbation of the effective stress field in host rocks and subsequently causes diversion of the direction of growing hydrofractures. Hydrofracturing in the model produces a non-static permeability in an over-pressured system, where the permeability does adjust the local fluid pressures and accordingly the evolved stresses. We tested the model for a number of different combinations of high fluid pressure gradients, gravity and tectonic stresses to produce complex patterns. We are able to define the first proxies that can be used to determine whether natural fracture, vein and fault networks are mainly due to tectonic stresses or high fluid pressure gradients.

5.8 References

1. Fyfe, W.S., N.J. Price, and A.B. Thompson, *Fluids in the Earth's Crust: Their Significance in Metamorphic, Tectonic, and Chemical Transport Processes*. 1978: Elsevier Scientific Pub. Co.
2. Dahm, T., *Numerical simulations of the propagation path and the arrest of fluid-filled fractures in the Earth.* Geophysical Journal International, 2000. 141(3): p. 623-638.
3. Hubbert, M.K. and W.W. Rubey, *Role of fluid pressure in mechanics of overthrust faulting: I. mechanics of fluid-filled porous solids and Its application to overthrust faulting.* Geological Society of America Bulletin, 1959. 70(2): p. 115-166.
4. Secor, D.T., *Role of fluid pressure in jointing.* American Journal of Science, 1965. 263(8): p. 633-646.
5. Gundersen, E., et al., *Fracture spacing during hydro-fracturing of cap-rocks.* Geofluids, 2011. 11(3): p. 280-293.
6. Gudmundsson, A. and S.L. Brenner, *How hydrofractures become arrested.* Terra Nova, 2001. 13(6): p. 456-462.
7. Bai, T. and D.D. Pollard, *Closely spaced fractures in layered rocks: initiation mechanism and propagation kinematics.* Journal of Structural Geology, 2000. 22(10): p. 1409-1425.
8. Bai, T. and D.D. Pollard, *Fracture spacing in layered rocks: a new explanation based on the stress transition.* Journal of Structural Geology, 2000. 22(1): p. 43-57.
9. Brenner, S.L. and A. Gudmundsson, *Arrest and aperture variation of hydrofractures in layered reservoirs.* Geological Society, London, Special Publications, 2004. 231(1): p. 117-128.
10. Behrmann, J.H., *Conditions for hydrofracture and the fluid permeability of accretionary wedges.* Earth and Planetary Science Letters, 1991. 107(3–4): p. 550-558.
11. Wang, C.-y. and X. Xinong, *Hydrofracturing and episodic fluid flow in shale-rich basins; a numerical study.* AAPG Bulletin, 1998. 82(10): p. 1857-1869.
12. Lister, J.R. and R.C. Kerr, *Fluid-Mechanical Models of Crack Propagation and Their Application to Magma Transport in Dykes.* J. Geophys. Res., 1991. 96(B6): p. 10049-10077.
13. Bons, P.D., M.A. Elburg, and E. Gomez-Rivas, *A review of the formation of tectonic veins and their microstructures.* Journal of Structural Geology, 2012. 43(0): p. 33-62.
14. Ramsay, J.G., *The crack-seal mechanism of rock deformation.* Nature, 1980. 284(5752): p. 135-139.
15. Price, N.J. and J.W. Cosgrove, *Analysis of geological structures*. 1990: Cambridge University Press.
16. Helgeson, D.E. and A. Aydin, *Characteristics of joint propagation across layer interfaces in sedimentary rocks.* Journal of Structural Geology, 1991. 13(8): p. 897-911.
17. Holland, M., et al., *Evolution of fractures in a highly dynamic thermal, hydraulic, and mechanical system - (I) Field observations in Mesozoic Carbonates, Jabal Shams, Oman Mountains.* Geoarabia, 2009. 14(1): p. 57-110.
18. Koehn, D., J. Arnold, and C.W. Passchier, *Fracture and Vein Patterns as Indicators of Deformation History: A Numerical Study.* Geological Society, London, Special Publications, 2005. 243(1): p. 11-24.
19. Laubach, S.E., et al., *Coevolution of crack-seal texture and fracture porosity in sedimentary rocks: cathodoluminescence observations of regional fractures.* Journal of Structural Geology, 2004. 26(5): p. 967-982.
20. Cox, S.F., *The application of failure mode diagrams for exploring the roles of fluid pressure and stress states in controlling styles of fracture-controlled permeability enhancement in faults and shear zones.* Geofluids, 2010. 10(1-2): p. 217-233.
21. Miller, S.A., et al., *Aftershocks driven by a high-pressure CO2 source at depth.* Nature, 2004. 427(6976): p. 724-727.

22. Segall, P. and S.D. Fitzgerald, *A note on induced stress changes in hydrocarbon and geothermal reservoirs.* Tectonophysics, 1998. 289(1-3): p. 117-128.
23. Sibson, R.H., *Fluid involvement in normal faulting.* Journal of Geodynamics, 2000. 29(3–5): p. 469-499.
24. Sibson, R.H. and J. Scott, *Stress/fault controls on the containment and release of overpressured fluids: Examples from gold-quartz vein systems in Juneau, Alaska; Victoria, Australia and Otago, New Zealand.* Ore Geology Reviews, 1998. 13(1-5): p. 293-306.
25. Collettini, C., N. De Paola, and N.R. Goulty, *Switches in the minimum compressive stress direction induced by overpressure beneath a low-permeability fault zone.* Terra Nova, 2006. 18(3): p. 224-231.
26. Hu, J.-C. and J. Angelier, *Stress permutations: Three-dimensional distinct element analysis accounts for a common phenomenon in brittle tectonics.* Journal of Geophysical Research: Solid Earth, 2004. 109(B9): p. B09403.
27. Bonafede, M. and S. Danesi, *Near-field modifications of stress induced by dyke injection at shallow depth.* Geophysical Journal International, 1997. 130(2): p. 435-448.
28. Jamtveit, B., et al., *Hydrothermal vent complexes associated with sill intrusions in sedimentary basins.* Geological Society, London, Special Publications, 2004. 234(1): p. 233-241.
29. Adachi, J., et al., *Computer simulation of hydraulic fractures.* International Journal of Rock Mechanics and Mining Sciences, 2007. 44(5): p. 739-757.
30. Hunt, J.M., *Generation and migration of petroleum from abnormally pressured fluid compartments.* AAPG Bulletin, 1990. 74(1): p. 1-12.
31. Roberts, S.J. and J.A. Nunn, *Episodic fluid expulsion from geopressured sediments.* Marine and Petroleum Geology, 1995. 12(2): p. 195-204.
32. Nunn, J.A. and P. Meulbroek, *Kilometer-Scale Upward Migration of Hydrocarbons in Geopressured Sediments by Buoyancy-Driven Propagation of Methane-Filled Fractures.* AAPG Bulletin, 2002. 86(5): p. 907-918.
33. Cathles, L.M. and A.T. Smith, *Thermal constraints on the formation of mississippi valley-type lead-zinc deposits and their implications for episodic basin dewatering and deposit genesis.* Economic Geology, 1983. 78(5): p. 983-1002.
34. Krynauw, J.R., D.R. Hunter, and A.H. Wilson, *Emplacement of sills into wet sediments at Grunehogna, western Dronning Maud Land, Antarctica.* Journal of the Geological Society, 1988. 145(6): p. 1019-1032.
35. Miller, S.A. and A. Nur, *Permeability as a toggle switch in fluid-controlled crustal processes.* Earth and Planetary Science Letters, 2000. 183(1–2): p. 133-146.
36. Cooke, M.L., et al., *Mechanical stratigraphic controls on fracture patterns within carbonates and implications for groundwater flow.* Sedimentary Geology, 2006. 184(3–4): p. 225-239.
37. Ghani, I., et al., *Dynamic Development of Hydrofracture.* Pure and Applied Geophysics, 2013: p. 1-19.
38. Zoback, M.D., *Reservoir geomechanics*. 2007: Cambridge University Press.
39. Segall, P., *Formation and growth of extensional fracture sets.* Geological Society of America Bulletin, 1984. 95(4): p. 454-462.
40. Engelder, T. and A. Lacazette, *Natural hydraulic fracturing*, in *Rock Joints: Proceedings of the international symposium on rock joints*, N.B.a.O. Stephansson, Editor. 1990, A.A. Balkema, Rotterdam: Loen, Norway. p. 35-44.
41. Olson, J.E., S.E. Laubach, and R.H. Lander, *Natural Fracture Characterization in Tight Gas Sandstones: Integrating Mechanics and Diagenesis.* AAPG Bulletin, 2009. 93(11): p. 1535-1549.
42. Biot, M.A., *General Theory of Three-Dimensional Consolidation.* Journal of Applied Physics, 1941. 12(2): p. 155-164.

43. Rice, J.R. and M.P. Cleary, *Some basic stress diffusion solutions for fluid-saturated elastic porous media with compressible constituents.* Rev. Geophys., 1976. 14(2): p. 227-241.
44. Secor, D.T., *Mechanics of natural extension fracturing at depth in the earth's crust*. 1969, Geological Survey of Canada. p. 3-48.
45. Flekkøy, E.G., A. Malthe-Sorenssen, and B. Jamtveit, *Modeling Hydrofracture.* Journal of Geophysical Research-Solid Earth, 2002. 107(B8).
46. Vinningland, J.L., et al., *Experiments and simulations of a gravitational granular flow instability.* Physical Review E, 2007a. 76(5): p. 051306.
47. Vinningland, J.L., et al., *Granular Rayleigh-Taylor instability: experiments and simulations.* Physical Review Letters, 2007b. 99(4): p. 048001.
48. Holland, M., N. Saxena, and J.L. Urai, *Evolution of fractures in a highly dynamic thermal, hydraulic, and mechanical system - (II) Remote sensing fracture analysis, Jabal Shams, Oman Mountains.* Geoarabia, 2009. 14(3): p. 163-194.
49. Hilgers, C., et al., *Fracture sealing and fluid overpressures in limestones of the Jabal Akhdar dome, Oman mountains.* Geofluids, 2006. 6(2): p. 168-184.
50. Boudier, F., et al., *Kinematics of oceanic thrusting in the Oman ophiolite: model of plate convergence.* Earth and Planetary Science Letters, 1985. 75(2–3): p. 215-222.
51. Breton, J.P., et al., *Eoalpine (Cretaceous) evolution of the Oman Tethyan continental margin: Insights from a structural field study in Jabal Akhdar (Oman Mountains)* Geoarabia, 2004. 9(2): p. 41-58.
52. Searle, M.P., *Structural geometry, style and timing of deformation in the Hawasina window, Al Jabal al Akhdar and Saih Hatat culminations, Oman mountains.* Geoarabia, 2007. 12(2): p. 99-130.
53. Ghani, I., et al., *Dynamic Development of Hydrofracture.* Pure and Applied Geophysics, in press.
54. Press, W.H., *Numerical Recipes in C: The Art of Scientific Computing*. 1992: Cambridge University Press.
55. Bons, P.D., D. Koehn, and M.W. Jessell, *Microdynamics Simulation*. 2007: Springer.
56. Allen, D.N.G., *Relaxation methods*. 1954: McGraw-Hill.
57. Malthe-Sørenssen, A., et al., *Modeling and Characterization of Fracture Patterns in the Vatnajökull Glacier.* Geology, 1998a. 26(10): p. 931-934.
58. Malthe-Sørenssen, A., et al., *Simulation of Extensional Clay Fractures.* Physical Review E, 1998b. 58(5): p. 5548-5564.
59. Cooke, M.L. and C.A. Underwood, *Fracture termination and step-over at bedding interfaces due to frictional slip and interface opening.* Journal of Structural Geology, 2001. 23(2-3): p. 223-238.
60. Gudmundsson, A., *Emplacement and arrest of sheets and dykes in central volcanoes.* Journal of Volcanology and Geothermal Research, 2002. 116(3–4): p. 279-298.
61. Fischer, M.P., et al., *Heterogeneous hydrofracture development and accretionary fault dynamics: Comment and Reply.* Geology, 1994. 22(11): p. 1052-1054.
62. Gudmundsson, A., *Fluid overpressure and stress drop in fault zones.* Geophysical Research Letters, 1999. 26(1): p. 115-118.
63. Bercovici, D., Y. Ricard, and G. Schubert, *A two-phase model for compaction and damage: 1. General Theory.* Journal of Geophysical Research: Solid Earth, 2001. 106(B5): p. 8887-8906.
64. Zoback, M.D. and H.-P. Harjes, *Injection-induced earthquakes and crustal stress at 9 km depth at the KTB deep drilling site, Germany.* J. Geophys. Res., 1997. 102(B8): p. 18477-18491.
65. Virgo, S., et al., *Development of fault and vein netowrks in a carbonate sequence near Hayl al-Shaz, Oman Mountains.* GeoArabia, 2013. 18(2): p. 99-136.

6. Summary and concluding remarks

In this chapter the findings previous chapters are summarized as a general conclusion of this thesis. The chapter is composed of two subsections, with the first section outlining the outcome of simulation experiments with regard to the objectives of this thesis. In the second section, the shortcomings of this work are discussed (inconsistency with quantitative analysis of fluid flow) and further development directions (random lattice of solid particles, thermo-pressure coupling, mineralization of fracturing fluid to study hydrofracturing in a more real geological scenario e.g., crack-seal vein growth) are suggested.

6.1 General conclusion

The mechanical interaction of fluid-solid phases in geopressured sediments is the sole agent in determining the dynamic growth of natural hydrofractures. Limitations to direct observation of this fracturing process under natural conditions (which claim millions of years for pressure buildup and several kilometers of depth) constrain the investigation of the matter through alternative means. This includes analogue experiments under controlled laboratory conditions, theoretical and numerical analysis to gain a better understanding of the controlling conditions for the mechanics of fracturing in relation to crustal fluid pressure. Therefore, the focus of this thesis is the development and the implementation of a computationally efficient coupled hydro-mechanical numerical model to simulate the propagating behavior of hydrofractures in specified problems of interest.

6.1.1 Efficiency of the numerical model

The coupled numerical scheme can efficiently replicate the process of hydrofracturing, which is believed to occur naturally under conditions of a low differential stress state when elevated pore fluid pressures in sedimentary basins approach lithostatic pressure and reduce the minimum effective horizontal stress below zero to reach the tensile strength of the rock. It has been shown that alike pure tensile fractures, fluid driven hydrofractures form and propagate parallel to the direction of the maximum principal compressive stress (σ_1), however during propagation the primary shape and orientation may divert corresponding to the contrastive interaction between the fracturing fluid pressure and the stress field in the system. In addition, simulation examples illustrate that the employed coupled scheme inherits the intimate mutual feedback among the solid-fluid entities in the form of time dependant changes both structure permeability and the pressure field according to poroelastic effects due to structural deformation.

The consistency between the simulated results and previous experimental and numerical results suggests that the described numerical procedure is worthy of simulating qualitative dynamic aspects of hydrofractures and reasonably justifies the assumptions made in the numerical program which attain much of its robustness from the use of simple Darcy based pressure diffusion equation sans redundant components in the description of fluid dynamics.

However, yet there stand some shortcomings, which bound the efficiency of the program and are particularly important when attempting to analysis the fluid flow or drainage through induced fracture planes quantitatively in deformed rocks. This might be resolve with the approximation of area reduction related to particles with broken bonds. One other hand the selection of large time steps for the solution of pressure diffusion in zones with fractured particles may result in problems. However, both of these approaches resulted in stability concerns in the current format of the elasto-plastic model, therefore additional work is still needed to determine more adequate solution of fracture to permeability relation and the respective appropriate conditions for stability to verify a general convergences in the time and space domains. Some other possible strategies have been referred to in chapter 4 in this regard.

6.1.2 Interplay between seepage forces and fracture propagation

It is well established that pore fluid pressure reduces the apparent fracture strength and hence affects the likelihood of rock failure by carrying a part of the total stress through the effective stress criterion (in conjunction with poro-elastic effects). Pore fluid flow under pressure gradients imparts seepage forces (frictional forces) on the solid phase which reflects the localized pore pressure variations in the form of coupling of pore-fluid diffusion with rock deformation. Inversely, the brittle deformation of the solid phase modifies the porosity and permeability and thus changes the rate of fluid flow. Fluid pressure and developing fractures influence each other depending on how effectively fractures can drain an existing fluid pressure.

It is possible to demonstrate in a series of simulation experiments that seepage forces introduce local perturbations of the effective stress field which accordingly promotes different failure patterns as regard to external tectonic loadings. In an extensional stress regime, where the horizontal principal compressive stress (σ_3) is significantly less than the vertical principal compressive stress (σ_1), the hydrofractures are invariably vertical to semi-vertical in orientation and form perpendicular to the minimum compressive stress. In laterally compressive regimes, hydrofracture exhibit an axisymmetric shear propagation from the localized sourced zone under the loading of gravity as well. Moreover, the gravitational loading is shown to have significant impact on the orientation of the induced hydrofractures and the upward drainage of the system.

The simulations that were performed with distinct background permeability in the porous elastic rock system manifested the significant dependency of critical effective tensile stress states on the pressure diffusion rate. It is shown that the higher the permeability the faster the pressure will diffuse and consequently the lower the increase in hydro-tensile stress will be until it is insufficient to induce extension fractures. On the contrary, low pressure diffusion due to lower background permeability facilitates build up of high stress gradients in a relatively short period of time that is adequate enough to induce tension fractures.

6.1.3 Control of physical properties and stress permutation

The presences of anisotropy in the form of statistical distributions of mechanical and hydraulic properties (Young modulus, breaking strength and primary porosity) in the coupled system is an important factor that has a major influence on the propagation of hydrofractures. Anisotropies can lead to substantial localization of distinct pressure diffusion rates and mode-I driving stress and result in the progression of process zones ahead of the pressure source. This process zone contains fractures while the larger scale system is still within an overall elastic behavior. With a continuous increase in pore pressure, microcracks in the process zones tend to link up and produce macro-crack in the direction of the pressure gradient and lead to a system failure in non-elastic behavior.

In addition, heterogeneities in terms of layers of contrasting mechanical and hydraulic properties (e.g., cap rock layer in geopressured sediments) also have shown to produce major influences on fracture propagation. A field of study that is often ignored in numerical simulations (studies of geopressured sediments with internal fluid pressure or injection of external fluid) is the effect of steep pressure gradients across impermeable layers. A range of stress-controlled features may therefore by self-generated by fluid overpressure in heterogeneous sedimentary sequences with varying magnitude of material properties and contribute to its structural permeability.

Stiff layers are shown to fail early and perpendicular to the layering due to concentration of high differential stresses by the seepage forces. However, in conjunction with the layer's low permeability (seal layer) under undrained boundary conditions, the pore fluid pressure at the seal-host layer interface contributes to the permutation of the principal stress tensor. As a consequence, a second set of bedding parallel fractures forms when the evolved total horizontal stress meets the horizontal resistance of the layer interface. Several authors advocate the occurrence of these conditions to high overpressure and low permeable sedimentary systems e.g., accretionary wedges. Reciprocally, a combination of low permeability and critical breaking strength of the respected layers alleviate the large scale vertical propagation of hydrofractures from the localized source to cross the seal layer and represent a complete seal failure.

In a lateral extensional regime, a reduction in the horizontal minimum compressive stress (σ_3) may per se lead to the formation of dilatant shear fracture of certain orientations with the bedding layers. The simulated structures under these condition are in agreement with field observations of veins in the Oman Mountains. The structures represent a positive correlation between purely strain induced bedding perpendicular tensile fractures in the stiffer layers and the large scale normal faulting of the whole sequence. The isolated layer confined fractures link up under the influence of high pressure gradients and lead to the concurrent process of large scale dilatation faulting and the fluid drainage promoting the role of tensile fractures and activated faults in crustal scale fluid transport.

6.2 Suggestion for further improvements

The primary objective of this work was the development of an adequate and computationally efficient coupled numerical tool to simulate and understand the dynamics of hydrofracturing corresponding to physical fluid-solid interaction and thus this work does not claim to investigate or explain all its relevant issues (quantitative fluid flow analysis, healing of fractures and crack-seal mechanism). These important issues of hydrofractures are not addressed in this thesis simply because these are beyond the scope of this work due to time constraint.

Several improvements can be done in order to enhance the domain of implementation of the model to get wider understanding of this complex subject. First, the use of hexagonal elastic lattice may develop preferred fracture orientations due to lattice effects. Therefore, a randomly generated elastic-particle model with a varying range of particle sizes is being suggested which would provide a configuration of the elastic solid medium that is closer to natural rock structures. Secondly, thermal anomalies also play a significant role in or interlinked with pore pressure evolution to induce fluid driven extension fractures as well as condition of fluid mineralization in many geological settings e.g., burial, regional uplift or magmatic intrusions. Hence, an adequate pressure-temperature diffusion coupling will be a more realistic approach towards simulations of hydrofracturing in natural conditions.

Further, introduction of sticky particles in the elastic model can provide solution to healing processes of the induced fractures. Due to sticky features, the particles with broken contacts can gain back a part of their cohesion once they are in contact again for a certain time. This can enable us to track the fractures through the system with respect to their generic time of formation and model vein growth system. Finally, a major drawback of the current model is its two dimensional configuration. However, an extension of the presented procedure to three-dimensional is straight forward is hinted in chapter 3 and chapter 4. Three-dimensional modeling would tremendously further enhance the understanding of permeability and transport problems of the system.

Acknowledgements

CURRICULUM VITAE

IRFAN GHANI